The role of capillary pericytes in cerebral blood flow changes during ischaemia and in Alzheimer's disease

Ross R. Nortley

A thesis submitted to University College London

for the degree of Doctor of Philosophy

Department of Neuroscience, Physiology and Pharmacology

University College London

March 2018

Abstract

Recently, it was found that brain capillary pericytes play a significant role in controlling cerebral blood flow. Pericytes may therefore also play an important pathological role when cerebral blood flow is compromised, both acutely, as occurs during ischaemic stroke, and chronically, as occurs in Alzheimer's disease. In this thesis I have investigated the role of brain capillary pericytes as follows.

(1) Ischaemia: Pericytes have been suggested to constrict capillaries and subsequently die in rigor during ischaemia, making them a therapeutic target after acute stroke when a long-lasting decrease of cerebral blood flow occurs despite re-opening of the occluded artery. I confirmed that pericytes constrict and die in rigor during ischaemia and demonstrated that the L-type Ca^{2+} channel blocker nimodipine inhibits ischaemia-induced pericyte constriction.

(2) Alzheimer's disease (AD): Vascular compromise occurs early in AD and amyloid β (Aβ) has been shown to reduce cerebral blood flow. In the cerebral vasculature most resistance is in capillaries, so Aβ might primarily act on contractile capillary pericytes. I used live and fixed human tissue to establish disease-relevance, and rodent experiments to define mechanism, to show that Aβ constricts brain capillaries at pericyte locations. Applying soluble Aβ oligomers to live human cortical tissue constricted capillaries by 25%. Using rat cortical slices this was shown to reflect Aβ evoking capillary pericyte contraction, with an EC_{50} of 4.7 nM, by generating reactive oxygen species and activating endothelin ET-A receptors. In freshly-fixed diagnostic biopsies from human patients investigated for cognitive decline, mean capillary diameters were 8.1% less in patients showing Aβ deposition than in patients without Aβ deposition. For patients with Aβ deposition, capillary diameter was 31% less at pericyte somata than away from the somata, predicting a halving of blood flow. Constriction of capillaries by Aβ will contribute to the cerebral energy deficit occurring in AD, which promotes further Aβ generation.

Statement of the candidate's contribution to this thesis

The work in this thesis is described in three results chapters. Experiments, data analysis, figure production and writing were almost entirely performed by Ross Nortley (with normal supervisorial input from David Attwell), with his specific contribution to each project listed below. In the introduction (Chapter 1), sections 1.2.6 to 1.2.11 describe the role of astrocytes in the flow of energy from the blood to neurons and the important role played by astrocytes in neurovascular coupling. These sections were formed from a review article written by Ross Nortley for Current Opinions in Neurobiology entitled 'Control of brain energy supply by astrocytes' (Nortley and Attwell, 2017) with Ross Nortley contributing 90% of the overall work to that manuscript.

(1) Control of human and rat capillary diameter by pericytes in physiological conditions. Brightfield studies (with and without fluorescence), immunocytochemistry and confocal imaging described in Chapter 3 were performed by Ross Nortley. Two-photon imaging described in this chapter was perfomed by Ross Nortley in collaboration with Dr. Christian Madry. Planning and execution of all experiments in this chapter, and analysis of all data, were by Ross Nortley. Confirmatory, blinded analysis of data on the time course of vessel diameter was performed by Dr. Anusha Mishra.

(2) Preventing pericyte constriction of brain capillaries and subsequent death in rigor during simulated ischaemia. Brightfield studies (with and without fluorescence) described in Chapter 4 were performed by Ross Nortley. Planning and execution of all experiments in this chapter, and analysis of all data, were by Ross Nortley. Confirmatory, blinded analysis of data on the time course of vessel diameter was performed by Dr. Anusha Mishra.

(3) Effect of amyloid β oligomers on capillary pericytes. Quantification of Aβ peptide concentration was performed by Ross Nortley in collaboration with Dr Vasiliki Kyrargyri. Brightfield studies described in Chapter 5 were performed by Ross Nortley. Two-photon imaging described in this chapter was performed by Ross Nortley in collaboration with Dr. Christian Madry. Pericyte death experiments with confocal imaging were performed by Ross Nortley in collaboration with an undergraduate project student, Hui Gong. Planning and execution of all experiments in this chapter, and analysis of all data, were by Ross Nortley. Confirmatory, blinded analysis of data on the time course of vessel diameter was performed by Dr. Anusha Mishra.

Acknowledgements

First and foremost I want to thank Professor David Attwell. During four really enjoyable years in his laboratory, he has provided me with peerless guidance, support and encouragement. Above all, I am grateful to him for all his kindness and friendship; I could not have had a better supervisor.

I would to thank all lab members past and present, whom I have had the good fortune to work and become friends with. A great bunch, they made working life in the lab really fun. They were always willing to help me out, offered sound advice, and their level of scientific knowledge and expertise perpetually impressed me.

I really enjoyed collaborating in experiments with Dr. Christian Madry, Dr. Vasiliki Kyrargyri, Nils Korte and Hui Gong, and I am grateful to Dr. Lorena Arancibia Carcamo and Dr. Nicola Hamilton-Whitaker who helped me get to grips with immunohistochemistry techniques and computer software for data analysis and creating figures. I would especially like to thank Dr. Anusha Mishra for her expert analytical input.

I would also like to thank Dr. Elisabeth Engl, Dr. Julia Harris, Dr. Anna Krasnow, Dr. Narges Bazargani, Dr. Matthew Hammond-Haley, Dr. Marc Ford, Dr. Fergus O'Farrell, Dr. Felipe Freitas, Rayane Benyahia, Chanawee Hirunpattarasilp and Pablo Izquierdo - it has been a pleasure to work with you all.

I would like to extend my gratitude to others outside of the Attwell Lab with whom we collabortated to investigate the role of capillary pericytes in Alzheimer's disease: Miss Huma Sethi, Dr. Zane Jaunmuktane, Professor Sebastian Brandner and Angela Richard-Loendt.

I am extremely grateful to the Wolfson Foundation who funded my PhD programme, and I wish to thank Professor Nick Wood, Professor John Hardy and Professor Nick Fox who gave me this opportunity and supported me over the last four and a half years. I also want to particularly thank Elizabeth Halton and Dr. Andrea Hodgetts who kept me organised and on track to complete my PhD programme.

Finally I want to thank family because without their love and support I could not have pursued and continued a career in medicine and science. I want to thank my mum, stepdad and my sister, my grandparents, my aunt, uncle and cousins, my wife's parents Pauline and Tariq and Rene and Helen, both my brother-in-laws, my sister-in-law, and most of all, I want to thank my beautiful wife Mei and our wonderful children Jack and Neezie.

Table of contents

List of figures

Chapter 1: Introduction

1.1 Overview

It has recently been found that brain capillary pericytes - contractile cells that can alter capillary diameter, and hence the resistance to blood flow - play a significant role in regulating cerebral blood flow to appropriately meet the energy demands of neural activity (Hall et al., 2014). Pericytes may therefore also play an important in pathologies where cerebral blood flow is compromised, both acutely, as occurs during ischaemic stroke (Ames et al., 1968; Hall et al., 2014; Majno et al., 1967), and chronically, as occurs in Alzheimer's disease (AD) (Iadecola, 2013; Iturria-Medina et al., 2016; Love and Miners, 2016). In this thesis I will describe experiments investigating the role played by brain capillary pericytes in both of these disorders, as follows.

(1) Ischaemia: It has been shown that pericytes constrict capillaries and subsequently die in rigor during ischaemia (Hall et al., 2014), making them an attractive therapeutic target in acute stroke. In this component of the thesis I will attempt to pharmacologically block pericyte constriction, and subsequent death in rigor, during simulated ischaemia.

(2) Alzheimer's Disease: Investigations into the vascular effects of Aβ in AD have focused on arteries and arterioles (Deane et al., 2003; Dietrich et al., 2010; Niwa et al., 2001), but in the brain parenchyma the majority of the vascular resistance is located in capillaries (Gould et al., 2017). In this component of the thesis I will investigate whether capillary pericytes are affected by Aβ oligomers, the molecular species that show a concentration that correlates best with cognitive decline in AD (Attems et al., 2004; Benilova et al., 2012; Caughley and Lansbury, 2003; Glabe, 2006; Klein et al., 2001).

Where possible (to maximise disease relevance), I use living human brain slices derived from neurosurgically-resected brain tissue (removed to access tumours) to study acute responses to Aβ and rapidly-fixed human brain biopsy tissue (with or without Aβ deposition) to assess pericyte responses to long-term accumulation of Aβ in AD. The mechanisms of effects seen in human tissue were then defined in more readily available rodent brain slices.

1.2 Brain Energy use and Neurovascular Coupling

1.2.1 Brain Energy

Normal functioning of the human brain is critically dependent on a high consumption of energy (derived from glucose and oxygen delivered in the blood), which is used mainly to reverse the ion fluxes that underlie synaptic potentials and action potentials (Attwell & Laughlin, 2001). ATP is generated from the complete oxidation of glucose within the mitochondria of neurons and glia (glycolysis and oxidative phosphorylation generate ~7% and 93% of ATP respectively). This ATP is mainly consumed (ignoring cell housekeeping energy use) on the reversal of ion fluxes through synaptic receptors (50%), reversal of Na^+ entry for action potentials (22%), reversal of Na^+ entry at the resting potential (20)%, recycling glutamate (4%) and reversal of presynaptic Ca^{2+} entry (4%) (Harris et al., 2012). Powering human brain cells is energetically expensive and whilst the human brain comprises only 2% of the body's mass, it consumes ~20% of the total oxygen used by the body (Mink et al., 1981). Moreover, if the energy supply of brain cells (which have virtually no fuel reserve) is compromised (as occurs during ischaemic stroke and cardiac arrest), they quickly become injured or die (Iadecola, 2017). To ensure that the fluctuating activity-dependent energy requirements of neurons

are met, the brain has evolved ‘neurovascular coupling’ mechanisms to regulate energy supply, which increase the blood flow to regions where neurons are active - a response termed ‘functional hyperaemia’ (Attwell et al., 2010). Once delivered to an active area, glucose must then be transferred from the blood to brain cells, where it is used to generate ATP, converted to other forms of energy substrate (such as lactate or glutamate) or converted in astrocytes to the only energy reserve the brain has, i.e. glycogen (McKenna et al., 2016; Waitt et al., 2017).

In this introduction to the thesis I will give an overview of the ‘flow’ of energy from blood to neurons. I will start with a description of the macroscopic blood supply and microvasculature of the brain, since this backround is necessary to understand the how ischaemic stroke occurs in the brain. I will then describe the cellular components and signaling pathways involved in neurovascular coupling, which provide essential context for my experiments trying to manipulate regulation of blood flow at the capillary level. Particular emphasis will be given to the important roles played by astrocytes and capillary pericytes (key components of the neurovascular unit). This will be followed by a description of the important role of pericytes in cerebral ischaemia (which causes stroke) and Alzheimer’s disease, with relevant background given for both pathologies.

1.2.2 Brain blood supply at a macroscopic level

The arterial supply of the cerebrum is divided into two separate systems: the deep perforating arteries which primarily arise at the base of the brain from the circle of Willis (see below) or its immediate branches, and the leptomeningeal arteries (pial arteries), which form an anastamotic network on

the surface of the hemispheres and stem from the terminal branches of the anterior, middle and posterior cerebral arteries, and the anterior choroidal artery. Both the deep perforator and leptomeningeal systems are supplied by a pair of anterior and posterior arteries (the internal carotid arteries and the vertebral arteries, respectively) and ultimately converge back towards each other, having passed through the cortical layers and the deep grey structures, respectively, to merge in the deepest areas of the subcortical white matter where there is a watershed area (Pantoni, 2010) (Figure 1.1).

The carotid system is made up of three major arteries: the common carotid, internal carotid (described below) and the external carotid. The right common carotid begins at the level of the sternoclavicular notch from the brachiocephalic artery, whilst the left carotid arises directly from the aortic arch. The common carotid arteries climb in the neck to the level of 4th cervical vertebra (just below the level of the angle of the jaw), where they each divide into the external and internal carotid arteries.

Entering the base of the skull through the floor of the cavernous sinus, the internal carotid artery runs forward to puncture its roof medial to the anterior clenoid process. Opposite the optic canal, where the ophthalmic artery branches off, the internal carotid artery then arches backward over the roof of the cavernous sinus before turning upwards once more, lateral to the optic chiasm. Here, the internal carotid artery ends by dividing into the anterior and middle cerebral arteries, and the posterior communicating artery.

The vertebral artery enters the cranium through the foramen magnum and winds gradually around to the anterior aspect of the brainstem to join its

counterpart from the opposite side, to form the singular basilar artery at the inferior border of the pons. After continuing superiorly, it divides into the two posterior cerebral arteries in the midline at the upper border of the pons.

By means of the anterior communicating arteries, which connect the anterior cerebral arteries, and the posterior communicating arteries, which unite the middle and posterior cerebral arteries, blood flowing from the carotid and vertebral systems becomes continuous in the circle of Willis (Figure 1.1), which rests in the interpeduncular cistern beneath the forebrain close to the optic chiasm and infundibulum of the pituitary gland.

The anterior cerebral artery for each hemisphere initially runs anteriorly above the optic nerve before turning upwards and running backwards over the corpus callosum in the longitudinal fissure. It is joined to its counterpart from the opposite hemisphere by the anterior communicating artery. This artery, through its superficial branches, supplies the anterior three quarters of the medial surface of the frontal lobe, including its medial-orbital surface, the frontal pole, a length of the lateral surface of the cerebral hemisphere along the superior border, and the anterior four fifths of the corpus callosum. Deep perforator branches of each anterior cerebral artery-the anterior lenticulostriate arteries and the recurrent artery of Heubner, arise proximally (near the circle of Willis) to supply the anterior limb of the internal capsule, the inferior portion of the head of the caudate nucleus and the anterior part of the globus pallidus.

Each middle cerebral artery breaks up into superficial and deep hemisphere branches as it passes laterally in the lateral cerebral sulcus.

Through its cortical branches it supplies the lateral convexity of the cerebral hemisphere encompassing the cortex and white matter of the frontal lobe, parietal lobe and superior parts of the temporal lobe and insula. The deep medial and lateral lenticulostriate branches of the middle cerebral arteries supply the putamen, part of the head and body of the caudate nucleus and the corona radiate.

The vertebral arteries and their important branches (the posterior inferior cerebellar and anterior spinal arteries) supply the majority of blood to the medulla, the medial lemniscus and nearly all of the lateral medullary region, the restiform body, the posteroinferior part of the cerebellar hemispheres and the ventral portion of the spinal cord.

The basilar artery along with its important branches (the superior cerebellar, anterior inferior cerebellar, and the pontine and labyrinthine arteries) supply the pons, the middle and superior cerebellar peduncles, the inner ear, the high midbrain and the medial subthalamic regions.

The posterior cerebral artery (terminal branch of the basilar) is joined by the posterior communicating artery branch of the internal carotid artery as it twists around the cerebral peduncles. The posterior cerebral artery and its perforator branches supply deep structures in the brain including the thalamus, substantia nigra, red nucleus, mammillary bodies, the lateral geniculate body as well as the posterior limb of the internal capsule. Its superficial, terminal branches supply the inferior surface of the occipital lobe, all of the temporal lobe (except the lateral surface) and the medial surface of

the occipital lobe (Hall-Craggs, 1990; Ropper and Brown, 2005; Tatu, Vuillier and Moulin, 2014).

The deep perforator branches of the cerebral arteries (described above) penetrate the brain via the anterior, posterior and lateral perforated substances. The perforator arteries stemming from the internal carotid artery, anterior and middle cerebral arteries, anterior communicating artery and anterior choroidal artery (the latter originates from the internal carotid artery and exceptionally from the middle cerebral artery) pass through the anterior perforator substance. Perforating arteries arising from the posterior cerebral artery enter the brain through the posterior perforated substance forming the interpenduncular arteries, which are classed as three rami: only the superior rami (thalamoperforating arteries) supply blood to the hemispheres; the middle and inferior rami supply the brainstem. The posterior cerebral artery also gives rise to the thalamogeniculate branches and the posterior choroidal arteries to supply blood to the thalamus and geniculate bodies.

The posterior communicating artery gives rise to perforating branches, most notably the premamillary artery, which passes through the lateral perforator substance. Rarely, a single arterial trunk - the artery of Percheron arises from the PCA to supply the paramedian thalami and the rostral midbrain bilaterally. (Tatu, Vuillier and Moulin, 2014).

1.2.3 Cortical blood supply at a microscopic level

The major cerebral arteries and their cortical branches supply the cerebral cortex from the surface by giving rise to a lattice of pial arterioles (with several layers of smooth muscle cells separated from the endothelium

by a prominent elastic lamina (Rogendorf & Cervós-Navarro, 1977)). These arterioles run, anastomose and penetrate into the brain cortex (along with surfacing intracortical veins) beneath the arachnoid mater of the hemispheres. The multiple anastomoses of the pial arteries reduce the loss of blood flow to the cortex when one pial artery becomes blocked (Shih et al., 2013). As pial arterioles plunge into the brain parenchyma, forming so-called penetrating arterioles, they do so surrounded by an extension of the subarachnoid space, the Virchow-Robin space, which is delineated by the vascular basement membrane and the glia limitans (Iadecola, 2017; Jones, 1970; Zhang et al., 1990).

Using corrosion casting of the human brain vasculature, Duvernoy classified human brain arterioles into six groups according to their depth and branching pattern. Group 1 arterioles dive only to the depth of cortical layer 1 (molecular layer) and may extend to cortical layer 2 (external granular layer), whilst Group 2 vessels reach the superficial part of cortical layer 3 (pyramidal layer). The most densely vascularized of the cortical layers- cortical layer 4 (the internal granular layer) is reached by Group 3 arterioles. Group 4 arterioles reach the multiform layer and inner limit of the subcortical white matter. Group 5 arterioles penetrate through the full thickness of the cortex and into the white matter, supplying all cortical layers as they pass through. Group 6 vessels are devoid of branches as they pass through the cortical layers to penetrate deepest and supply the subcortical white matter (Duvernoy et al., 1981).

Penetrating arterioles, as they progress deeper, replace their single layer of continuous smooth muscle cells with non-continuous spans of

smooth muscle cells (Rogendorf & Cervós-Navarro, 1977)) to become intraparenchymal arterioles, which display a less distinct elastic lamina. At this level, the glial membrane and vascular basement membrane come closer together to obliterate the perivascular space and the arteriole becomes enwrapped by astrocytic endfeet.

Branching further, intraparenchymal arterioles lose their smooth muscle cell wall (but retain their close apposition of astrocyte endfeet) and give rise to the dense and highly collateralised capillary bed, which has evolved to ensure adequate and adaptable delivery of O_2 and glucose to neurons. The diffusion distance from a neuron to an adjacent capillary rarely exceeds 15μm (Iadecola, 2017; Jones, 1970; Winkler et al., 2014; Zhang et al., 1990). Capillaries are covered by spatially isolated pericytes (discussed in detail below) - mural cells embedded within the basement membrane - which extend circumferential and longitudinal processes around and along the vessel wall, and of which a sub-population are contractile (Grant et al., 2017; Hall et al., 2014; Mishra et al., 2016; Peppiatt et al., 2006).

Throughout this microvascular bed, effective and robust neurovascular intercommunication is dependent upon the coordinated action of the multiple cell types that constitute the 'neurovascular unit' (NVU): neurons, vascular cells (endothelial cells, vascular smooth muscle cells, pericytes) and glial cells (astrocyte endfeet and microglia) (Bell et al., 2010; Winkler et al., 2011).

1.2.4 Cerebral small vessel disease and its classification

Pathological processes of various aetiologies affecting cerebral capillaries, small arteries, arterioles and venules may be grouped together

and referred to as cerebral small vessel disease. It must be remembered however, that the term small vessel disease often has different meanings, depending its contextual usage (in the pathological, clinical and neuroimaging arenas), and is commonly exlusively applied to diseases of arterial/arteriolar vessels (and not capillaries and venules). Small vessel diseases are usually systemic disorders and affect several different organs, though some small vessel pathological processes predominantly or even exclusively affect the brain. Indeed, cerebral small vessel disease is thought to be the most frequent neurological disease, and plays a crucial role in three major overlapping fields: stroke, dementia and ageing. For example, in most cases of neuropathologically confirmed Alzheimer's disease, post-mortem examination reveals parenchymal vascular disease- both amyloid angiopathy and arteriosclerotic small vessel disease (Pantoni, 2010).

Arterioscletotic disease (including fibrinoid necrosis, lipohyalinosis, microatheroma, microaneurysms and segmental disorganization) and sporadic and hereditary cerebral amyloid angiopathy represent (according to a recently proposed aetiological classification of cerebral small vessel diseases) the two most prevalent types of small vessel diseases of cerebal small vessels – Type 1 and Type 2, respectively. Type 3 cerebral small vessel diseases comprise inherited or genetic small vessels diseases (distinct from cerebral amyloid angiopathy), such as cerebral autosomal dominant arteriopathy with subcortical ischaemic strokes and leukoencephalopathy (CADASIL) and Fabry's disease. Type 4 disorders represent inflammatory and immunologically mediated cerebral small vessel diseases including primary angiitis of the CNS and vasculitis associated with connective tissure

disorders such as systemic lupus erythematosus and Sjögren's syndrome, whilst Type 5 cerebral small vessel disease represents venous collagenosis, where deposition of collagen thickens the walls of small veins and venules located close to the lateral ventricles, resulting in luminal narrowing and sometimes vessel occlusion. Finally, Type 6 cerebral small vessel disease is comprised of all other disorders of small vessels, such as radiation-induced vasculopathy and non-amyloid microvessel degeneration in Alzheimer's disease (Pantoni, 2010).

1.2.5 Neurovascular coupling and functional hyperaemia: 'feedback' and 'feedforward' mechanisms

In the past, there was a prevailing concept that functional hyperaemia resulted from active neurons generating a metabolic signal, such as a fall in O_2 or glucose concentration or a rise in carbon dioxide concentration ('negative feedback signaling': Cohen et al., 1997). It was also believed that cerebral blood flow was regulated solely by pre-capillary arterioles because capillaries lack a smooth muscle wall. Over the last 30 years however, it has been demonstrated that ('feedforward') neurotransmitter-mediated (particularly glutamate) signaling by neurons and astrocytes also plays a key role in regulating cerebral blood flow, and that capillaries, in addition to arterioles, are likely to control blood flow (Attwell et al., 2010) (see Figs. 1.2, 1.3 below).

Currently, it is thought that *both* 'feedback' and 'feedforward' signaling pathways are involved in coordinating the hyperaemic response, and that both pathways may work in concert to mediate neurovascular coupling at the

arteriolar and the capillary levels (Iadecola, 2017; Attwell et al., 2010): Driving the 'feedforward' signal, glutamate release from active synapses activates post-synaptic glutamate receptor (GluRs), triggering Ca^{2+}-dependent signaling pathways. These result in the release of vasoactive factors (including K^+, nitric oxide and prostanoids) to elicit a vascular response in local arterioles and capillaries. In tandem, 'feedback' mechanisms may be triggered when a reduction in tissue O_2 (hypoxia) from increased energy use (induced by neuronal activation) or the accumulation of vasodilatory metabolic by-products (adenosine, CO_2, H^+ and lactate) drive an additional feedback component to secure an appropriate increase in blood flow to meet the metabolic demands of the tissue (Freeman & Li, 2016; Iadecola, 2013).

1.2.6 Neuronal control of neurovascular coupling

Neuronal signaling is thought to be the *primary* initiator of the local vascular response (see Fig. 1.2), with neurons signaling either directly to the vasculature or through intermediary cells such as astrocytes (see sections 1.2.6 – 1.2.13 below). Direct neuronal signaling has been shown to depend upon synaptic glutamate release activating N-methyl-D-aspartate (NMDA) receptors (assumed to be predominantly on postsynaptic interneurons, where nitric oxide synthase is expressed; Brenman et al., 1996; Kornau et al., 1995, although there is a suggestion that NMDA receptors are also present on endothelial cells: András et al., 2007; Krizbai et al., 1998; Sharp et al., 2003) and α-amino-3-hydroxyl-5-methyl-4-isoxazole propionic acid (AMPA) receptors. These increase intracellular [Ca^{2+}], activating the Ca^{2+}-dependent enzymes neuronal nitric oxide synthase (nNOS) and cyclooxygenase 2 (COX-2). nNOS and COX-2 produce the powerful vasodilators NO and

prostaglandins, respectively (Attwell et al., 2010). Neuron-derived adenosine and K^+ (at a K^+ concentration less than 12mM) are also potent vasodilators (Iadecola, 1993; Filosa et al., 2006; Ko et al., 1990) and may too participate in increasing cortical blood flow, either directly or via astrocytes. Moreover, inhibitory γ-aminobutyric acid (GABA) interneurons express vasoactive agents (such as the vasoconstrictors neuropeptide Y (NPY) and vasoactive intestinal peptide (VIP), and vasodilatory nNOS), and are also likely to play a prominent role in mediating functional hyperaemia (Cauli and Hamel, 2010; Uhlirova et al., 2016b; Iadecola, 2017).

Aminergic and cholinergic neurons also participate in regulating vascular tone. There are diffuse adrenergic, dopaminergic, serotinergic and cholinergic projections from several subcortical nuclei: the locus coeruleus, the ventral tegmental area, the raphe and the basal forebrain, respectively. Projections from these nuclei frequently terminate near astrocytic endfeet (Cohen et al., 1996; Hamel, 2006) and are thought to possess a less spatially localised capability to regulate resting cerebral blood flow. The amine transmitters are vasoconstricting and provide a basal constricting tone to arterioles (and pericytes) against which the vasodilators can cause relaxation and locally increase flow (Cohen et al., 1996; Zhang et al., 1995; Hamel, 2006; Toussay et al., 2013; Iadecola, 2017). Acetylcholine, on the other hand, provides a spatially poorly localised increase of blood flow (Biesold et al., 1989; Sato et al., 2001).

In addition to direct signaling from neurons to the vasculature, astrocytes can transmit signals from neurons to the vasculature to increase local cerebral blood flow (described in detail below). It has been proposed

that synaptic glutamate release activates type 1 metabotropic glutamate receptors (mGluR1 and mGluR5) on astrocytes, triggering astrocytic [Ca^{2+}] rises and astrocytic production of vasoactive agents (Gordon et al., 2008; Mulligan & MacVicar, 2004; Zonta et al., 2003), although a lack of mGluRs on astrocytes in adult animals and further investigation have led to the idea that astrocyte $[Ca^{2+}]_I$ may rise as a result of activation of astrocyte P2X1 receptors (Sun et al., 2013; Mishra et al., 2016). Interestingly, the pathway by which dilation is evoked at the arteriole level may differ from that by which blood flow is increased by capillary dilation, as discussed below, with astrocytes being mainly involved in signalling to capillary pericytes (Mishra et al., 2016; Biesecker et al., 2016).

1.2.7 The role of astrocytes in regulating blood flow and energy supply in the CNS

Astrocytes, with 'endfoot' processes abutting blood vessels supplying glucose, and finer processes surrounding synapses (the brain's major energy consumers), are potentially important regulators of brain energy supply. There continues to be intense debate, however, about the role of astrocytes, both in regulating local blood flow to power active neurons, and in transforming glucose to other molecules that are the immediate substrate for ATP production.

1.2.8 The role of astrocyte $[Ca^{2+}]_i$ transients in adjusting brain energy supply

Astrocytes, which are present in the brain at similar numbers to neurons (von Bartheld et al., 2016), are ideally positioned between the vasculature and neurons to fulfil several key roles in regulating the flow of

energy to neurons, including mediation of neurovascular coupling. Astrocytes extend fine processes that ensheath neuronal synapses and more substantial 'endfeet' that wrap much of the surface of the brain vasculature. For example, astrocyte processes cover ~63% of the surface area of capillaries, with most of the rest of the endothelial tube being covered by pericytes (the role of which is discussed below), and <1% of the endothelium facing clefts between these cells (Mathiiesen et al., 2010). This topographical arrangement allows astrocytes to detect changes in neuronal activity (and hence metabolic demand) by sensing neurotransmitter release, and to relay this information to the vasculature to alter the energy supply. Regulation of blood flow is achieved by vascular smooth muscle cells and pericytes altering their tone to adjust the diameter of arterioles and capillaries respectively, and thus alter blood flow (discussed further below).

The first evidence that astrocytes are able regulate arteriole diameter came from brain slices, where the Carmignoto group showed that raising astrocyte $[Ca^{2+}]_i$ with metabotropic glutamate receptor (mGluR) agonists dilated arterioles by generating a cyclooxygenase derivative of arachidonic acid (Zonta et al., 2003). Subsequently, the MacVicar group showed that raising astrocyte $[Ca^{2+}]_i$ by optically uncaging Ca^{2+} led to arteriole constriction (later found to become a dilation at physiological oxygen levels (Gordon et al., 2008; Mulligan & MacVicar, 2004). Similarly, Nedergaard's group reported that *in vivo* an mGluR-evoked arteriole dilation occurred in response to neuronal activity and was mediated by a cyclooxygenase derivative (Takano et al., 2003). Subsequently, there has been debate over whether the astrocyte $[Ca^{2+}]_i$ transients evoked by neuronal activity are too small, too

slow, or too infrequent to have a causative role in neurovascular coupling (Lind et al., 2013; Nizar et al., 2013; Winship et al., 2007), and whether $[Ca^{2+}]_i$-raising mGluRs even exist in adult astrocytes (Sun et al., 2013). These arguments partly reflected the fact that conclusions had been based on measuring Ca^{2+} signals in astrocyte cell bodies, rather than in the fine astrocyte processes near synapses which presumably respond first to neuronal activity. In addition, these studies employed bulk loading of Ca^{2+}-sensing dyes, which may go into both astrocytes and neurons, making it hard to be certain which cell type is generating observed Ca^{2+} signal (Bazargani & Attwell, 2016; Otsu et al., 2015; Reeves et al., 2011).

In addition to releasing enzyme-derived chemical messengers, astrocyte $[Ca^{2+}]_i$ transients driven by neuronal activity may also signal to blood vessels by releasing K^+ ions onto vessels, through Ca^{2+}-activated K^+ (BK) channels in astrocyte endfeet (Filosa et al., 2006). In the physiological voltage range, increasing $[K^+]_o$ hyperpolarises vascular smooth muscle, by increasing the conductance of, and thus increasing outward current through, inward rectifier K^+ channels. This hyperpolarisation reduces Ca^{2+} influx through voltage-gated channels, and leads to vessel dilation. A similar mechanism has been suggested to initiate a propagating hyperpolarization along capillary endothelial cells, to send a signal instructing arterioles to dilate (see secton 1.2.13 below) (Longden et al., 2017).

1.2.9 Astrocytes mediate neurovascular coupling at the capillary level

Despite a general focus on neurovascular coupling at the arteriole level, it was recently demonstrated that the majority of the hydraulic resistance (which can be reduced to increase blood flow in the cortical

vasculature) is located in capillaries rather than arterioles (Blinder et al., 2013; Gould et al., 2017). This has shifted attention to the role of pericytes - spatially isolated contractile cells on capillaries - in controlling cerebral blood flow. Indeed, *in vivo* data suggest that a major fraction of the increase in blood flow evoked by neuronal activity reflects active relaxation of capillary pericytes (Hall et al., 2014; Kisler et al., 2017).

Dialysing astrocytes in brain slices with a high concentration of the rapid calcium buffer BAPTA was found to inhibit pericyte-mediated capillary dilation evoked by neuronal stimulation, while having no effect on arteriole dilation (Mishra et al., 2016) (perhaps surprisingly, given previous reports (Gordon et al., 2008; Takano et al., 2006) of astrocyte $[Ca^{2+}]$ regulating arteriole dilation), suggesting a role for astrocyte $[Ca^{2+}]_i$ transients in regulating brain energy supply at the capillary level. Further pharmacological analysis demonstrated that the signalling evoked by neuronal activity to dilate the two types of vessel in brain slices was different. Arterioles were dilated by nitric oxide release (presumably from interneurons), and capillaries were dilated by prostaglandin E_2, which was generated from arachidonic acid derived from the sequential action (in astrocytes) of phospholipase D2, diacylglycerol lipase and cyclooxygenase 1. (Note however that other studies (Gordon et al., 2008; Takano et al., 2006) have reported that arachidonic acid metabolites such as PgE_2 can also dilate arterioles, suggesting that different neurovascular coupling mechanisms may occur in different circumstances). The astrocyte $[Ca^{2+}]_i$ transients evoked by neuronal activity to initiate capillary dilation were surprisingly shown to be produced, not by mGluRs as discussed above, but by postsynaptically released ATP activating $P2X_1$ receptors on

astrocytes (Mishra et al., 2016) (Fig. 1.3). Similarly, in the retina, astrocyte (Müller cell) $[Ca^{2+}]_i$ transients were found to dilate intermediate layer capillaries but not arterioles (Biesecker et al., 2016). It has been suggested that a low level of neuronal activity can evoke arteriole dilation in the absence of astrocyte endfoot $[Ca^{2+}]_i$ transients, which are only detectable when a higher level of neuronal activity occurs (Institoris et al., 2015) and it will be interesting to determine whether this dilation is mediated by NO, as found by Mishra et al. (2016). If so, this might imply that low levels of neuronal activity increase blood flow solely by dilating arterioles, while higher activity also dilates capillaries via astrocytes and pericytes.

The control of capillary diameter by astrocytes and pericytes may be relevant to developing strategies for preventing deleterious decreases of blood flow that occur in pathology (discussed in detail below). After ischaemia (Hall et al., 2014), in epilepsy (Leal-Campanario et al., 2017) and in spinal cord injury models (Li et al., 2016) localised constrictions of capillaries produced by pericytes reduce local blood flow, which will contribute to neurodegeneration. An important issue for the future will be whether the control of pericyte tone by astrocytes can be harnessed therapeutically to maintain a normal energy supply to the tissue in such situations.

1.2.10 Tonic regulation of cerebral blood flow by astrocytes

Changes of blood flow evoked by neuronal activity, in part generated through astrocytes as discussed above, initiate the signals detected by the widely used BOLD fMRI (blood oxygen level dependent functional magnetic resonance imaging) technique. However, a tonic regulation of cerebral blood flow by astrocytes may be of equal importance for brain function. Introducing

the calcium chelator BAPTA into astrocytes in brain slices was found to produce a constriction of arterioles that was prevented by blocking cyclooxygenase 1, but was unaffected by blocking neuronal activity with TTX (Rosenegger et al., 2015). Thus, either the mean resting level of astrocyte $[Ca^{2+}]_i$, or $[Ca^{2+}]_i$ transients generated independently of action potentials, may tonically activate the prostaglandin-mediated pathway described above (Mishra et al., 2016), although it is surprising that in this case it is affecting arterioles rather than capillary pericytes. Recently, astrocyte $[Ca^{2+}]_i$ transients generated independently of action potential evoked transmitter release were characterised as resulting from bursts of Ca^{2+} efflux through the mitochondrial permeability transition pore (Agarwal et al., 2017). Although these transients occur in TTX, their rate was raised when neuronal activity was increased by blocking synaptic inhibition with picrotoxin. This may occur because the mitochondrial permeability transition pore opens more when demand for oxidative phosphorylation is greater during neuronal activity (Agarwal et al., 2017). If so, this would provide another astrocyte-mediated mechanism to increase the supply of glucose and oxygen substrates for oxidative phosphorylation when needed.

Another way in which astrocytes may play a key role in regulating cerebral blood flow tonically is in response to changes of CO_2 level (Howarth et al., 2017). When $[CO_2]$ rises, astrocyte $[Ca^{2+}]_i$ rises, possibly as a result of activation of Na^+/HCO_3^{--} co-transport into the cell followed by a slowing or reversal of Na/Ca^{2+} exchange (Turovsky et al., 2016). This $[Ca^{2+}]_i$ rise activates cyclooxygenase 1 (COX1) to generate vasodilating prostaglandin E_2. The enzyme downstream of COX1 that synthesizes prostaglandin E_2

depends for its activity on glutathione, which can fall in concentration in disease or old age, suggesting a possible mechanism by which cerebral blood flow and energy supply might be reduced in these conditions (Howarth et al., 2017).

1.2.11 Signalling from the vasculature to neurons via astrocytes

Remarkably, communication between neurons and the vasculature via astrocytes may be bidirectional. Increasing the flow and pressure within arterioles in brain slices has been found to constrict the arterioles and raise $[Ca^{2+}]_i$ in astrocyte processes via activation of TRPV4 channels (Kim et al., 2015). This astrocyte $[Ca^{2+}]_i$ rise leads, perhaps via release of the gliotransmitter ATP which is converted extracellularly into adenosine, to increased spiking activity of inhibitory interneurons and a hyperpolarization and decreased spiking activity of pyramidal neurons (Kim et al., 2015). At present the functional significance of this pathway for matching neuronal activity to supply of energy substrates is uncertain.

1.2.12 Astrocyte control of neuronal energy use

After arriving in the blood, glucose crosses cerebral vascular endothelial cells via facilitative (sodium-independent) GLUT1 glucose transporters, before uptake mainly via GLUT1 and GLUT3 into glial cells and neurons, respectively (Fig. 1.3). Here, it undergoes conversion to glucose-6-phosphate by hexokinase, before being processed by the glycolysis pathway to generate ATP and pyruvate, by the pentose phosphate pathway to generate NADPH, or (in astrocytes only) being converted to the energy store glycogen (Mergenthaler et al., 2013). Pyruvate generated by glycolysis can either be used directly (in the same cell) by oxidative phosphorylation to

generate a much larger amount of ATP per glucose than glycolysis provides, or can be converted to lactate and exported from the cell, either to be lost from the brain or to be taken up into another cell and converted back to pyruvate to be used in oxidative phosphorylation (Mergenthaler et al., 2013).

Neurons are the principal consumers of brain energy (~80%), which they use mainly to reverse the ion entry generating synaptic and action potentials (see above) (Attwell & Laughlin, 2001). The vasculature-wrapping morphology of astrocytes described above might suggest that glucose may be initially transferred from blood vessels into astrocytes before being distributed to neurons through the astrocyte cytoplasm, and even through astrocyte-astrocyte gap junctions to more distant regions (Rouach et al., 2008) (although modelling based on transporter data (Simpson et al., 2007) has indicated that most glucose could in fact reach neurons by diffusion through the extracellular space: Fig. 1.3). The influential astrocyte-neuron lactate shuttle (ANLS) hypothesis (Pellerin & Magistretti, 2012) proposed an appealing mechanism by which neuronal activity could thus be linked to energy supply. When neurons are active and releasing glutamate, uptake of the glutamate into astrocytes and its subsequent conversion to glutamine were postulated to trigger glycolysis in the astrocytes, generating lactate (made from pyruvate via astrocytic lactate dehydrogenase (LDH): Fig. 1.3) that could then be exported to neurons and used as fuel for oxidative phosphorylation (after conversion by neuronal LDH back to pyruvate). Export of the lactate would occur via monocarboxylate transporters (MCTs) or perhaps a channel-based mechanism (Sotelo-Hitschfeld et al., 2015).

The ANLS hypothesis was based partly on the affinities of the LDH and MCT isoforms present in neurons and astrocytes being suited to transfer lactate from astrocytes to neurons, however the overall direction of the lactate flux is determined by concentrations of the reactants involved in the reactions catalysed by LDH and not by the MCT and LDH affinities (Bak & Schousboe, 2017). The ANLS hypothesis was also based on the notion that astrocytes are much more glycolytic than neurons, which were hypothesised to generate ATP by oxidative phosphorylation using astrocyte-derived lactate as a substrate. Indeed, 6-phosphofructo-2-kinase/fructose-2,6-biphosphatase 3 (Pfkfb3), which promotes glycolysis by converting fructose-6-phosphate to fructose-2,6-bisphosphate which allosterically activates the rate-limiting glycolytic enzyme phosphofructokinase, is more highly expressed in astrocytes than in neurons (Herrero-Mendez et al., 2009; Zhang et al., 2016). Further downstream in glycolysis, astrocytes and neurons differ in the splice variant they express of the enzyme pyruvate kinase, which generates pyruvate from phosphoenolpyruvate, as a result of which it has been suggested that astrocytes are more able than neurons to regulate their glycolytic rate to match the prevailing energetic conditions (Zhang et al., 2014). Furthermore, in cultured cells, the activity of pyruvate dehydrogenase (PDH), which regulates entry of pyruvate into the TCA cycle, is more inhibited by phosphorylation in astrocytes than in neurons, thus diverting pyruvate from the TCA cycle and promoting lactate formation (Halim et al., 2010; Zhang et al., 2014).

Despite these data suggesting that astrocytes use glycolysis more than neurons, it certainly is not the case that all astrocyte ATP generation is

via glycolysis, while all neuronal ATP is produced by lactate-fuelled oxidative phosphorylation in mitochondria. Tracing a fluorescent glucose analogue has suggested that neuronal activity promotes its uptake mainly into neurons rather than astrocytes, consistent with neurons being important users of glycolysis (Lundgaard et al., 2015). Astrocytes have mitochondria even in their fine processes (Derouiche et al., 2015), and indeed neuronal activity localises mitochondria at positions in astrocyte processes that are near synapses (Jackson et al., 2014; Stephen et al., 2015) presumably in order to power glutamate uptake that occurs there. Furthermore, if neuronal ATP were made using oxidative phosphorylation fuelled by astrocyte-derived lactate under all circumstances, then blocking LDH would inhibit the rise in oxygen consumption evoked by stimulating neuronal activity, but in brain slices blocking LDH has no such effect (Hall et al., 2012). It may be asked why the effect of an astrocyte-selective inducible deletion or knock-down of MCTs or LDH has not yet been reported (as has been performed for oligodendrocyte-axon energetic interactions (Lee et al., 2012)), as an incisive test of the idea that lactate trafficking from astrocytes to neurons is crucial for neuronal function. In fact when this was done for MCT1 in astrocytes or MCT2 in neurons (Suzuki et al., 2011), although it inhibited long-term memory, it had no effect on memory acquisition or short-term memory, arguing against an obligatory role for lactate transport via MCT1 and MCT2 to power neuronal function on a rapid time scale (but see below).

1.2.13 Astrocytes and long-term energy reserves

Conversion of glucose to glycogen in astrocytes provides a limited reserve of energy, which may be important for sustaining neuronal function in

periods of intense energy use. This may occur during long-term term memory formation, since this is inhibited by preventing glycogenolysis or MCT-mediated transfer of lactate to neurons (Suzuki et al., 2011). However, estimates from experiments blocking ATP synthesis suggest that glycogen can sustain neuronal function for only a few minutes (even in brain slices where energy use is reduced compared to the *in vivo* situation) (Allen et al., 2005). A more significant long-term contribution of astrocytes to brain energetics lies in the fact that they take up over 90% of the glutamate released as a neurotransmitter - a molar amount comparable to the amount of glucose used by the brain (Marcaggi & Attwell, 2004). If this glutamate were lost to the blood, then it would be necessary to approximately double the glucose supply to the brain in order to provide carbon skeletons for glutamate synthesis, in addition to the glucose needed to make ATP.

1.2.14 The role of endothelial cells in neurovascular coupling

To permit co-ordinated dilation of both downstream and upstream vessels during hyperaemic responses (whilst avoiding deleterious 'flow steal' from interconnected territories), it is necessary for local neuronal signals to be conveyed to upstream arterioles remote from the area of neuronal activation (Segal, 2015). It has been proposed that local vascular responses to neuronal activity are conducted retrogradely along blood vessels to recruit larger pial arterioles upstream, rather than brain-derived vasoactive factors reaching pial arterioles by diffusion through the subarachnoid space (Iadecola, 1993; Ngai & Winn, 2002; Woolsey & Rovainen, 1991). There is increasing evidence that the endothelium, which can generate powerful vasoactive agents (e.g. NO, prostanoids and endothelin) is not only capable

of regulating blood flow in response to chemical and mechanical signals (e.g. blood pressure), but also plays a role in the transmission of neuronal activity to upstream vessels (Iadecola, 2017). Recently, it was demonstrated that a highly localised endothelial lesion in a single somatosensory pial arteriole prevented vasodilation (following somatosensory activation) being conducted beyond that precise location. Moreover, wide-field endothelial disruption in pial arteries was shown to significantly attenuate the haemodynamic response to neuronal activity following somatosensory stimuli, particularly the early, rapid increase and peak in blood flow (Chen et al., 2014).

Propagation of vasomotor signals along the endothelium of the cerebral vasculature is probably initiated by activation of inwardly rectifying potassium (K_{IR}) channels to generate a hyperpolarization (Longden et al., 2017) rather than activation of Ca^{2+}-activated potassium (K_{Ca}) channels (which drive endothelial vasomotor signal propagation in systemic vessels (Segal, 2015)). Cerebral capillary endothelial cells are exquisitely sensitive to K^+, which is generated during neuronal activity when neurons are depolarised and released from astrocyte end feet when a rise in astrocyte $[Ca^{2+}]_i$ opens K^+ channels. A rise in $[K^+]_o$ triggers endothelial cell hyperpolarisation, a vasodilatory signal, by increasing the conductance of inward rectifier K^+ channels. This hyperpolarization then spreads through the endothelial cell, and is conducted (at a speed of 2 mm/second) to penetrating arterioles. The voltage spread reflects ionic currents travelling though endothelial cell gap junctions, and from endothelial cells to arteriolar smooth muscle cells through myoendothelial junctions (Longden et al., 2017; Segal, 2015).

1.2.15 Control of cerebral blood flow by arterioles

To increase blood flow, signals reflecting neuronal activity, whether arriving at the vasculature directly, via astrocytes or through hyperpolarising endothelial signals, must engage the effectors of the vasomotor response: arteriolar smooth muscle cells and capillary pericytes. Smooth muscle cells (SMCs) (classically regarded as the primary mechanical apparatus involved in hyperaemia) wrapped around resistance vessels are capable of contracting and relaxing in response to a wide range of vasoactive agents, as well as to changes in intra-luminal pressure, which alters vessel diameter and resistance to flow (Cohen et al., 1996; Cohen et al., 1997; Iadecola, 2017; Koller & Toth; 2012). The contractile state of SMCs is dependent upon the interplay between their membrane potential, intracellular Ca^{2+} and Ca^{2+}-sensitivity of the contractile apparatus, which ultimately controls the interaction of contractile proteins (Cipolla, 2010; Iadecola, 2017; Longden et al., 2017). Whilst it was previously believed that cerebral blood flow was regulated solely by pre-capillary arterioles (because capillaries lack a continuous smooth muscle wall), emerging evidence suggests that a subgroup of capillary pericytes contain smooth muscle actin, are contractile and also play a major role in controlling CNS blood flow in health and disease (Biesecker et al., 2016; Hall et al., 2014; Kisler et al., 2017; Li et al., 2016; Mishra et al., 2016; Nehls & Drenckhahn, (1991); Peppiatt et al., 2006; Winkler et al., 2011; Yemisci et al., 2011).

1.2.16 Capillary pericytes

Pericytes are isolated, multi-functional, potentially contractile cells apposed to capillaries, which play a crucial role in angiogenesis, blood-brain barrier preservation, glial scar formation and the generation of pleuripotent

cells (Armulik et al., 2010; Dore-Duffy et al., 2006; Göritz et al., 2011; Lindahl et al., 1997). Their presence was first described by Carl Josef Eberth in 1871 and two years later by Charles-Marie Benjamin Rouget, who described them as contractile cells surrounding the endothelial cells of small blood vessels. In 1923, Zimmerman termed them 'pericytes' because of their peri-endothelial location (Eberth, 1871; Krueger & Bechmann, 2010; Rouget, 1873; Zimmerman, 1923).

In the central nervous system, pericytes (together with vascular smooth muscle cells) are thought to originate from the ectoderm-derived neural crest (Armulik et al., 2011). Pericyte proliferation, maturation and recruitment to, and stabilization of the microvasculature is reliant on paracrine and juxtacrine signalling between pericytes and endothelial cells (Armulik et al., 2005). Briefly, pericyte recruitment to vessels is dependent on platelet derived growth factor receptor β (PDGRFβ) secreted from endothelial cells binding to the PDGRFβ receptors expressed on the surface of developing pericytes. Mice lacking PDGRFβ or its receptor exhibit pericyte deficient vessels which leads to microvascular haemorrhage and neonatal death (Levéen et al., 1994; Soriano, 1994; Lindahl et al., 1997; Armulik et al., 2011). Other pathways implicated in pericyte recruitment to the vasculature include the angiopoietin/TIE pathway (Armulik et al., 2011), the stromal derived factor 1-a (SDF-1α)/CXCR4 axis (Song et al., 2009), heparin-binding epidermal growth factor (HB-EBF) signalling through EGF receptors (ErbB) (Iwamoto et al., 2003; Nanba et al., 2006), and sonic hedgehog (Shh) signalling (Passman et al., 2008; Lamont et al., 2010).

To distinguish them from several other cell types populating the

periendothelial compartments of blood vessels (vascular smooth muscle cells, fibroblasts, macrophages), pericytes are defined or described using a combination of criteria including location, morphology and gene/protein expression pattern. They may be identified by their expression of platelet derived growth factor receptor β (PDGRFβ) (Lindahl et al., 1997; Winkler et al., 2010) and of neural/glial antigen 2 (NG2) (Huang et al., 2010) which is a co-receptor for PDGFβ. Other examples of markers (surface antigens) used to identify pericytes include CD13 (alanyl (membrane) amino peptidase) (Kunz et al., 1994) α-SMA (alpha-smooth muscle actin) (Nehls and Drenckhahn, 1993) and desmin (Nehls et al., 1992), although it is important to appreciate that there is no known pericyte-specific marker (Armulik et al., 2011). In a recent paper, the Nissl dye Neurotrace showed promise as a new tool to study pericytes (or subtypes thereof) (Damisah et al., 2017), but other approaches are still needed to reliably phenotype mural cells (Iadecola, 2017).

Pericytes are spatially isolated cells with a bump-on-a-log morphology (see Fig. 1.4), present on the outside of capillaries, and are enveloped by the vascular basement membrane (as confirmed by electron microscopy). They possess a prominent round nucleus which is distinguishable from the cigar shaped nucleus of endothelial cells. (Dore-Duffy and Cleary, 2011). Pericyte density along the vasculature varies between different organs but microvessels in the central nervous system are thought to have the greatest pericyte coverage with a 1:1 - 1:3.1 ratio between endothelial cells and pericytes. This provides an approximate 30% coverage of the abluminal surface (Sims, 1986; Mathiiesen et al., 2010; Armulik, 2011). For neocortical

capillaries in postnatal day 21 rats the pericyte soma density was found to be 2.2±0.2 per 100μm of capillary length (Hall et al., 2014).

Pericytes differ in their morphological characteristics and gene/protein expression depending on their position on the microvasculature. The location-specific morphology and protein expression of pericytes was recently highlighted by Hartmann *et al.* (2015) using two Cre-recombinase driver mouse lines, one driven by the promoter for the NG2 proteoglycan and the other by the promoter for PDGFRβ. They demonstrated that the single smooth muscle cell layer on arterioles is succeeded by 'hybrid smooth-muscle pericyte cells' on pre-capillary arterioles which interlock with 'mesh-pericytes' at the arteriole-capillary interface (a point of transition where immunostaining delineated α-SMA rich arterioles and α-SMA-poor capillaries). The hybrid smooth-muscle pericyte cells strongly express α-SMA, have a protruding ovoid cell body, are elongated in comparison to smooth muscle cells and enveloped the entire endothelium. Mesh pericytes on the capillary side of the arteriole-capillary interface possessed mesh-like processes which enwrap the vessel and exhibit much smaller amounts of α-SMA. In the middle of the capillary bed, pericytes exhibited long processes that spanned the microvasculature in single strands or pairs which twist in a helical fashion. On post-capillary venules, mesh pericytes became more prevalent again, before giving way to venular pericytes which display a stellate morphology (see Fig. 1.5). Other investigators have also shown that pericytes with more circumferential processes at the arteriolar end of the capillary bed express more smooth muscle α-actin than those in the middle of the capillary bed, but mid-capillary pericytes have also been shown to

express α-SMA (Hill et al., 2015; Bandopadhay et al., 2003).

The topographically-dictated diversity of perictye morphology and gene expression likely reflects the requirement for pericytes to perform disparate functions along the continuum of the microvasulature. Pericytes with circumferential processes located towards the arteriolar side of the capillary bed express α-SMA and appear suited to perform a contractile function (Grant et al., 2017). Pericytes with long, thin processes extending longitudinally and expressing less α-SMA (located in the middle of the capillary bed) may have a role in maintaining the blood-brain barrier and, in concert with astrocytes, may play a key role in coordinating neurovascular coupling (see below). Potentially, however, pericytes extending longitudinal processes may still be able to alter blood flow by controlling the stiffness of the capillary wall and regulating its deformability by passing red blood cells (O'Farrell et al., 2017). Pericytes located on the venular side of the capillary bed may have a primary role in regulating the entry of immune cells across the blood-brain barrier (Attwell et al., 2015).

Given the fact that some pericytes express little or no α-smooth muscle actin, it has been suggested that γ-actin might mediate the contraction of some pericytes (Grant et al., 2017). Although there is no information on this for CNS pericytes, recent work found that cardiac pericytes across the capillary bed commonly possess γ-smooth muscle actin, as well as β -smooth muscle actin, in addition to α-smooth muscle actin which is found mainly in pericytes populating the arteriolar end of the capillary bed (DeNofrio et al., 1989; O'Farrell et al., 2017).

1.2.17 Control of cerebral blood flow by capillary pericytes

A major theme of this thesis is the control of cerebral blood flow by pericytes both physiologically and in pathology. In normal physiological conditions, alterations of pericyte tone in response to neuronal activity control capillary constriction and dilation to regulate cerebral blood flow (Peppiatt et al., 2006; Fernández-Klett et al., 2010; Hall et al., 2014). Moreover, it was shown that most of the noradrenergic neurons from the locus coeruleus that terminate near the brain vasculature, terminate nearer to capillaries than arterioles, suggesting that these neurons may signal to capillaries, as well as arterioles, to alter blood flow (Cohen et al., 1997).

Pericytes on neocortical and cerebellar capillaries have been shown to undergo sustained constriction in response to application of noradrenaline *in vitro* (mimicking its release from the locus coeruleus *in vivo*), while application of glutamate, following noradrenaline-evoked constriction, leads to pericyte relaxation and capillary dilation (in some instances, dilation occurs without the requirement for pre-exposure to noradrenaline) (Hall et al., 2014). The pathways by which noradrenaline and glutamate alter pericyte tone *in vivo* remain incompletely understood, but it has been shown *in vitro* that resting pericyte tone may be sustained by noradrenaline and that pericyte dilation is dependent on two particular downstream effects of glutamate release: the generation of prostaglandin E_2 (PgE_2) by astrocytes (see above) and production of nitric oxide to block synthesis of the vasoconstrictor 20-HETE (Hall et al., 2014; Mishra et al., 2016; Peppiatt et al., 2006). Pericyte tone has been shown *in vitro* to be dependent on intracellular [Ca^{2+}] changes: pericytes contract in response to intracellular [Ca^{2+}] rises (Wu et al., 2003; Kamouchi et

al., 2004), with calcium influx likely to occur via L-type Ca^{2+} channels, agonist activated Ca^{2+} permeable channels and capacitative Ca^{2+} entry pathways (Kamouchi et al., 2004). It has also been demonstrated that electrical stimulation-evoked constriction of retinal perictyes is abolished in the absence of extracellular Ca^{2+}, supporting the premise that pericyte constriction is dependent upon Ca^{2+} influx (Peppiatt et al., 2006)

In vivo experiments with 2-photon imaging of mouse somatosensory cortex show that, in response to sensory input (electrical stimulation of the whisker pad), first and second order capillaries consistently dilate before penetrating arterioles (more than a second earlier), indicating that pericyte relaxation generates the initial phase of cerebral vessel dilation, and capillary dilation is not a passive response to increased blood pressure following arteriolar dilation. Additionally, resting capillary diameter was found to be greater in capillary regions populated by pericyte somata than in regions lacking pericyte somata and, following sensory stimulation, capillary segments apposed by pericytes dilated more than segments devoid of pericytes (Hall et al., 2014). Dilating capillaries may also relay a hyperpolarizing, vasodilatory signal to arterioles, mediated by gap junctions between endothelial cells, to further increase blood flow (Iadecola et al., 1997; Peppiatt et al., 2006; Puro, 2007).

The observation that hyperaemia is generated at vessels downstream of penetrating arterioles was further confirmed by Hill *et al* (2015) who investigated blood flow regulation at various locations along the vascular tree, in living transgenic mice with pericytes labelled by fluorescent proteins with

expression driven by promotors for NG2 and α-SMA. They showed that optogenetic activation of a light gated proton channel (channelrhodopsin 2, ChR2) specifically in NG2-expressing cells (smooth muscle cells and cortical pericytes), or whisker stimulation, or cortical spreading depolarization, produced diameter changes of microvessels smaller than 10 μm in diameter, with branch orders ranging from first to third after the penetrating arteriole (i.e. vessels normally called capillaries). They also demonstrated that only microvessels with mural cells that had a circumferential morphology and expressed α-SMA have the capacity to regulate blood flow. Contrary to convention, they defined these mural cells (even when spatially isolated) as smooth muscle cells, and their associated microvessels, regardless of branch order, as arterioles. Because of this shift in nomenclature, capillary pericytes, re-defined as mural cells with non-circumferential processes and no expression of α-SMA, are inevitably non-contractile and unable to directly regulate blood flow. If differences of nomenclature are set aside however, the findings of Hill *et al.* strongly complement those of earlier work rather than contradicting them.

Under normal physiological conditions therefore, capillary pericytes have important dual roles in regulating cerebral blood flow. First, they detect increased metabolic demand in areas of neuronal activity and second, they effect a response by dilating capillaries to increase blood flow to those areas, whilst possibly triggering arteriolar dilation to further augment cerebral blood flow.

1.3 Structure and circuitry of the neocortex

In this thesis the role of capillary pericytes in controlling blood flow during ischaemia and in Alzheimer's disease is examined in the neocortex. This section gives an overview of the structure and function of the cortex.

The grey matter of the cerebral cortex in humans is 2-3 mm thick, highly convoluted (such that its surface area is several hundred square centimetres) and made up of six distinct layers containing hundreds of different neuronal types and a diverse range of glia. Within it, neurons come in 2 main varieties. Glutamatergic pyramidal neurons, so called because of their prominent, typically superficial-pointing apical dendrites, are excitatory in nature. GABA (γ-aminobutyric acid)-containing inhibitory neurons (also called local circuit neurons or interneurons), possess a more diverse morphology, e.g. basket cells with characteristic axonal ramifications forming 'baskets' around cell bodies and chandelier cells which make multiple strings of contact ('chandeliers') around axonal initial segments. Pyramidal neurons extend axons locally as well as to distant intracortical, subcortical and subcerebral targets. As pyramidal axons project from the grey matter, they coalesce to form the cortical white matter, whereas axons from inhibitory neurons remain confined to the grey matter and usually make only short-range and local connections (Molyneaux et al., 2007; Shipp, 2007).

Importantly, there is regional specialisation of function across the surface area of the cortex, in so called 'cortical regions' (e.g. Broca and Wernicke language related areas, primary motor cortex, primary visual cortex). A cortical region simply represents an area where neurons which perform similar roles can communicate with each other more easily and efficiently because they are in immediate proximity to one another. During

cortical recordings, it has been shown that neurons in a radial column (perpendicular to the cortical surface) share broadly similar response properties when input to that column is activated; their receptive fields may all be located on the same patch of skin, for example. Moreover, moving through sensory areas of the cortex parallel to the cortical laminae, it was demonstrated that neighbouring columns have neighbouring receptive fields, thus giving rise to a topological cortical map of the relevant sensory surface. The cortical regions are impressively interconnected with each other and with subcortical structures, and the layering of the cortex (which is remarkably uniform over the expanse of the sheet) represents the radial organisation of these input and output connections. In sum, the cerebral cortex is a cellular sheet with extrinsic connectivity, composed of inter-lamina and inter-regional projection (pyramidal) neurons and local circuit neurons (interneurons), organised in horizontal layers, which are intersected by radial stereotypically interconnected columns (Rakic, 2009; Shipp, 2007).

By convention a neuron ‘belongs’ to the cortical layer in which its body is sited regardless of how many layers its apical and basal dendrites span. The cortex is created ‘inside out’, with nascent pyramidal neurons migrating radially away from the proliferative zone to form layer VI first and layer II last (layer I in adults is almost devoid of cell bodies). Inhibitory neurons have more diverse origins and migrate tangentially, with some subtypes following an ‘outside-in’ sequence of neurogenesis. The cortical layers are delineated as follows. Layer 1 is the molecular layer and most superficial. It is largely made up of dendritic tufts originating from pyramidal cell bodies located in deeper cortical layers, and terminal axons from the intralaminar thalamic

nuclei. Layer 2 is the outer granular layer and contains glutamatergic stellate cells (these are smaller and less spatially polarised than pyramidal cells, and possess multiple spiny dendrites) and small pyramidal cells. Layer 3, the outer pyramidal layer contains more impressive pyramidal cells and stellate neurons. The inner granular layer- 4 is densely populated by stellate cells, which receive thalamic input connections. Like layer 2, layer 4 receives sensory input, and is thickest in sensory cortical regions e.g. visual cortex. Impulses received by layers 2 and 4 are then transmitted by interneurons to adjacent and superficial and deep layers, and then to appropriate efferent neurons in layer 5, termed the inner pyramidal layer (the main output layer) containing large pyramidal neurons. From layer 5, pyramidal projections are sent to subcortical structures, other cortical regions and the spinal cord. The specialised pyramidal neurons of layer 6, the innermost layer, project mainly to the thalamus (Fitzgerald et al., 2007; Ropper & Brown, 2005; Shipp, 2007).

1.4 Cerebral ischaemia, stroke, the no-reflow phenomenon and the role of capillary pericytes

Ischaemia is an insufficient supply of blood to an organ or tissue, usually as a result of a narrowing or blockage of an artery. If severe, the inadequate supply of blood, oxygen and glucose can result in damage to the tissue. Cerebral ischaemia is a common consequence of atherosclerotic cardiovascular disease and, as discussed above (in section 1.2), brain tissue relies on a continuous supply of energy in the form of oxygen and glucose which, if interrupted (even for only a brief period), sets in motion a complex sequence of pathophysiological events including cellular excitotoxicity, inflammation and programmed cell death (Dirnagl et al., 1999). Within a few

minutes of cerebral ischaemia, the core region supplied by the compromised blood supply is fatally injured and undergoes necrotic cell death. The infarcted cerebral tissue is, however, surrounded by an area that is less severely affected - the ischaemic penumbra. The penumbral region remains viable for a much longer period (hours to days), and may be salvageable, if blood flow and energy supply can be restored within hours of the onset of blood flow reduction (Dimagl et al., 1999; Broughton et al., 2009; Woodruff et al., 2011).

A component of this thesis is dedicated to experiments aimed at preventing pathological responses of pericytes after ischaemia. In this section I will therefore discuss the pathobiology of brain ischaemia, clinical intervention for stroke with thrombolysis/mechanical clot retrieval and the role of capillary pericytes in stroke and its associated no-reflow phenomenon.

1.4.1 Pathobiology of brain ischaemia

When the supply of oxygen and glucose to brain cells is severely reduced during cerebral ischaemia, ATP production from oxidative phosphorylation ceases (after a brief period when ATP is made from glycogen-fuelled glycolysis). Consequently, ATP-dependent ion pumps such as Na^+/K^+-ATPases (which maintain a high $[Na^+]_o$ and $[K^+]_i$) fail, leading to a breakdown in the maintenance of these essential ion concentration gradients (Lipton, 1999). Ca^{2+}-ATPase pumps are similarly affected leading to a rise in $[Ca^{2+}]_i$ (Dimagl et al., 1999).

With the rise in $[Na^+]_i$ and $[K^+]_o$, neurons and glia depolarise, activating somatodendritic and pre-synaptic voltage-dependent Ca^{2+} channels, which

initially trigger exocytotic release of glutamate into the extracellular space (Dirnagl et al., 1999), but this ceases after a few minutes. Nevertheless, the concentration of glutamate in the extracellular space rises to a concentration of ~100 μM during ischaemia (Phillis et al., 1996; Globus et al., 1991). This is primarily due to the reversed operation of glutamate transporters: reversal of glutamate uptake occurs when ischaemia causes run down of ionic gradients (Rossi et al., 2000). This rise of glutamate concentration plays a key role in generating the "anoxic depolarization" of neurons and glia to ~-20 mV, which abolishes information processing in the central nervous system within a few minutes of the onset of ischaemia. This occurs via a positive feedback loop, where energy lack raises $[K^+]_o$ and $[Na^+]_i$ and depolarizes cells, releasing glutamate, which acts on its receptors to generate further depolarization and K^+ release (Rossi et al., 2000). Cytotoxic oedema develops during the run down of ionic gradients when water passively follows Na^+ and Cl^- entering neurons via ion channels and transporters during glutamate receptor overactivation (as the influx of Na^+ and Cl^- is larger than the efflux of K^+) (Dirnagl et al., 1999; Simard et al., 2007).

Activation of NMDA receptors and metabotropic glutamate receptors contributes further to Ca^{2+} overload, and the intracellular calcium concentration rises from its normal level of 20-100 nM to ~2.5 μM during ischaemia (Lipton, 1999). Intracellular calcium overload initiates a series of cytoplasmic and nuclear events that are profoundly injurious to brain tissue, such as activation of proteolytic enzymes that degrade cytoskeletal proteins, activation of phospholipases which break down membranes and trigger free-radical production, and activation of endonucleases that degrade genetic

material, thus causing cell membrane, mitochondrial and DNA damage (Dimagl et al., 1999). Within the core of the ischaemic region, excitotoxic mechanisms are profound, and lead to rapid cell necrosis caused by cell swelling. Within the ischaemic penumbra, excitotoxic mechanisms are not immediately lethal, and trigger more-delayed detrimental mechanisms. These include tissue inflammation mediated predominantly by microglia (but also by endothelial cells and astrocytes) and blood-brain barrier breakdown with accompanying vasogenic oedema. Ultimately, the rise of cytoplasmic $[Ca^{2+}]_i$ leads to Ca^{2+} entry into mitochondria, causing a release of the respiratory enzyme cytochrome C into the cytoplasm, where it activates caspase enzymes to trigger apoptotic cell death (Bramlett & Dietrich, 2004; Broughton et al., 2009; Dimagl et al., 1999; Woodruff et al., 2011).

1.4.2 Stroke

The definition of stroke is clinical and based on the sudden onset of loss of focal neurological function lasting more than 24 hours (or any duration if CT or MRI imaging show an ischaemic or haemorrhagic lesion relevant to the symptoms). It reflects infarction or haemorrhage in the relevant region of the central nervous system (Hankey, 2017; Sacco et al., 2013). A transient ischaemic attack is now defined as a focal dysfunction of less than 24 hours with no evidence of infarction on imaging (Sacco et al., 2013).

Stroke is the second largest cause of global mortality (accounting for approximately 10% of 53 million deaths worldwide in 2010) (Feigin et al., 2014) and is a leading cause of adult disability in the United Kingdom (Townsend et al., 2012) and United States (Roger et al., 2011). In the UK

alone, there are approximately 152,000 strokes per year (Townsend et al., 2012) and around half of survivors are left dependent for activities of daily living. On the modified Rankin Scale [mRS], ~40% of stroke survivors are disabled (mRS score 3–5) between 1 month and 5 years after stroke (with 20% classed as disabled before the stroke) (Luengo et al., 2013; RCP National Sentinal Stroke Clinical Audit, 2010). Case fatality rates following stroke are approximately 15% at 1 month, 25% at 1 year and 50% at 5 years (Luengo et al., 2013).

Approximately 87% of strokes worldwide are ischaemic in nature (Wechsler, 2011): ischaemic stroke describes arterial occlusion by a thrombus (formed *in situ* or following embolisation), which reduces cerebral blood flow sufficiently to cause cellular injury and ultimately, tissue infarction (see section 1.4.1) (Fisher, 1997; Lo et al., 2003; Wechsler, 2011). Aetiological subtypes of ischaemic stroke are classified according to the TOAST classification (a categorisation system of subtypes of ischaemic stroke mainly based on aetiology that was developed for multicentre clinical trials), the ASCOD phenotyping system (A: atherosclerosis; S: small vessel disease; C: cardiac pathology; O other cause; D; dissection) and the Causative Classification System (Adams et al., 1993; Amerenco et al., 2013; Ay et al., 20107; Hankey, 2017). The aetiology of one third of stroke cases remains unknown, of which a subgroup is now defined as having embolic strokes of undetermined source (Hankey, 2017; Hart et al., 2014).

Known risk factors for ischaemic stroke are hypertension, hypercholesterolaemia, carotid stenosis and atrial fibrillation. Likely causal risk factors are cigarette smoking, excess alcohol consumption and insulin

resistance/diabetes mellitus. Other modifiable risks factors include physical inactivity, obesity, psychological stress, high saturated fat intake and a low nutrition diet (Hankey, 2017), and there are also some rare, highly penetrant gene mutations that cause young-onset stroke

In experimental models of stroke, the duration and the severity of ischaemia have been shown to determine whether irreversible damage occurs (Jones et al., 1981). Treatments aimed at restoring blood flow as quickly as possible following the onset of symptoms should therefore have a beneficial impact in stroke and, as studied in this thesis, preventing deleterious changes in pericyte function could play an important role in this.

From the 1990s onwards, randomised controlled thrombolysis trials have shown that the probability of a favourable outcome is increased by treatment of patients with intravenous tissue plasminogen activator (rt-PA) to disrupt the culprit thrombus within 3 hours (The National Institute of Neurological Disorders and Stroke rt-PA Stroke Study Group, 1995) or up to 4.5-6 hours (Hacke, 2008; IST3 Collaborative group, 2011) of stroke onset. Meta-analysis of thrombolysis trial data has shown that rtPA, 0.9 mg/kg administered within 4.5 hours of ischaemic stroke increases the odds ratio of no disability at 3-6 months by a third without having an effect on mortality. This treatment, however, is associated with an increased risk of symptomatic intracerebral haemorrhage (Emberson et al., 2014). Furthermore, over half of patients treated with alteplase (rt-PA) show a lack of recovery, which may be attributable to inadequate reperfusion, or reperfusion occurring too late, to prevent tissue infarction (Wechsler, 2011; von Kummer, 2009). Recently, analysis of individual patient data pooled from five randomized controlled

clinical trials of mechanical thrombectomy showed that endovascular thrombectomy using stent-retriever device technology in conjunction with rt-PA treatment is highly beneficial, as compared to rt-PA alone, in patients with intracranial internal carotid or middle cerebral artery occlusion presenting within 6 hours of stoke onset. The rate of angiographic revascularisation at 24 hours and functional independence at 90 days is doubled without increasing the risk of symptomatic intracerebral haemorrhage or all-cause mortality. (Badhiwala et al., 2015; Berkhemer et al., 2015; Campbell et al., 2015; Goyal et al., 2015; Goyal et al., 2016; Saver et al., 2015; Jovin et al., 2015). Encouragingly, in patients with imaging evidence of occlusion of the intracranial internal carotid artery or the first segment of the middle cerebral artery, and with a clinical deficit disproportionate to their imaged infarct volume, mechanical thrombectomy significantly improved their level of disability at 90 days compared with standard stroke care alone (Nogueira et al., 2017). This was the case for thrombectomy performed 6-24 hours after the onset of stroke, including on those who woke up with new stroke symptoms where the time of onset cannot be known.

1.4.3 The role of pericytes in the no-reflow phenomenon in the brain

Despite the significant advances in treatment and outcomes for patients with stroke, it has been demonstrated that, even after re-opening of a blocked artery (achieved for example by either rt-PA or endovascular thrombectomy) following which there is a brief increase of local blood flow (reactive hyperaemia), there is a long-lasting decrease of cerebral blood flow by about 50% (the ‘no-reflow’ phenomenon) (Hauck et al., 2004). As long ago as the 1950s, it was appreciated that cerebral ischaemia may modify the state of the

blood or injure blood vessels and thus impair the return of blood flow, compounding the initial ischaemic damage to the parenchyma (Crowell et al., 1955; Kowada et al., 1968; Neely and Youmans, 1963). In the late 1960's it was demonstrated that obstruction of the arterial supply to the rabbit brain, followed by reperfusion, leads to widespread non-perfusion of stretches of arterioles and capillaries, as revealed with the addition of a contrast agent. Capillary occlusion was not always complete, but often capillary stenosis-blocked the passage of red blood cells (Majno et al., 1967). It was postulated that the obstacle producing circulatory impairment following cerebral ischaemia resulted from either intravascular plugging by fibrin, red blood cells, platelets or leucocytes adherent to the capillary wall, or a reduction of the vascular lumen (possibly from intraluminal endothelial cell swelling or perivascular astrocyte end-feet swelling), or a combination of the two (Ames et al., 1968; Majno et al., 1967). The no-reflow phenomenon discovered in the brain was also observed in other organs such as the kidney, the heart and the skin, and was thought to result from similar pathophysiological mechanisms (Flores et al., 1972; Kloner et al., 1974; Summers & Jamison, 1971; Willms-Kretschmer & Majno, 1969).

It has been shown that capillary pericytes contract and constrict capillaries in pathological states following ischaemia, following spinal cord injury and during epilepsy (Hall et al., 2014; Leal-Campanario et al., 2016; Li et al., 2017). Furthermore, during ischaemia, pericytes rapidly die in their contracted state (i.e. in rigor) to impede subsequent capillary dilation. Under strongly ischaemic conditions, it has been demonstrated *in vitro* that neocortical grey matter and cerebellar white matter capillaries are constricted

by pericytes within ~15 minutes and pericytes die in rigor within ~40 min (Hall et al., 2014). *In vivo*, pericytes have been shown to constrict following middle cerebral artery occlusion (MCAO) (Yemisci et al., 2009) and die following 90 min of MCAO (followed by 22.5 hours recovery) (Hall et al., 2014). Again, disregarding superficial differences of nomenclature, Hill et al. (2015) have also demonstrated focal constrictions by microvascular mural cells, expressing α-SMA and NG2 at the arteriole-capillary interface, following MCAO for 90 min. These focal constrictions caused red blood cell (RBC) perfusion block in downstream capillaries (Hill et al., 2015). An increase in pericyte [Ca^{2+}], following ion pump inhibition by ATP depletion, may partly explain why pericytes constrict in ischaemia. Blockade of AMPA/kainate, NMDA and ionotropic glutamate receptors significantly reduced pericyte death in brain slices subjected to simulated ischaemia (fixed and labelled with NG2 and/or isolectin B4 to identify pericytes: Hall et al., 2014), suggesting that glutamate excitotoxicity plays a role in pericyte death in ischaemia (although patch-clamp data suggest these receptors are not on pericytes themselves). Removal of external calcium also significantly reduced pericyte death, as did (to a much smaller extent) blockade of NO production. O_2^{*-} scavenging or blockade of metabotropic glutamate receptors, action potentials or production of 20- HETE did not reduce pericyte death (Hall et al, 2014).

Contraction and subsequent death in rigor of pericytes during cerebral ischaemia may therefore help to explain the long-lasting capillary narrowing and trapping of leukocytes and red blood cells that underlies the no-reflow phenomenon (O'Farrell & Attwell, 2014). Indeed, recent work has suggested

that pericytes play a similarly important role in contributing to the no-reflow phenomenon in the heart. Occlusion of a rat coronary artery, followed by reperfusion, blocked 40% of cardiac capillaries and halved perfusion blood volume in the affected region. Capillary blockages were strongly co-localised with pericytes, where capillary diameter was reduced by 37%. Additionally it was shown that treatment with adenosine, a known pericyte relaxant, after the period of ischaemia decreased capillary block by a quarter and increased perfusion volume by 57% (O'Farrell et al., 2017).

1.5 Alzheimer's Disease

First described in 1906 by the Bavarian psychiatrist Alois Alzheimer (Alzheimer, 1906), Alzheimer's disease (AD) is the most common form of dementia - a term encompassing a range of neurological disorders characterised by memory loss and cognitive impairment (Winblad et al., 2016). AD accounts for 50-70% of dementia cases and represents a major public health concern that has been identified as a research priority (Querfurth and La Ferla, 2010).

In 2015 there were an estimated 47 million people worldwide with dementia, a figure predicted to triple by 2050 (Prince et al., 2015; Wimo and Prince, 2010). The estimated cost of dementia to the UK is £23 billion annually (www.alzheimers.co.uk, 2016) and in 2015 alone dementia was estimated to have cost the world economy US$818 billion, a figure that will continue to rise as the number of people with dementia rises (Prince et al., 2015). Unsurprisingly, it has been stated that dementia is the greatest global challenge for health and social care in the 21st century (Livingstone et al., 2017).

A component of this thesis is dedicated to experiments aimed at understanding the early vascular effects of Alzheimer's disease, in particular those that occur at the capillary level. In this section I will therefore discuss the pathobiology of Alzheimer's disease and the possible role of vascular changes in it.

1.5.1 Epidemiology of Alzheimer's disease

AD is characterised neuropathologically by the accumulation of aggregated β-amyloid (Aβ) in extracellular plaques and blood vessels and intracellular neurofibrillary tangles comprised mainly of hyperphosphorylated tau (neuritic plaques, neurofibrillary tangles and neuropil threads), together with extensive neuronal damage and loss (Braak and Braak, 1991). Following a pre-symptomatic phase spanning decades (Bateman et al., 2012), AD causes a progressive deterioration of memory and other cognitive abilities, with sufferers becoming doubly incontinent, bedbound and stripped of the very essence of themselves prior to death within 3 to 9 years of diagnosis (Hardy and Allsop, 1991; Huang and Mucke, 2012). The relatives and carers of patients with AD have to cope with seeing a family member or friend become ill and decline whilst responding to their needs, increasing dependence and changes in behaviour (Livingstone et al., 2017). Advancing age is the strongest risk factor for AD and the incidence of the disease doubles every 5 years after the age of 65 years of age (Querfurth and La Ferla, 2010). Post-mortem studies suggest however, that the prevalence of AD decreases beyond the age of 98 years of age and the development of AD, like Parkinson's disease, is not an inevitable consequence of ageing (Nelson et al., 2011).

Epidemiological studies have shown that known risk factors for vascular diseases, including hypertension, diabetes, hypercholesterolaemia, obesity, smoking and the apolipoprotein-ε4 genotype, are also important risk factors for sporadic AD (Barnes and Yaffe, 2011), suggesting that their pathogenic mechanisms are connected (Kalaria, 2000). Indeed, pathological specimens from many patients with AD show evidence of significant microvascular disruption including endothelium, pericyte and vascular smooth muscle loss and degeneration, a reduction in capillary density, a thickened vascular basement membrane and a loss of tight junctional and adherens junctional proteins which compromise the blood brain barrier BBB and allow the accumulation of plasma proteins in the brain (Zlokovic, 2011). Other potentially modifiable risk factors for AD include head injury, hearing loss, depression, low educational attainment and physical inactivity (Barnes & Yaffe, 2011; Livingstone et al., 2017; Mortimer1991; Norton et al., 2014; Plassman et al., 2000).

1.5.2 Mechanisms underlying Alzheimer's disease

Over 20 years ago, the amyloid cascade hypothesis postulated Aβ as the causative agent in AD pathology and that neurofibrillary tangles, cell loss, vascular damage and dementia follow as a direct result of its deposition (Hardy and Higgins, 1992). Whilst it is still widely held that excessive Aβ generation is the primary initiator of AD pathogenesis, the mechanisms by which Aβ causes synaptic failure (Selkoe, 2002) and neuronal death have yet to be fully elucidated. It is now thought likely that Aβ initiates a complex network of downstream pathological processes to produce the neuropathological and clinical syndrome that is AD (Musiek and Holtzman,

2015). Furthermore, it is now recognised that small assemblies of a few Aβ molecules, rather than the histologically visible plaques, are the likely key initiators of the cognitive decline that occurs in AD (Benilova et al., 2012; Heneka et al., 2013; Walsh et al., 2012).

Monomeric Aβ peptides are natural products of metabolism consisting of 36-43 amino acids with a molecular weight of approximately ~ 4kDA produced through sequential proteolytic cleavage of amyloid precursor protein (APP) by β- and γ-secretase. The aspartyl protease β-site APP cleaving enzyme 1 (BACE1), cleaves APP predominantly at a unique site, whereas the γ-secretase complex (a protein complex with presenilin 1 at its catalytic core) cleaves the resulting carboxy-terminal fragment at several sites, with a predilection for positions 40 and 42, leading to formation of $A\beta_{1–40}$ and $A\beta_{1-42}$ peptides, which are the major species produced in AD (Querfurth and La Ferla, 2010). Alternative processing of APP at the α-site prevents the formation of amyloid β, because the α-site is located within the amyloid β fragment (Querfurth and La Ferla, 2010; Thorlakur et al., 2012). Aβ (particularly $A\beta_{1-42}$) spontaneously self-aggregates into multiple physical forms. Oligomeric Aβ (2 to 6 peptides) aggregates form intermediate assemblies (protofibrils) before coalescing further into fibrils (with a so-called cross-β structure where individual strands lie perpendicular to the fibril axis), which then further arrange into β-pleated sheets to form the insoluble fibres of advanced neuritic plaques (Ahmed et al., 2010; Benilova et al., 2012). Together with other proteins implicated in neurodegenerative disease such as tau (Wang and Mandelkow, 2016) and α-synuclein (Luk et al., 2012), aggregated Aβ has the ability to seed normal forms of the protein to initiate

spread of these deposits in a prion-like fashion through the brain (Juanmuktane et al., 2015).

The precise mechanisms underlying the aggregation, deposition and spread of Aβ in AD are not fully understood, but are likely to involve activation of innate immune responses and the NACHT-, LRR- and pyrin- (PYD) domain-containing protein 3 (NLRP3) inflammasome, following Aβ detection by microglial pattern-recognition receptors (the CD36 scavenger receptor and the Toll-like receptor 4(TLR-4) receptor) (Heneka, et al., 2013). (Microglia can also be activated by low nanomolar concentrations of Aβ oligomers before they are deposited as fibrils, in a process that requires the scavenger receptor SR-A and the Ca^{2+}-activated potassium channel KCa: Heneka et al., 2015). The NLRP3 inflammasome comprises NLRP3, the adaptor protein apoptosis-associated speck-like protein containing a CARD (ASC), and the effector caspase-1. Activation of this inflammasome leads caspase-1 releasing highly pro-inflammatory cytokines of the interleukin 1β (IL-1β) family, which have been shown to suppress long-term potentiation in the hippocampus, to impair microglial clearance of Aβ, and to be toxic to neurons (Heneka et al., 2013; Heneka et al., 2015; Lynch, 2014). Moreover, NLRP3 inflammasome activation has been found both in the brains of patients with AD and in the brains of APPSwe/PSEN1dE9 transgenic mice - an AD mouse model where genetic deficiency of NLRP3 or caspase-1 protect against age-related microglial IL-1β production, Aβ-related pathology and cognitive decline (Heneka et al., 2013). Other AD mouse models also show early activation of IL-1β release, suggesting that the NLRP3 inflammasome could play an important role in the progression and spread of Aβ pathology in AD.

This idea has recently garnered further support (Venegas et al., 2017) after it was shown that activating NLRP3 can lead to the formation of ASC helical fibrils (observable as paranuclear specks within microglia) which are released into the intercellular space. Here, microglia-derived ASC specks bind rapidly to Aβ and increase the formation of Aβ oligomers and aggregates, thus acting as an inflammatory-driven seed for Aβ pathology (Lu et al., 2014; Masumoto et al., 1999; Venegas et al., 2017).

It is worth noting however, that whilst a large body of evidence supports Aβ as a key initiator in the pathogenesis of AD, there is a poor correlation both temporally and anatomically between its deposition as plaques, neuronal loss and clinical symptoms in sporadic AD. In contrast, a strong correlation with the onset and progression of disease symptoms and neurodegeneration in AD is found with the levels of Aβ oligomers (Benilova et al., 2012; Heneka et al., 2013; Walsh et al., 2012) and with tau accumulation (Arriagada et al., 1992; Josephs et al., 2008; Musiek & Holtzman, 2015; Williams et al., 2008).

The human genetics of AD make a strong case for Aβ being the primary initiator of the disease. Mutations in genes which encode the Aβ precursor (β-amyloid precursor protein (APP)), or its cleaving enzymes (PSEN1 and PSEN 2 encoding the presenilin 1 and 2 catalytic subunits of the γ-secretase complex respectively) that generate Aβ, are sufficient to cause familial, early onset AD (Bettens et al., 2013). Additionally, individuals with Down syndrome (trisomy 21), who have an extra copy of APP, develop the full neuropathological changes of advanced AD by their fourth or fifth decade

(Hardy and Allsop, 1991). Mutations in APP, PSEN1 and PSEN2 tend to favour increased production of the more aggregation-prone 42-amino-acid form of Aβ ($Aβ_{1-42}$) both in vivo and in vitro (Herrup, 2014) and several APP mutations have been found to increase the propensity of Aβ to aggregate rather than to increase its total production. Furthermore, it was recently discovered that an APP mutation (A673T, an alanine-to-threonine mutation very near the β-secretase cleavage site) that significantly lowers Aβ production is protective against AD, and also protects against cognitive decline in the non-AD population (Thorlakur et al., 2012).

The strongest genetic risk factor linked to sporadic AD - APOE, located on chromosome 19 - has a gene-dose dependent effect on increasing risk and lowering age of onset of the disease. Apolipoprotein E (ApoE) is a polymorphic protein encoded by the APOE gene, with high expression in the human brain (where it is produced predominantly by astrocytes and microglia). There are three common human isoforms, ApoE2, ApoE3 and ApoE4, which differ from one another by a single amino acid substitution. Those carrying a single copy of the APOE ε4 allele (~25% of the population) have an ~4x increased risk of AD, whilst those homozygous for APOEε4 (~2% of the population) carry a ~12x increased risk. The ApoE3 isoform is associated with a decreased risk of AD. ApoE4 has several effects in AD: it may be processed into neurotoxic fragments, and it is thought to act as a chaperone for Aβ which may explain why it strongly modulates Aβ pathology, promoting and exacerbating both the aggregation and deposition of Aβ (Huang and Mucke, 2012; Masters et al., 2015; Musiek and Holtzman, 2015). Additionally, mice that express APOE4 show disinhibition of a cyclophilin A

signalling mechanism in brain capillary pericytes, resulting in microvascular degeneration, leakage of the blood-brain barrier, and neurodegeneration independent of Aβ (see below) (Bell et al., 2012; Scheltens et al., 2016).

Importantly, it has recently been shown that ApoE4 influences tau pathogenesis, neuroinflammation and tau-mediated neurodegeneration independently of Aβ (Shi et al., 2017). These findings build on previous work which demonstrated that ApoE3 (but not ApoE4) is able to bind to a self-binding motif on tau *in vitro* (Strittmatter et al., 1994), that neuronal human APOE4 expression *in vivo* results in tau hyperphosphorylation (Brecht et al., 2004) and that APOE4 has a strong association with levels of CSF tau and phosphorylated tau protein (after correction for the effect of APOE on Aβ levels) in genome-wide association (GWAS) studies (Deming et al., 2017). Using a P301S tauopathy mouse model (which overexpresses 1N4R human tau, leading to tau hyperphosphorylation) on either a human ApoE knock-in (KI) or ApoE knock-out (KO) background, it was shown that P301S/ApoE4 mice have significantly higher brain tau levels and greater somatodendritic tau redistribution by three months of age compared with P301S/ApoE2, P301S/ApoE3 or P301S/ApoE-KO mice (Shi et al., 2017). By nine months, P301S/ApoE4 develop greater brain atrophy and neuroinflammation than PS301S/ApoE2 and P301S/ApoE3 mice while P301S/ApoE-KO mice are mostly protected from these changes. *In vitro* experiments (Shi et al., 2017) showed higher levels of innate immune reactivity of ApoE4-expressing microglia following lipopolysaccharide treatment, and co-culture of P301S tau-expressing neurons with ApoE4-expressing mixed glia (including astrocytes) yielded higher levels of TNF-α and decreased neuronal viability

compared to ApoE2, ApoE3 or ApoE-KO co-cultures. Furthermore, in individuals with a sporadic primary tauopathy (cortico-basal degeneration, fronto-temporal dementia and progressive supranuclear palsy), possession of an APOEε4 allele was associated with more severe regional neurodegeneration, and individuals with symptomatic AD who are positive for Aβ (who usually have associated tau pathology) demonstrate a faster rate of disease progression (Shi et al., 2017).

There are also important APOE associations with cerebral amyloid angiopathy (CAA)-associated vasculopathic changes. CAA is characterised by deposition of Aβ in the walls of leptomeningeal and cortical blood vessels (compromising their integrity), and has a prevalence of approximately 20-49% in non-demented elderly persons and 50-60% in demented elderly persons (Charidimou et al., 2011); it is thought to be responsible for up to a third of all intracranial haemorrhage (ICH) in the elderly (Pezzini and Padovani, 2008) and is the most frequent vascular pathology encountered in AD (Attems et al., 2005). CAA may also lead to ischaemic cerebral injury by altering cerebral blood flow and compromising vessel luminal patency (Brandner, 2011; Charidimou et al., 2011; Smith & Greenberg, 2009).

APOE alleles are the only known genetic risk factors for sporadic CAA. APOE ε4, in both postmortem and clinical series, increases the risk of sporadic CAA related lobar ICH and the number of ε4 alleles relates to clinical severity (Biffi et al., 2010; Charidimou et al., 2011; Greenberg et al., 1995; Premkumar et al., 1996; Verghese et al., 2011). APOE ε2 allele carriers also have an increased risk of CAA-related lobar ICH (Biffi et al., 2010; Charidimou et al., 2011; Nicoll et al., 1997). Both APOE ε2 and ε4

alleles are also associated with a younger age of first ICH, an increased risk of haematoma expansion, a poorer clinical outcome and a higher chance of recurrence (Biffi et al., 2011; Charidimou et al., 2011; Greenberg et al, 1996; Montaner, 2011; O'Donell et al., 2000). Possession of APOE ε2 and ε4 allelic variants together has a compounding effect, and patients with both these alleles have the earliest disease onset and highest risk of early ICH recurrence (Charidimou et al., 2011; Greenberg et al., 1998; O'Donell et al., 2000) .It is thought that the ε2 and ε4 alleles may promote CAA related haemorrhage by distinct mechanisms: ε4 by promoting Aβ deposition and ε2 by inducing structural changes in amyloid laden vessels, making them liable to rupture (Biffi et al., 2011; Charidimou et al., 2011; Montaner, 2011; McCarron et al., 1999; Walker et al., 2000).

Two distinct pathological subtypes of CAA have been described: CAA type 1 or capillary CAA (more closely associated with parenchymal amyloid deposition in AD), is characterised by Aβ in cortical capillaries (with or without involvement of other vessels) and CAA type 2, where Aβ deposits are restricted to leptomeningeal and cortical arteries, arterioles and, rarely, veins (Thal et al., 2002). The APOE ε4 allele is most strongly associated with CAA type 1 while APOE ε2 is more associated with CAA type 2 (Thal et al, 2002). In a recently published neuropathological study of the presence of CAA and its subtypes, and the presence of hemorrhages and infarcts in 284 autopsy cases of demented and non-demented individuals, it was shown that capillary CAA and CAA severity were associated with allocortical microinfarcts, comprising the CA1 region of the hippocampus. Allocortical microinfarcts, capillary CAA and CAA severity were, thereby, found to be associated with

cognitive decline. It was also found that allocortical microinfarcts, CAA severity and capillary CAA were associated with one another and with the development of cognitive decline. Furthermore, AD cases with capillary CAA were shown to develop dementia symptoms not only due to AD-related Aβ plaque and neurofibrillary tau pathology, but also due to hippocampal microinfarcts that were associated with capillary CAA and CAA severity (Hecht et al, 2018).

GWAS studies have enabled the identification of 20 or more genetic loci associated with the risk of AD. Many of these are frequent population polymorphisms (that are of less importance to an individual's risk of developing the disease) that have highlighted the importance of pathways concerned with immune regulation, inflammatory responses, cholesterol, lipid metabolism and endosomal recycling in the pathogenesis of sporadic AD (Karch & Goate, 2015; Scheltens et al., 2016). Novel genome-sequencing approaches have identified rare gene mutations such as those in TREM2, a microglial receptor involved in the removal of Aβ, which greatly increases the risk of developing AD. Genome-wide profiling of gene expression in the brains of patients with sporadic AD suggests the involvement of upregulation of TYROBP - a tyrosine kinase binding protein that is a key regulator of genes directing immune and microglial signalling cascades related to the reactive oxygen species burst during pathogen phagocytosis (Scheltens et al., 2016; Zhang et al., 2013).

Soluble Aβ oligomers (dimers and trimers), larger Aβ oligomers and structures such as amylospheroids (ASPD), which are spherical Aβ assemblies of 10-15 nm diameter, rather than Aβ deposited in amyloid

plaques, are thought to produce most of the harmful effects of Aβ (Attems et al., 2004; Benilova et al., 2012; Caughley and Lansbury, 2003; Glabe, 2006; Klein et al., 2001; Matsumura et al., 2011; Noguchi et al., 2009; Shankar et al., 2008). This may help to explain the anatomical and temporal disparity that exists between the development and location of amyloid plaques, neuronal loss and the onset of clinical dementia (Musiek and Holtzman, 2015). Synthetic human $A\beta_{1-42}$ (Lambert et al., 1998) and soluble, low-number oligomers of naturally secreted human $A\beta_{1-42}$ (Walsh et al., 2002) have been shown to inhibit the maintenance phase of hippocampal long-term potentiation (LTP). This has been demonstrated both *in vivo* by microinjection of $A\beta_{1-42}$ oligomers into living rats (Walsh et al., 2002) and *in vitro* by application of $A\beta_{1-42}$ to hippocampal slices (Townsend et al, 2006). Moreover, $A\beta_{1-42}$ oligomers have been shown to reversibly interfere with the memory of learned behaviour in awake, behaving rats (Cleary et al., 2005). Strengthening the evidence derived from synthetic and rodent cell derived Aβ, Shankar et al. (2008) have shown that soluble Aβ oligomers (principally dimers) isolated directly from human AD brains, potently and consistently induced several AD–like phenotypes in normal adult rodents, decreasing dendritic spine density, inhibiting LTP and facilitating LTD in hippocampus, and thus interfering with the memory of a learned behaviour.

Whether the toxic effects of Aβ can be ascribed to a single oligomeric Aβ species or whether a mixture of various oligomers and/or aggregates is needed to trigger neurodegeneration in AD remains unresolved (Benilova et al, 2012; Musiek and Holtzman, 2015). Proposed mechanisms of oligomeric Aβ toxicity include:

(i) binding of oligomeric species to cellular receptors (variously suggested to be PrPC; APP; NMDAR; AMPAR; mGluR; α7-AcChR; insulin R),

(ii) pore or channel formation by Aβ leading to aberrations of ion homeostasis and $[Ca^{2+}]_i$, and

(iii) oxidative stress and injury to the cell membrane.

All of these may lead to tau hyperphosphorylation, aggregation and neurofibrillary tangle formation, and tau-dependent or -independent synaptic dysfunction with inhibition of LTP and promotion of LTD (Benilova et al., 2012).

Aβ may be removed from the brain parenchyma via mechanisms including (i) 'glymphatic' drainage (Xie et al., 2013) and (ii) enzymatic break down by neprilysin, insulin-degrading enzyme, tPA and matrix metalloproteinases (MMPs), although it is predominantly cleared by (iii) low density lipoprotein receptor-related protein-1 (LRP-1)-mediated transendothelial trafficking to circulating blood plasma (Shibata et al., 2000; Querfurth and La Ferla, 2010; Tachibana, et al., 2017; Zlokovic, 2011). Intravascular Aβ is also transported across the BBB by endothelial cells in the vessel wall expressing the receptor for advanced glycation end products (RAGE). RAGE however cannot completely eliminate brain derived Aβ.

RAGE-mediated transport of systemically administrated $Aβ_{1-40}$ into the CNS of wild-type mice led to a decrease in CBF measured by laser Doppler, which was found to be mediated by the vasoconstrictive peptide endothelin-1 (ET-1) (Deane et al., 2003). This observation was a starting point for a major component of my thesis, examining the effects of Aβ on the cerebral

vasculature at the capillary level. This work is presented in Chapter 5. The following section reviews the background to these experiments.

Recently, it has been argued that there is an over-reliance on the amyloid cascade hypothesis given the growing amount of data that are inconsistent with a linear pathway that begins with Aβ formation and ends with the dementia we know as AD (Herrup, 2015). Observations that support the proposition to reject the current linear structure of the amyloid cascade hypothesis include the following: APP, PSEN, BACE and microtubule-associated protein tau (MAPT) polymorphisms show little association with AD (Bertram et al. 2007; http://www.alzgene.org); individuals (a quarter to a third of all older persons) with substantial plaque burden can have normal cognition (Klunk et al., 2009; Villemagne et al., 2011); an inability reproduce AD-like dementia or most AD-associated pathology by overexpressing APP with or without second or third AD-associated transgenes in animal models of AD (no neurofibrillary tangles are formed, and though there is synaptic loss, there is little or no neurodegeneration) (Götz and Ittner, 2008; Hochgräfe et al., 2013; Hock er al., 2001; Kim et al., 2013; Kitazawa et al., 2012; LaFerla and Green, 2012; Webster et al., 2014); a number of failed anti-amyloid vaccination, anti-amyloid antibody and β- and y-secretase-targetting clinical trials based on the hypothesis (Doody et al., 2013; Doody et al., 2014; Egan et al., 2018; Holmes et al., 2008; Orgogozo et al., 2003; Salloway et al., 2014; Serrano-Pozo et al. 2010)

Whilst evidence from sporadic AD suggests that amyloid (at any stage of aggregation) may not by itself be sufficient to cause AD, none of these data argue against Aβ playing a leading role in the pathogenesis of AD.

Indeed, those in favour of abandoning the amyloid cascade hypothesis still insist that along with APP and the secretases, Aβ should remain central any revised hypothesis of the origins of AD (Herrup, 2015).

1.5.3 The role of capillary pericytes in Alzheimer's disease

There is a growing body of evidence that neurovascular dysfunction, reduced CBF and BBB breakdown have an important role in the development and progression of AD. Furthermore pericytes, as key regulators of BBB integrity and coordinators of neurovascular coupling, may play a pivotal role in the pathogenesis of AD.

Pericyte degeneration and loss has been observed in both the hippocampus and cortex of human AD cases (Sagare et al., 2013), and leads to BBB breakdown and reduced clearance of soluble Aβ from the brain (pericytes express the Aβ clearance receptor LRP-1, that binds and internalizes Aβ for degradation within the lysosome). The mechanism(s) underpinning the loss of pericytes in AD are not fully understood, but may require prolonged exposure of pericytes to high concentrations of Aβ (Sagare et al., 2013; Wilhelmus et al., 2007) that overwhelm the LRP-1 clearance pathway. In turn, the loss of pericytes and the LRP-1 Aβ-degradation pathway, promote Aβ accumulation to create a potential 'feed-forward' mechanism, and also lead to loss of BBB function which is maintained by pericytes (Armulik et al., 2010; Daneman et al., 2010; Zlokovic, 2008). BBB breakdown in AD leads to leakage of serum proteins into the parenchyma, and extravasation of red blood cells (microhaemorrhages) that release haemoglobin (with associated iron), which promotes the formation of toxic

reactive oxygen species (ROS). Leakage of albumin and immunoglobulin G (IgG) through the BBB promotes the development of vasogenic oedema, contributing to hypoperfusion, hypoxia and ultimately injury to nervous tissue. Furthermore, a defective BBB leads to potentially toxic blood-derived proteins (including circulating Aβ) entering the brain (Zlokovic, 2011). Degradation of the BBB in AD may be due to upregulation of a cyclophilin A (CypA) - nuclear factor κB (NF-κB) - matrix metalloproteinase 9 (MMP9) pathway in brain pericytes, which has been demonstrated in mice overexpressing ApoE4 (but not ApoE2 or ApoE3, providing an insight into how APOE genotype affects the brain microvasculature). Activation of the CypA-NFκB-MMP9 pathway in pericytes leads to enzymatic breakdown of endothelial tight junction complexes and neuronal uptake of multiple blood-derived neurotoxic proteins, followed by a cerebral blood flow reduction (Bell et al., 2012).

MRI (with contrast agent) studies have shown that during normal ageing there is increased hippocampal BBB permeability, which worsens in those with mild cognitive impairment and precedes measureable changes in hippocampal volume. Furthermore these studies found that in patients with early Alzheimer's disease and vascular cognitive impairment there is BBB breakdown in the hippocampus, cortical and subcortical regions (Kisler et al., 2017; Montagne et al., 2015; Nir et al., 2013; Taheri et al., 2011; Van de Haar et al., 2016).

Reductions in cortical blood flow (CBF) have been demonstrated in patients with AD, and population studies of both human AD cases and studies in transgenic AD mouse models have shown that CBF compromise likely precedes neurodegenerative change in AD (Iadecola, 2004; Iturria-

Medina et al., 2016; Zlokovic, 2011). Indeed, in the earliest stages of AD, CBF studies using ultrasound imaging, fluorodeoxyglucose positron emission tomography (PET), single-photon emission computed tomography (SPECT) studies, and different MRI techniques, have suggested that CBF reductions precede cognitive decline, hippocampal and cortical atrophy, changes in CSF levels of Aβ, tau and phosphorylated tau and amyloid β (Aβ) deposition. CBF reductions are observed in individuals with genetic risk factors for AD, including APOE4 carriers (Iturria-Medina et al., 2016; Kisler et al., 2017; Kogure et al., 2000; Michels et al., 2016; Montague et al., 2016; Reiman et al., 2004; Ruitenberg et al., 2005; Sheline et al., 2010; Thambisetty et al., 2010; Wirth et al., 2016). Neurovascular uncoupling in AD has also been studied using BOLD functional MRI (fMRI) (in particular with assessment of the brain resting state 'default mode network', which reflects synchronised changes in local blood flow: Mateo et al., 2017). This showed that neurovascular dysfunction occurs early in sporadic disease (before detectable Aβ pathology), in the presymptomatic stage of patients with autosomal dominant AD, and in cognitively normal individuals with genetic risk factors for sporadic AD (APOE4 carriers) (Kisler et al., 2017).

The precise mechanism by which CBF becomes disrupted in early AD is not yet fully understood, but it has been shown that Aβ, through its vasculotoxic and/or vasoactive effects, can cause both arterial and arteriolar vasoconstriction (Dietrich et al., 2010; Suo et al., 1998; Thomas et al., 1996; Zhang et al., 1997), and neurovascular uncoupling, leading to reduced CBF (Niwa et al., 2000; Park et al., 2004; Iadecola, 2004). The mechanisms include Aβ binding to the scavenger receptor CD36 on vascular smooth

muscle cells and pericytes to generate reactive oxygen species [ROS], Aβ-mediated NADPH oxidase generation of ROS, and transport of Aβ from the circulation into the brain by the receptor for advanced glycosylation products (RAGE), triggering production of the potent vasoconstrictor endothelin (Park et al., 2005; Park et al., 2011; Deane et al., 2003)).

In a transgenic mouse model of pericyte degeneration (lack of PDGFRβ, in the absence of Aβ), capillary CBF responses to neuronal stimuli are diminished, resulting in brain hypoxia, metabolic stress and, over time, impaired neuronal excitability and neurodegenerative changes (Kisler et al., 2017). These findings suggest that when Aβ causes pericyte degeneration this may contribute to neurovascular dysfunction and neurodegeneration in AD.

Pericyte loss has also been shown to promote Aβ-dependent neurodegenerative changes in a murine model in which pericyte-deficient mutants ($Pdgfr\beta^{+/-}$ mice) were crossed with mice overexpressing the Swedish mutation of human APP ($APP^{sw/0}$). In this model, it was demonstrated pericyte loss impaired the clearance of soluble $A\beta_{1-40}$ and $A\beta_{1-42}$, leading to increased deposition of Aβ within the brain parenchyma, and promoted further pericyte loss. Additionally, the loss of pericytes compromised cerebral vessel integrity leading to microvascular regression. Significantly, within 9 months, $APP^{sw/0}$;$Pdgfr\beta^{+/-}$ mice displayed the full spectrum of AD pathology - Aβ deposition, neuronal accumulation of hyperphosphorylated tau species, neuronal loss within the cortex and hippocampus. and poor performance on hippocampal-dependent behavioural tests (compared with $APP^{sw/0}$, $Pdgfr\beta^{+/+}$ littermate controls or $Pdgfr\beta^{+/-}$ mice of the corresponding age: Sagare et al.,

2013). Interestingly, it has been recently reported that 3 weeks following stereotaxic injection of mesenchymal stem cell-derived pericytes into one brain hemisphere of 18-20 month-old APP/PS1 amyloid model mice, cerebral blood flow in that hemisphere was enhanced compared to that in the contralateral control hemisphere. The observed increase in cerebral blood flow may have been due to improved microvascular modulation by the implanted pericytes or by pericyte endocytic LRP1-mediated clearance of $A\beta_{1-40}$ and $A\beta_{1-42}$ (Tachibana et al., 2017).

Reduced CBF leads to a reduction in protein synthesis, which is crucial for processes such as the long-term potentiation and synaptic plasticity required for learning and memory. If prolonged or severe, CBF reduction maylead to ischaemic injury (that in isolation leads to cognitive impairment: Shih et al., 2013). In turn, brain injury increases amyloid precursor protein (APP) expression and Aβ cleavage in affected regions, thus driving an additional and detrimental 'feed-forward' loop (Iadecola, 2004).

1.5.4 Vascular dementia and Alzheimer's disease

After AD, vascular dementia (VaD) in its pure form, or mixed VaD and AD, account for the vast majority of remaining dementia cases. Population-based clinicopathological studies have yielded prevalence estimates of 2.4–23.7% for pure VaD and 4.1–21.6% for mixed AD and VaD (the variability in types and location of vascular disease, the existence of mixed pathology, and the absence of internationally accepted consensus criteria for VaD neuropathology, possibly explain the deficiency in sensitivity and specificity of ante-mortem clinical diagnostic criteria and the variability in prevalance

estimates reported in autopsy series) (Elahi and Miller, 2017; Grinberg et al., 2013; Korczyn, 2002). Overlap of AD neuropathology (amyloid plaques and neuro- fibrillary tangles) with cerebrovascular lesions such as atherosclerosis of the circle of Willis and its branches, leukoaraiosis, and lacunar infarcts, microbleeds, microinfarcts, and cerebral amyloid angiopathy (CAA) has been reported in up to 50% of cases of dementia (Benedictus et al., 2013; Charidimou et al., 2011; Honig et al., 2005; Iadecola, 2013; Jellinger, 2013; Richardson et al., 2012; Roher et al., 2004; Toledo et al., 2013; Yarchoan et al., 2012). Ischemic lesions of the 'watershed' or 'borderzone' regions between arterial territories have also been reported in AD, suggesting hypoperfusion and cerebral amyloid angiopathy play an important role in their mechanisms (Iadecola, 2013; Miklossy, 2003; Suter et al., 2002). Vascular lesions are also seen in other age-related neurodegenerative diseases, such as Parkinson's disease, and frontotemporal lobar degeneration (FTLD), but the coexistence with AD is the most frequent (Iadecola, 2013; Toledo et al., 2013).

The decrease in pure VaD and related increase in mixed pathologies with age are now well established, and suggest complex interrelationships between vascular disease, cerebral ageing and accumulation of abnormal proteins in neurodegeneration (Elahi and Miller, 2017; James et al., 2012; Pendlebury and Rothwell, 2009).

1.6 Aims of the thesis

1) To investigate pericytes as a therapeutic target in acute stroke

Based on the premise that, during ischaemia, pericyte constriction and

death in rigor lead to a long-lasting capillary constriction that will decrease effective reperfusion of ischaemic brain tissue (even following arterial thrombolysis/mechanical thrombectomy), pericytes represent an attractive therapeutic target for the treatment of acute stroke. It seems reasonable to propose that a treatment preventing pericyte constriction and death in ischaemia would have a beneficial effect in acute stroke.

I will investigate, for the reasons explained in Chapter 4, whether blockade of L-type Ca^{2+} channels with nimodipine, blockade of endothelin A (ET_A) receptors with BQ-123 and blockade of thromboxane A_2 (TXA_2) receptors with ICI 192605 during simulated ischaemia would prevent pericyte constriction. This work is described in Chapter 4.

2) To investigate the vasoactive response of pericytes to Aβ as a therapeutic target in Alzheimer's Disease

Whilst it has been conclusively demonstrated that arterial and arteriolar smooth muscle constricts in response to application of amyloid β species, no work to date has examined whether contractile pericytes constrict capillaries in response to Aβ. I therefore investigated whether capillary pericytes are affected by Aβ oligomers, the molecular species believed to be responsible for Aβ's toxic effects in AD (Attems et al., 2004; Benilova et al., 2012; Caughley and Lansbury, 2003; Glabe, 2006; Klein et al., 2001). Where possible, to maximise disease relevance, I used living human brain slices derived from neurosurgically-resected brain tissue (removed to access tumours) to study acute responses to Aβ and rapidly-fixed human brain biopsy tissue (with or without Aβ deposition) to assess pericyte responses to

long-term accumulation of Aβ in AD. The mechanisms of any effects seen in human tissue were then defined in more readily available rodent brain slices. This work is described in Chapters 3 and 5.

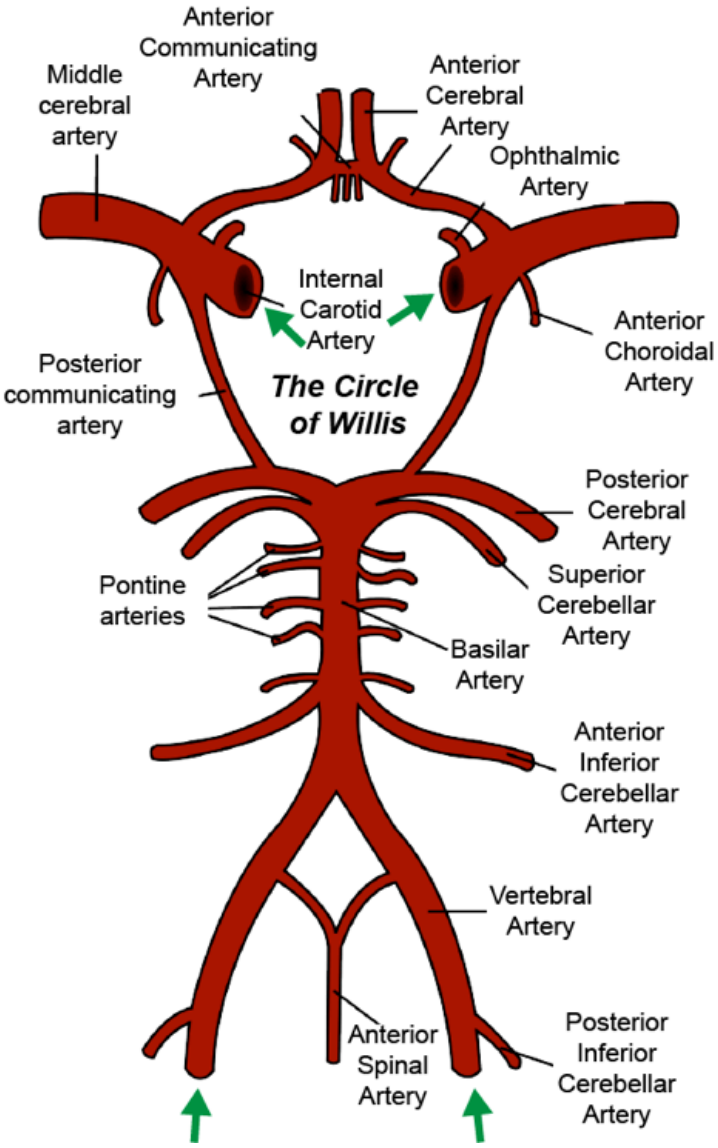

Figure 1.1 The Circle of Willis.

The major arterial branches of the Circles of Willis are shown. Blood enters the system through paired internal carotid and vertebral arteries. Deep perforator system (not shown): The middle cerebral artery gives origin to two main groups of perforators: the medial and lateral lenticulostriate arteries. Infrequently, the thalamotuberal artery may originate from the middle cerebral artery but far more commonly it originates from the posterior communicating artery. The anterior cerebral artery gives origin to the anterior lenticulostriate arteries and the recurrent artery of Heubner. The anterior choroidal artery takes its origin from the internal carotid artery and exceptionally from the middle cerebral artery. In addition, a small group of perforators comes directly from the internal carotid artery. Perforating arteries arising from the posterior cerebral artery to form the interpenduncular arteries, thalamogeniculate branches and the posterior choroidal arteries. The posterior communicating artery also gives rise to perforating branches, most notably the premamillary artery (Ghika et al., 1990). Green arrows = direction of blood flow into the circle. (Figure courtesy of Fergus O'Farrell, Attwell Lab)

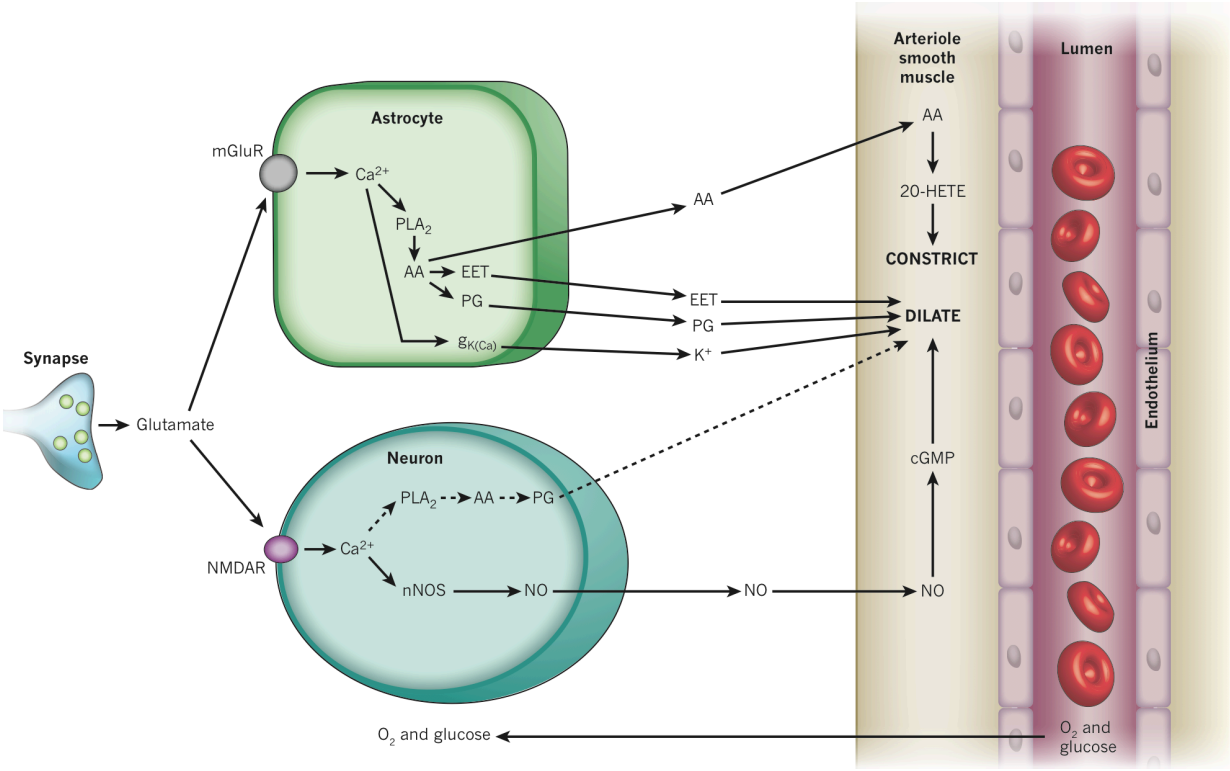

Figure 1.2 Major pathways by which glutamate may regulate cerebral blood flow.

Pathways from astrocytes and neurons (left) that regulate blood flow by sending messengers (arrows) to influence the smooth muscle around the arterioles that supply oxygen and glucose to the cells (right, shown as the vessel lumen surrounded by endothelial cells and smooth muscle). In neurons, synaptically released glutamate acts on *N*-methyl-D-aspartate receptors (NMDAR) to raise $[Ca^{2+}]_i$, causing neuronal nitric oxide synthase (nNOS) to release NO, which activates smooth muscle guanylate cyclase. This generates cGMP to dilate vessels. Raised $[Ca^{2+}]_i$, may also (dashed line) generate arachidonic acid (AA) from phospholipase A_2 (PLA_2) which is converted by COX2 to prostaglandins (PG) that dilate vessels. Glutamate raises $[Ca^{2+}]_i$ in astrocytes by activating metabotropic glutamate receptors (mGluR), generating arachidonic acid and thus three types of metabolite: prostaglandins (by COX1/3, and COX2 in pathological situations) and EETs (by P450 epoxygenase) in astrocytes, which dilates vessels, and 20-HETE (by ω-hydroxylase) in smooth muscle, which constricts vessels. A rise of $[Ca^{2+}]_i$ in astrocyte endfeet may activate Ca^{2+}-gated K^+ channels ($g_{K(Ca)}$), releasing K^+, which also dilates vessels. (Taken from Attwell et al., 2010)

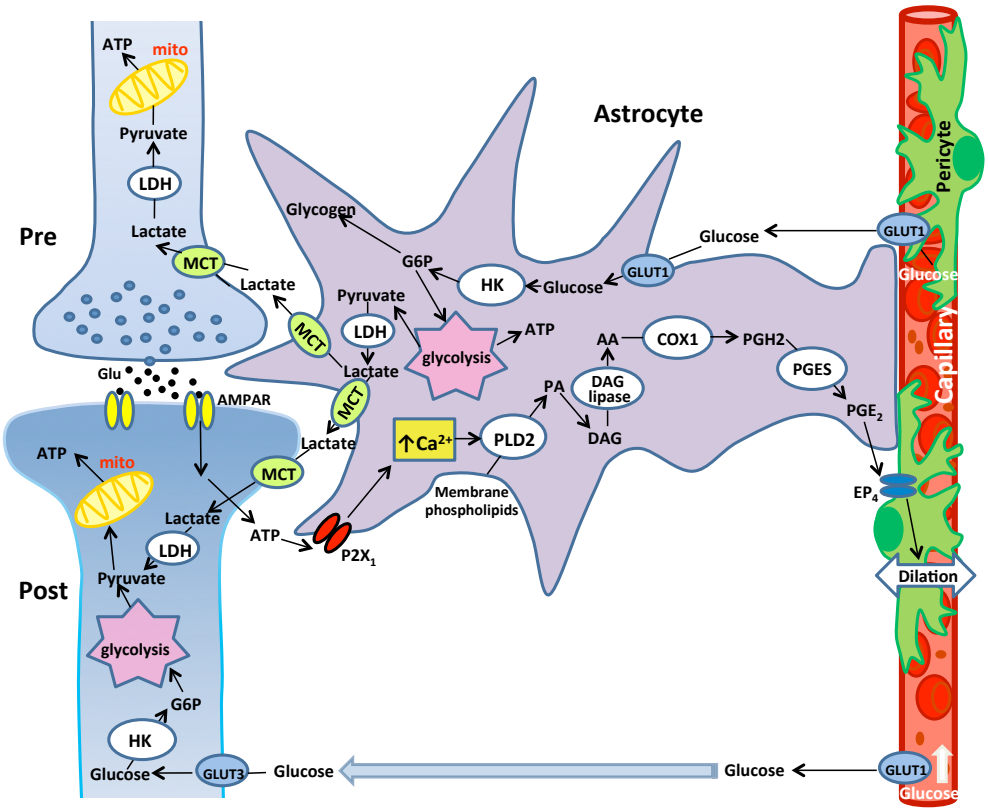

Figure 1.3 How astrocytes regulate brain energy supply.

Astrocytes regulate both glucose supply in the blood and the use of that glucose to make ATP in different cell types. On the right a capillary provides glucose (and oxygen) in the blood. This nutrient supply can be regulated by changes in the tone of contractile pericytes (or smooth muscle around upstream arterioles). Pericytes dilate capillaries when astrocytes experience a rise in $[Ca^{2+}]_i$, for example when ATP released from postsynaptic neurons

(stimulated by presynaptic glutamate release acting on AMPARs) activates astrocyte $P2X_1$ receptors. This activates an enzyme cascade that leads to the release of prostaglandin E_2, which dilates pericytes. Glucose leaves the capillary by transport on GLUT1, and then diffuses extracellularly to neurons and astrocytes where it is taken up by GLUT3 or GLUT1, respectively, and then converted by hexokinase to G6P, a precursor for glycolysis and for glycogen formation. Glycolysis generates ATP, and either pyruvate to enter the tricarboxylic acid cycle and oxidative phosphorylation in mitochondria (not shown in the astrocyte for clarity) or lactate (via LDH), which can be exported from the cell by monocarboxylate transporters (MCT). Once lactate is taken up into neurons by an MCT, it is converted back to pyruvate by LDH and is processed by the citric acid cycle and oxidative phosphorylation in mitochondria. The ATP thus generated is used mainly for powering the sodium/potassium pump.

Abbreviations: Pre: presynaptic terminal; Post: postsynaptic terminal; Glu: glutamate; AMPAR: AMPA receptor; $P2X_1$: a Ca^{2+}-permeable receptor for ATP; PLD2: phospholipase D2; PA: phosphatidic acid; DAG: diacylglycerol; COX1: cyclooxygenase 1; PGH2: prostaglandin H_2; PGE2: prostaglandin E_2; EP_4: receptor for PGE2; GLUT1: glucose transporter 1; GLUT3: glucose transporter 3; HK: hexokinase; G6P: glucose-6-phosphate; MCT: monocarboxylate transporter; LDH: lactate dehydrogenase; mito: mitochondrion.

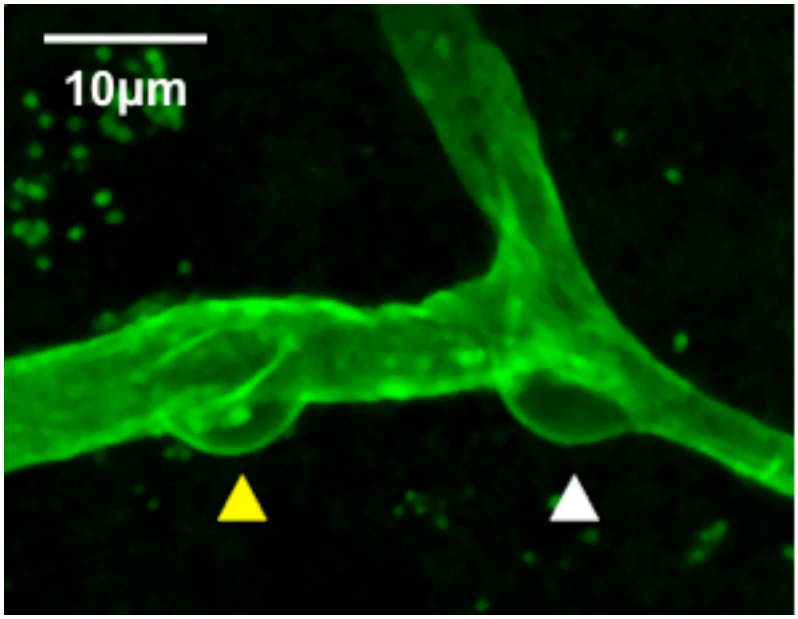

Figure 1.4 Pericyte morphology.

Confocal image showing Isolectin B_4 labelled human cortical pericytes with 'bump on a log' morphology on a straight section (yellow arrowhead) and at branch points (white arrowhead) of capillaries.

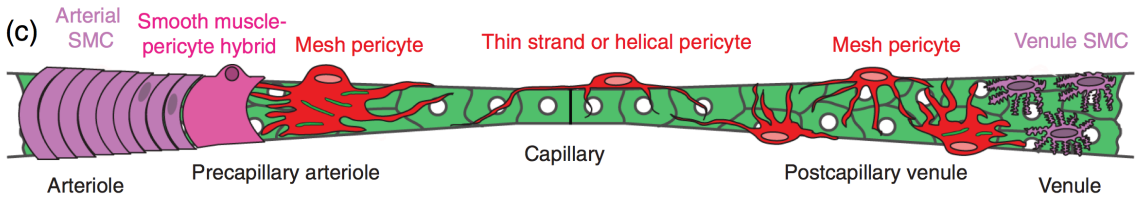

Figure 1.5 Continuum of mural cell types along the cerebral vasculature. From left to right: Smooth muscle cells form concentric rings on arterioles. Hybrid smooth muscle-pericyte cells reside on pre-capillary arterioles and interlock with mesh pericytes at the arteriole–capillary interface, which occurs where penetrating arterioles ramify into the capillary bed. Pericytes in capillary beds typically exhibit long processes that traverse the microvasculature in single strands or pairs that twist in a helical fashion. Mesh pericytes become more prevalent again as capillaries turn into post-capillary venules. Stellate-shaped smooth muscle cells cover the walls of parenchymal venules. (Taken from Hartmann et al., 2015)

Chapter 2: Methods

In this chapter I will describe the principal methods for the experiments detailed in this thesis. Experimental techniques and details specific to particular experiments are described in the Methods section of each Results chapter.

2.1 Solutions

All solutions for human and rodent experiments were prepared using ultrapure de-ionised water (Milli-Q, Millipore Corporation). Aqueous stock solutions of salts (using powdered salts of compounds dissolved in water or dimethyl sulfoxide (DMSO)) were used for the preparation of artificial cerebrospinal spinal fluid (aCSF) and other drug-containing solutions.

2.1.1 Extracellular solution

Human and rodent brain slices were superfused with solution (artificial cerebrospinal fluid, aCSF) containing (mM) 124 NaCl, 2.5 KCl, 26 $NaHCO_3$, 1 $MgCl_2$, 1 NaH_2PO_4, 10 glucose, 2 $CaCl_2$, 1 Na ascorbate. For all live imaging experiments this solution was equilibrated with a gas mixture of 20% O_2/75% N_2/5% CO_2, which (unlike when bubbling with 95% O_2/5% CO_2 which generates hyperoxic conditions) produces a physiological level of oxygen in the slice near the capillaries being imaged (Hall et al., 2014). Artificial CSF was delivered to the microscope imaging bath via a peristaltic pump (Masterflex) at ~4 ml/min and heated to 33-36°C by manually adjusting the electrical current passing through a pair of heating resistors mounted on a brass block encasing the perfusion inlet. The temperature was measured in the imaging bath using a thermo-electric effect thermometer.

2.1.2 Pharmacology experiments in live cortical slices

Human and rodent brain slices were superfused with extracellular fluid (as described above) with and without any of the following added: 500 μM glutamate, 2 μM noradrenaline, 10 nM endothelin, 1μM ET-A receptor blocker (BQ-123), 1 μM ET-B receptor blocker (BQ-788), 1μM L-NNA to block nitric oxide synthase, 10-250 nM oligomeric $A\beta_{1-42}$ (nominal concentrations are given for Aβ here - for the corrected concentrations after oligomerisation see section 2.4 below), 150 U/ml superoxide dismutase (SOD1), 1μM RAGE blocker (FPS-ZM1), 250 nM oligomeric scrambled $A\beta_{1-42}$, 250 nM oligomeric $A\beta_{1-40}$, 5 nM endothelin, 1 mM H_2O_2 to generate reactive oxygen species.

2.1.3 Ischaemic solution

To mimic ischaemia, rodent neocortical brain slices were superfused with ischaemic solution made up as for extracellular solution but with glucose replaced with 7 mM sucrose and oxygen removed by equilibrating solutions with 5% CO_2 and 95% N_2. In addition, 2 mM iodoacetate and 25 μM antimycin were added to inhibit ATP generation by glycolysis and oxidative phosphorylation respectively (a procedure termed chemical ischaemia). Ischaemic solution was heated to 33-36°C and delivered to the microscope imaging bath as for delivery of aCSF solution (described above).

For ischaemia plus nimdopine experiments, nimodipine was dissolved in dimethyl sulfoxide (DMSO) at 100 mM, and added to the ischaemia solution at a final concentration of 3 μM (so that the final DMSO concentration is less than 0.01% v/v of total solution volume).

For experiments examining pericyte death during ischaemia, propidium

iodide (PI, 7.5 μM) was added to ischaemic solution to label cells dying by necrosis (i.e. cells that had lost the selective permeability of their plasma membrane). Propidium becomes fluorescent when it binds to DNA, which is only possible if it can cross the cell membrane.

For endothelin A receptor blocker experiments, the endothelin A receptor blocker BQ-123, or the endothelin B receptor blocker BQ-788 were dissolved at 10 mM in double distilled water and added to the superfusion solution at a final concentration of 1 μM.

The thromboxane A_2 receptor blocker, ICI192605, was dissolved at 4 mM in DMSO and added to ischaemic solution at a final concentration of 1 μM, so that the final DMSO concentration was less than 0.01% v/v of total solution volume.

2.2 Human and rodent brain slices

2.2.1 Live rodent brain slices

Experiments used P21 Sprague-Dawley rats of either sex. All animal procedures were carried out in accordance with UK regulations (the UK Animals (Scientific Procedures) Act 1986 and subsequent updates). Animals were humanely killed using a Schedule 1 protocol. Rats were cervically dislocated and then decapitated to ensure exsanguination. The procedure for brain removal and subsequent processing was performed as previously described (Mishra et al., 2014). The rat head was placed in a small pot containing ice-cold slicing solution comprising (in mM) 93 N-methyl-D-glucamine chloride (NMDG), 2.5 KCl, 30 $NaHCO_3$, 10 $MgCl_2$, 1.2 NaH_2PO_4, 25 glucose, 20 HEPES, 5 Na ascorbate, 0.5 $CaCl_2$, 3 Na pyruvate, and 1

kynurenic acid (added to block glutamate receptors), bubbled with 95%O_2/5%CO_2 (to give a pH of 7.4) for a brief period. The rat scalp was then cut with scissors along the midline from the base of the neck anteriorly towards the nose. Skin flaps were reflected laterally to reveal the skull. The skull was then cut with fine scissors along the midline, posterior to anterior (along the sagittal suture), and two further mediolateral cuts were made on either side at the nasal end, such that two skull flaps were created which could be carefully reflected laterally with forceps to reveal the brain beneath. The brain was then gently retracted away from the base of the skull using a small spatula and placed (dorsal side facing upwards) in a Sylgard (Dow Corning, cat no. 184)-coated Petri dish containing ice-cold slicing solution. The brain was cut with a razor blade coronally to remove the cerebellum and posterior fifth of the hemispheres and to remove the anterior quarter of the hemispheres. The brain section was then mounted onto the slicing block with a thin layer of cyanoacrylate glue, supported by a cube-shaped piece of agarose, with the posterior cut edge facing downward and the inferior surface of the brain facing the agarose block (See Fig. 2.1a,b).

Coronal slices of rat neocortex (250-300 μm) were then prepared (Peppiatt et al., 2006; Mishra et al., 2014) on a vibratome (Leica VT1200S) in ice-cold slicing solution bubbled with 95% O_2/5% CO_2 to give a pH of 7.4 (See Fig. 2.1c). The cut slices were then transferred for a 'heat recovery' ten-minute incubation period in the same solution maintained at ~35°C. It has been found that more capillaries remain healthy in brain slices from P12 and P30 rats when sliced using NMDG-based slicing method with heat recovery than when sliced in standard slicing solution (Mishra et al., 2014; Nashmi et

al., 2002; Zhao et al., 2011). Slices were then incubated at room temperature (21-23 °C) in a similar recovery solution with the 93 NMDG-Cl, 10 $MgCl_2$, 0.5 $CaCl_2$ and 5 Na ascorbate replaced with (in mM) 92 NaCl, 1 $MgCl_2$, 2 $CaCl_2$ and 1 Na ascorbate, until used in experiments (See Fig. 2.1d).

2.2.2 Live human brain slices

This component of the work received ethical approval (REC number 15/NW/0568) and all patients gave prospective, fully informed written consent.

During elective neurosurgical operations for tumour treatment (predominantly glioma resection), apparently normal cortical tissue was removed by Miss Huma Sethi, Consultant Neurosurgeon, Division of Neurosurgery, National Hospital for Neurology and Neurosurgery, to gain access to the tumour (which would otherwise have been discarded). All patients from whom tissue was obtained gave prospective, fully informed written consent. Age, sex and the clinical indication for their surgery (for example resection of a glioma) were the only clinical details passed on by the surgeons; all other patient information remained confidential. All human tissue was handled, stored and disposed of in accordance with the Human Tissue Act (2004).

Immediately following resection, the human tissue sample was placed in ice cold brain slicing solution containing (mM) 93 N-methyl-D-glucamine chloride, 2.5 KCl, 30 $NaHCO_3$, 10 $MgCl_2$, 1.2 NaH_2PO_4, 25 glucose, 0.5 $CaCl_2$, 20 HEPES, 5 Na ascorbate, 3 Na pyruvate, 1 kynurenic acid (to block glutamate receptors, to prevent excitotoxic damage to neurons), oxygenated

by gassing with 95% O_2/5% CO_2, and transported in less than 15 minutes to the laboratory. Tissue was mounted onto a slicing block supported by a cube-shaped piece of agarose with a thin layer of cyanoacrylate glue. The tissue was then cut into 200 μm sections on a vibratome (Leica VT1200S) and the slices were incubated at 34^{o}C (for heat recovery) in the same solution for ten minutes, and then incubated at room temperature until used in experiments in a similar solution (Mishra et al., 2014) with the NMDG-Cl, $MgCl_2$ and $CaCl_2$ replaced by (mM) 92 NaCl, 1 $MgCl_2$ and 2 $CaCl_2$. Each patient's tissue typically generated ~2 brain slices. When sufficient tissue was present, histological examination of the slices using haematoxylin and eosin staining, was performed by Dr. Zane Jaunmuktane, Consultant Neuropathologist, Division of Neuropathology, National Hospital for Neurology and Neurosurgery, to assess tumour infiltration into the nominally normal tissue.

2.3 Imaging of the microvasculature

2.3.1 Brightfield Imaging of cortical capillaries

Healthy capillaries (<10 μm in diameter with no rings of arteriolar smooth muscle around them) were selected (Mishra et al., 2014) and regions of them were imaged which: (i) were in focus in a single image plane over at least 30 μm (along the length of a capillary), and (ii) exhibited a candidate pericyte with a bump-on-a-log morphology. Images 100 μm square were obtained using an Olympus BX50WI microscope with low power (4x) and high power (40x) water-immersion objectives, a brightfield light source, an epifluorescent xenon lamp, a Coolsnap HQ2 CCD camera and Image Pro Plus acquisition software. Typically 1 image was taken every 30 seconds with

an exposure time of 10 msec.

2.3.2 Brightfield imaging of cortical arterioles

Healthy arterioles (>10 μm in diameter with a clearly visible, continuous smooth muscle wall were selected and regions of them were imaged which were in focus in a single image plane extending over at least 30 μm. Image acquisition was as described above for capillaries.

2.3.3 Two-photon imaging of live capillaries and labelled pericytes

In some experiments pericytes were identified prior to imaging by incubating slices for 30 min in 10 μg/ml isolectin B_4 conjugated to Alexa 488 or Alexa 647, which binds to α-D-galactose residues in the basement membrane secreted by pericytes and endothelial cells, and outlines pericytes (Mishra et al., 2014) since they are surrounded by the basement membrane. This allowed 2-photon imaging (using a Zeiss LSM710 microscope, with excitation wavelength 800 nm) of the endothelial tube and the pericytes on it.

Incubation of live slices in the fluorescent Nissyl dye, neurotrace 500/525 at 1:25 dilution (described by Damisah et al., 2017 to label capillary pericytes *in vivo*), together with 10 μg/ml isolectin B_4 conjugated to Alexa 647, for 30 minutes allowed clear identification of pericyte somata and their processes extending around and along the capillary wall during 2-photon imaging, again using a Zeiss LSM710 microscope. Z-stacks were obtained with 1 μm step size and captured digitally using Zen software (Carl Zeiss Microscopy).

2.3.4 Vessel diameter analysis

Capillary and arteriole internal diameters were measured (using MetaMorph software (Molecular Devices)) on sequential image frames by manually placing a measurement line (perpendicular to the vessel) on the image (maintained at a specific point of reference along the vessel throughout the imaging sequence to ensure the same region of vessel was measured throughout). With the image scale calibrated (by taking an image of a graticule), diameters measured using this method were recorded in μm for the whole time series of the experiment. During analysis of the results (by myself and, to provide an independent check on the results, Dr. Anusha Mishra, Post-Doctorate Research Fellow, UCL), those measuring capillary diameters were blinded to the timing and identity of the drug applications. Diameter measurements were logged and exported to Microsoft Excel for analysis.

2.3.5 Assessing pericyte death during live imaging

The number of dead pericytes per 100 μm of capillary was measured during live imaging by identifying PI labeled cells with a pericyte morphology (using fluorescence imaging) which also had a pericyte morphology in the corresponding brightfield images. As stated above, pericytes produce a characteristic ‘bump on a log’ appearance as they wrap around endothelial cells (EC) on the outside of the capillary, and are completely surrounded by the basal lamina. They can be distinguished from ECs, which have elongated, cigar-shaped nuclei, by their prominent round nuclei (Dore-Duffy and Cleary, 2012). Previous studies have shown a mean density of pericyte

somata along neocortical capillaries in P21 rats of 2.2±0.2 per 100 μm of capillary length (Hall et al., 2014). Fluorescence images were obtained every 5 minutes (excited with an epifluorescence xenon lamp, passing through filters appropriate for the propidium fluorophore) with an exposure time of 2.5 sec.

Assessing pericyte death in fixed tissue

Brain slices (250 μm thick) were incubated in a multi-well plate at 35°C, with 95% O_2 /5% CO_2 blown gently on the surface, in aCSF, or aCSF with $A\beta_{1\text{-}42}$ or ET-1 added. All extracellular solutions contained isolectin B_4 conjugated to Alexa 488 to label the basement membrane, and hence pericytes which are enveloped by this (see above), and 7.5 μM propidium iodide (PI) to label cells with membranes that had become non-specifically permeable (Hall et al., 2014). After 3 hours incubation, slices were fixed in 4% paraformaldehyde, and washed 3 times with PBS, mounted on glass slides. The slices were then imaged on a Zeiss LSM 700 laser-scanning confocal microscope with a 20x water immersion objective. Z-stacks were obtained with 1 μm depth increment, and captured digitally using Zen software (Carl Zeiss Microscopy). Laser excitation at 488 nm and 543 nm was used to visualise isolectin B_4 conjugated to Alexa 488, and PI, respectively. Importantly, isolectin IB_4 and PI acquisition settings were kept the same between slices and different experiments to help to eliminate bias in the identification of pericytes and dead cells. A custom-written ImageJ script (courtesy of Lorena Arancibia-Carcamo, UCL NPP) was used to blind Hui Gong (a UCL life sciences undergraduate working in the Attwell lab under my supervision) and myself to the experimental condition during analysis.

Pericytes were identified using the IB4 labelling of the basement membrane, and PI labelling was used to assess cell death. To avoid counting cells killed by the slicing procedure, quantification of the percentage of pericytes that were dead excluded cells within 20 μm of the slice surface.

2.4 Amyloid Preparation

2.4.1 Oligomerising Aβ and assessing the form and concentration of Aβ applied

The method employed to generate oligomeric Aβ preparations was modified from that previously described (Lambert et al., 2001). Synthetic $A\beta_{1-42}$ (Bachem H-1368.1000), $A\beta_{1-40}$ (Bachem H-1194.1000) and scrambled $A\beta_{1-42}$ (Bachem H-7406.1000) were suspended in 1,1,1,3,3,3 hexafluoro-2-propanol (hexafluoropropanol HFIP; 52527, Sigma) at 1 mM, vortexed to obtain a homogenous solution, and aliquoted to microcentrifuge tubes. The HFIP was removed by overnight evaporation and completely lyophilized via a Speed-Vac. The Aβ peptide films were stored desiccated at -20^{o}C until further processed. The peptide films were then resuspended at 5 mM in DMSO, bath-sonicated for 10 min and vortexed for 30 sec. To form Aβ oligomers, this solution was diluted to 100 μM Aβ with phosphate-buffered saline, vortexed for 15-30 sec and incubated at 4^{o}C for 24 h. Immediately before use, the oligomeric preparations were centrifuged at 14,000 g for 10 min at 4^{o}C (to remove any fibrils that might be present) and the supernatants were further diluted to the final experimental concentrations with external solution.

Quantification of Aβ peptide concentration was performed (in collaboration with Dr Vasiliki Kyrargyri, a post-doc in the lab) using a Pierce

BCA protein assay kit (Thermoscientific 23227), calibrated against a known concentration of bovine serum albumin, taking into account the different chromophoric development of albumin and Aβ peptides by multiplying by a factor of 1.51 (Jan et al., 2010; as described in the Abeta_Quantitation_Protocol.pdf from www.amidebio.com). This showed that the amount of the molecule remaining as soluble monomers and oligomers was 28.7±2.9% (n=4) of the nominal concentration for $A\beta_{1-42}$, 39.9±1.5% (n=3) for $A\beta_{1-40}$, and 43.6±2.3% for scrambled $A\beta_{1-42}$. Concentrations stated in the Results have been corrected for these factors.

The Aβ oligomeric preparations were analysed via SDS-PAGE using 10-20% tris-glycine gels (EC61352BOX, Invitrogen). Samples of 50 µg Aβ peptides were added to tris-glycine SDS Sample Buffer (LC2676, Invitrogen). Equal volumes of each sample (10 µl) were loaded onto gels along with SeeBluePlus2 (Invitrogen) pre-stained molecular weight markers, and electrophoretically separated at 100 V. Gels were stained for total protein using a SilverXpress Silver Staining kit (LC6100, Invitrogen) according to the manufacturer's protocol. $A\beta_{1-42}$ and $A\beta_{1-40}$ formed monomers and oligomers, while scrambled $A\beta_{1-42}$ formed only monomers, as shown in Fig. 5.1, Chapter 5.

2.5 Immunohistochemistry of human tissue from neurosurgical operations

Human neocortical brain samples were fixed in 4% paraformaldehyde (PFA) for 24 hours and then washed 3 times (10 minutes each time) in phosphate-buffered saline (PBS). Samples were then transferred to 30%

sucrose/PBS at 4°C for 24 hours. Samples were washed again 3 times (10 minutes each time) with PBS before being cut into slices (200 μm) on a vibratome (Leica VT1000S) in 0.2M glycine/PBS and transferred to a 48 well plate. Slices were then incubated for 4-6 h with 0.5% Triton X, 10% goat serum in 0.2 M glycine/PBS at 21°C, then with primary antibodies for PDGFRβ (Santa Cruz, cat. no. sc432, 1:200), NG2 (Millipore, cat. No. AB5320, 1:200) and α-SMA (Santa Cruz, cat. no. CGA7, 1:200) at 4°C overnight with agitation and then for 4-8 hours with Alexa Fluor 647 conjugated secondary antibody at 4°C with agitation. Slices were then washed once in PBS containing DAPI nuclear stain (1:50,000) for 10 minutes and then washed again in twice (10 minutes each time) in PBS. Slices were mounted on standard glass microscope slides using DAKO mounting medium and 0.17 mm-thick glass coverslips sealed with colourless nail varnish. Slides were allowed to dry (in the dark) for more than 24 hours before slices were imaged on a Zeiss LSM700 laser scanning confocal microscope with a 20x water immersion objective. Laser excitation at 405 nm, 488nm and 633nm was used to visualise DAPI, FITC-IB_4 conjugated to Alexa 488 and Alexa 647 conjugated secondary antibodies, respectively. Z-stacks were obtained with a 1 μm depth increment and at a resolution of 768x768 pixels with a bit depth of 8 bit. Images were digitally captured using Zen software (Carl Zeiss Microscopy).

2.6 Human biopsy data

Diagnostic brain biopsies, comprising cortex and subcortical white matter, were performed as part of routine clinical investigation at the National Hospital for Neurology and Neurosurgery, Queen Square, London, to exclude

treatable causes of neurological symptoms the patients had presented with. All patients gave informed consent for the biopsy. The use of human tissue samples was licensed by the NRES, UK (University College London Hospitals NRES license for using human tissue samples, project ref 08/0077). The storage of human tissue was licensed by the Human Tissue Authority, UK (License #12054).

Biopsies (volume typically 1 cm^3) were all from the right frontal lobe. The biopsies were fixed in 10% buffered formalin less than 30 minutes after the resection, for a minimum of 12 hours. The formalin fixed tissue was dehydrated through graded alcohols and embedded in paraffin wax, from which 4 μm thick sections were cut for routine haematoxylin and eosin staining and a panel of immunohistochemical stains. As part of the diagnostic work up, the sections were immunostained for Aβ with immunoperoxidase-labelled antibody 6F3D (DAKO, 1:50), for phosphorylated tau with antibody AT8 (Innogenetics, 1:100), and for this study in addition with antibody against PDGFRβ (RD systems, cat. no. MAB1263, 1:20) to label pericytes. This was performed on a Roche Ventana Discovery automated staining platform following the manufacturer's guidelines, using biotinylated secondary antibodies and streptavidin-conjugated horseradish peroxidase and diaminobenzidine as the chromogen. The extent of parenchymal amyloid β deposition was assessed semi-quantitatively as absent, moderate or severe by a neuropathologist.

In addition, to quantify Aβ deposition objectively, the images of the immunoperoxidase label for Aβ were imported into ImageJ, and split into red, green and blue channels. Then the light intensity in the blue channel (which

gave best distinction of the immunoperoxidase label from the background tissue haemotoxylin labelling) was measured in the region of the biopsy where diameters were measured, normalised by the intensity in a region of the section showing no visible Aβ label, and converted to a percentage of light absorbed by the Aβ. Normalising by the intensity in a region without any tissue absorption gave values that were 5.8±0.5% larger, which did not materially change the form of the graphs presented in Chapter 5.

The mean age of patients without Aβ deposition was 50.5±5.5 (n=6, 4 women and 2 men), and of those with Aβ deposition was 62.1±4.2 (n=7, 4 women and 3 men, not significantly different, p=0.11). Regressing mean capillary diameter against age from all patients or from the patients lacking Aβ deposition showed that there was no significant dependence on age (p=0.5 and p=0.82 respectively; see Chapter 5, Fig. 5.9c).

Images were analysed to assess capillary diameter with the analyst (Ross Nortley) blinded to the level of Aβ deposits. A standard 5x4 grid of 20 squares (each with sides 400 μm long) was superimposed on each image, and all capillaries with clearly demarcated endothelial walls visible in each square had their diameter measured (see Fig. 2.2). The image squares were treated as the experimental unit for statistical analysis. Analysis of the diameter as a function of distance from the nearest visible pericyte employed a subset of all the measured diameters, because often no pericyte was visible on some short capillary segments.

2.7 Statistics

2.7.1 Tests for normality and p-value

Data normality was assessed with Shapiro-Wilk tests. Comparisons of normally distributed data were made using 2-tailed Student's t-tests. Equality of variance was assessed with an F test, and heteroscedastic t-tests were used if needed. Data that were not normally distributed were analysed with Mann-Whitney tests. P values were corrected for multiple comparisons using a procedure equivalent to the Holm-Bonferroni method (for N comparisons, the most significant p value is multiplied by N, the 2nd most significant by N-1, the 3rd most significant by N-2, etc.; corrected p values are significant if they are less than 0.05). Assessment of whether the slope of linear regressions differed significantly from zero was obtained using the t-statistic for the slope. P values comparing vessel diameters in the absence and presence of drugs were calculated for the last data point in each graph shown, or for an exposure time of 45-60 minutes if no graph is shown. Statistical analysis was performed in Microsoft Excel, OriginPro 9 (OriginLab Corporation) or SPSS (IBM Corporation).

2.7.2 Calculation of effect of vessel constriction on flow

We assume that pericytes are regularly spaced on capillaries at an interval of 2L. For flow governed by Poiseuille's law, the resistance of a segment of capillary of length L (from a pericyte soma to midway between two pericytes) and radius r_1 is given by

$$k.L/r_1^4$$

where k is a constant. If Aβ-induced pericyte contraction reduces the capillary

diameter from a value of r_1 at the midpoint between pericytes to r_2 near the pericyte soma (see Fig. 5.7a, b, d in Chapter 5), then if this reduction is linear with distance the resistance of the capillary segment from the soma to the midpoint is given by

$$k.L.(r_1^2 + r_1.r_2 + r_2^2)/(3.r_1^3.r_2^3)$$

so the factor by which the resistance is altered is

$$[1 + (r_1/r_2) + (r_1/r_2)^2].(r_1/r_2)/3$$

This was used to calculate the predicted flow reduction to be produced by the 30% pericyte constriction reported at pericyte somata in Fig. 3d and the main text. In reality the flow reduction will be greater because the diameter at the pericyte soma is actually larger than at the midpoint between pericytes in control conditions (see Chapter 5), and because Poiseuille's law does not apply for small capillary diameters for which the effective blood viscosity increases as the diameter decreases below 10 μm (Pries et al., 1990).

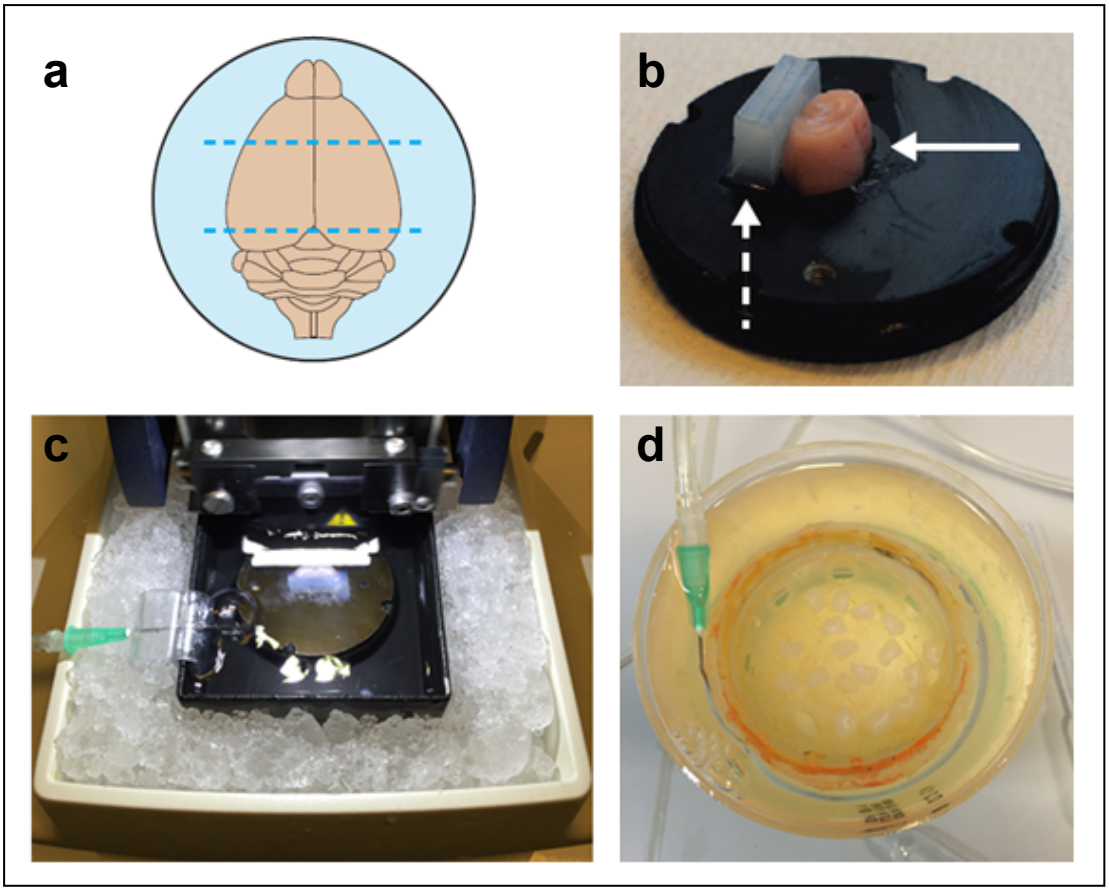

Figure 2.1 Live brain slicing.

(a) The brain is cut along the dashed lines to remove the cerebellum and a portion of the posterior hemisphere, together with a small section of frontal lobe. (b) The cut brain is then mounted onto a slicing block, supported by a cube of agarose gel. (c) The slicing block is fixed in a vibratome and the brain is cut to produce 250-300 µm thick slices in oxygenated NMDG slicing solution. (d) Slices are transferred to recovery solution for 30-40 minutes following 15 minutes of warm recovery in NMDG slicing solution. Adapted from Mishra et al, 2014.

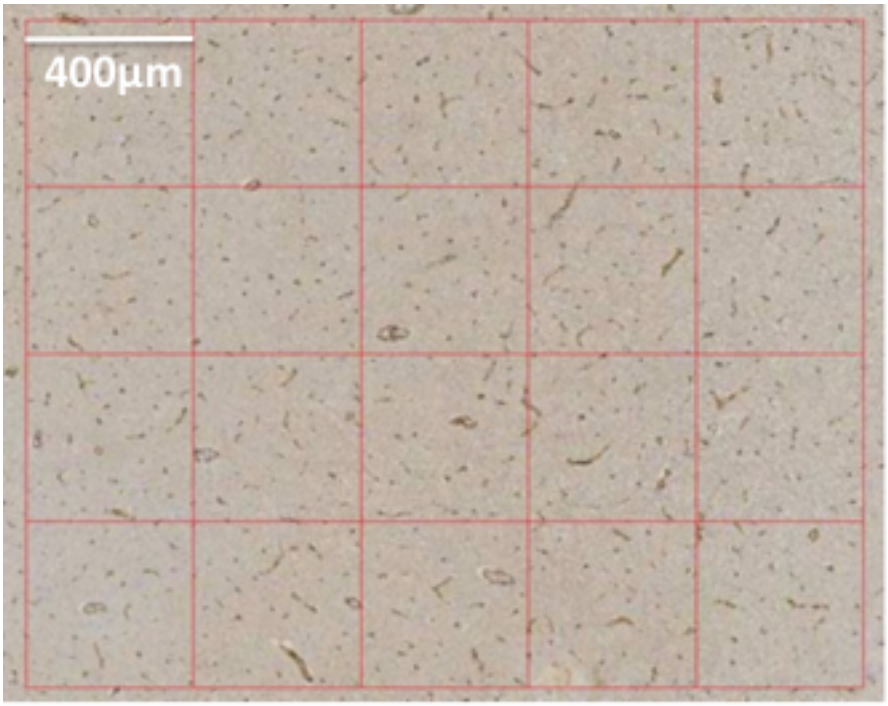

Figure 2.2 Analysis of human frontal lobe cortex biopsy.

Images of PDGFRβ-labelled capillaries and pericytes from human frontal lobe cortical biopsies were performed using a standard a 5x4 grid of 20 squares (each with 400µm sides). The image squares were treated as the experimental unit for statistical analysis.

Chapter 3: Control of human and rat capillary diameter by pericytes in physiological conditions

3.1 Introduction

Although it is now fairly well accepted that pericytes in the rodent CNS can alter their tone to constrict and dilate their underlying capillaries (see Chapter 1), no experiments have been performed on human pericytes *in situ* on capillaries to assess whether they can also regulate cerebral blood flow. Furthermore, although the powerful vasoconstrictor endothelin may constrict capillaries by acting on pericytes in the retina (Chakravarthy et al., 1992; Kawamura et al., 2002; but see Butryn et al., 1995), the kidney (Kennedy-Lydon et al., 2015; Pallone & Silldorff, 2001), and the ureter (Borysova et al., 2013), it is unknown whether endothelin also constricts capillaries in the brain. Finally, there is intense debate about whether all pericytes constrict or only some of them can constrict owing to a selective expression of α-smooth muscle actin in the pericytes on larger capillaries at the arteriole end of the capillary bed (Hall et al., 2014; Hill et al., 2015, Hartmann et al., 2015; Grant et al., 2017). Indeed, Grutzendler's group have proposed that mid-capillary bed pericytes, that can be labelled by the Nissl stain NeuroTrace, cannot constrict capillaries (Damisah et al., 2017). To address these deficits in our knowledge, in this chapter I describe experiments:

(i) providing a basic characterisation of the anatomy and physiology of pericytes on capillaries in slices made from nominally healthy human brain tissue (taken in order to access gliomas) from patients undergoing neurosurgical operations;

(ii) examining whether rodent cortical capillaries are constricted by endothelin

acting on pericytes;

(iii) testing whether supposedly non-contractile rodent pericytes labelled with NeuroTrace can be made to constrict capillaries by applying endothelin.

3.2 Methods

3.2.1 Preparation and imaging of live human brain slices

The human component of work in this chapter received ethical approval (REC number 15/NW/0568) and all patients gave prospective, fully informed written consent. All human tissue was handled, stored and disposed of in accordance with the Human Tissue Act (2004).

During elective neurosurgical operations for tumour treatment, apparently normal cortical tissue was removed to gain access to the tumour (which would otherwise have been discarded). Immediately following resection, the human tissue sample was placed in ice cold brain slicing solution oxygenated by gassing with 95% O_2/5% CO_2, and transported in less than 15 minutes to the laboratory. Live human tissue slices were prepared and stored for experiments as described in section 2.2.2. When sufficient tissue was present, histological examination of the slices using haematoxylin and eosin staining was undertaken by a neuropathologist to assess tumour infiltration into the nominally normal tissue.

Bright field imaging of capillaries in human cortical brain slices during superfusion with aCSF with and without drugs, was performed as described in section 2.2.2.

3.2.2 Immunohistochemistry and confocal imaging of human tissue

Preparation of human cortical brain slices for immunohistochemistry and

confocal imaging was performed as described in Section 2.5.

3.2.3 Preparation and imaging of rodent brain slices with Neurotrace labelling

Preparation of rodent brain slices and brightfield imaging of capillaries and arterioles during superfusion with aCSF with and without drugs was performed as described in Sections 2.2.1.

In some of these rodent experiments pericytes were identified, during brightfield imaging with fluorescence and during 2-photon imaging. by incubating live slices in the fluorescent Nissyl dye, NeuroTrace 500/525 (1:25 dilution, with or without 10 μg/ml isolectin B_4 conjugated to Alexa 647, for 30 minutes) which was described by Damisah et al., 2017 to label capillary pericytes *in vivo*. This allowed clear identification of pericyte somata and their processes extending around and along the capillary wall. Fluorescence during brightfield imaging was obtained by excitation with an epifluorescence xenon lamp, passing through filters appropriate for the NeuroTrace dye) and 2-photon imaging was performed using a Zeiss LSM710 microscope (see Section 2.3.3 for further details).

Vessel diameter measurements and statistical analysis were performed as described in Section 2.7.

3.3 Results

3.3.1 Human neocortical capillary pericyte morphology and frequency

Human neocortical capillary pericytes could be identified by their ‘bump on a log’ morphology on the abluminal surface of vessels, surrounded by

fluorescently-tagged Griffonia simplicifolia isolectin B4 (IB4) labelling (Fig. 3.1a-b). Labelling blood vessels and pericytes with IB4 was successful only if performed on live cortical slices (whilst incubated in recovery solution); labelling performed on cortical tissue after PFA fixation was not effective. Pericytes were observed on the straight parts of capillaries as well as at capillary branch points, as reported previously for rodent CNS (Peppiatt et al., 2006; Hall et al., 2014). Human cortical pericytes were strongly labelled by antibody to the growth factor receptor PDGFRβ (Fig. 3.1b) and simultaneous labelling with DAPI demonstrated the round nuclei of pericytes (Fig. 3.1b). However, labelling for the other classical pericyte markers NG2 and CD13 was not successful, for reasons that are unclear.

As for arteriole smooth muscle (Fig. 3.2a), 36% of pericytes labelled for α-smooth muscle actin (Fig. 3.2b). The pericyte soma density was 1.53±0.01 per 100 μm of capillary (Fig. 3.2c) derived from 52 pericytes counted over 3413 μm of capillaries in confocal stacks from tissue from a 71 year old male with a probable glioma, and 42 pericytes counted over 2723 μm of capillaries in confocal stacks from tissue from a 55 year-old female with a probable meningioma; for both patients there was insufficient tissue to send it for histopathological examination to assess tumour infiltration.

3.3.2 Human pericytes constrict in response to noradrenaline and dilate in response to glutamate

In rodent CNS, pericytes constrict capillaries in response to superfused noradrenaline (mimicking noradrenaline release from the locus coeruleus), and dilate in response to superfused glutamate (mimicking neuronal activity),

as shown in Fig. 3.3a-b (reproduced from Figure 4 of Peppiatt et al., 2006). I tested whether human pericytes in the tissue from neurosurgical patients showed similar responses. Following a period of perfusion with aCSF, 5 (out of 8) human neocortical capillaries with a stable internal diameter were seen to constrict following application of noradrenaline (NA) (2 μM), with the internal diameter decreasing by 36±11%. There was a relaxation of constricted vessels following aCSF washout with capillary internal diameter returning on average to 89.7±5.6% of baseline (n=3 vessels tested). Following application of glutamate (0.5 mM) (in the presence of 2 μM noradrenaline), there was a dilatory response in 3 of 5 capillaries tested that were constricted by noradrenaline, with the mean internal diameter increasing by 50.1±14.0% of the constricted diameter (Fig. 3.3c-d) or 26.8±7.7% of the original vessel diameter before application of NA).

3.3.3 Variability in the responses to noradrenaline and glutamate

The eight vessels tested in the preceding section were from neocortical brain tissue slices obtained from four patients. One vessel constricted to NA (2 μM), dilated in response to application of glutamate (0.5 mM) in the presence of the NA, and relaxed following washout of both drugs in tissue obtained from a 62 year old male with a suspected glioma (there was evidence of tumour infiltration of this tissue on histopathological review). In tissue obtained from a 55 year old female with a suspected meningioma, one out of two vessels tested constricted in response to the application of NA (2 μM) but did not dilate in response to the application of glutamate with the NA and failed to relax following washout (this vessel was deemed not to have had a reliable response to noradrenaline). The second vessel tested from this

patient showed no response to the application of NA or glutamate (in the presence of noradrenaline). There was insufficient tissue from this patient to send it for histopathology. In tissue from a 73 year-old female with a suspected high-grade glioma, two out of three vessels tested constricted and dilated in response to the application of NA (2 μM) and glutamate (0.5 mM) (in the presence of noradrenaline) respectively, and histopathological examination of this tissue showed no evidence of tumour invasion. Two vessels tested in tissue obtained from a 73 year-old male with a probable glioma constricted to application of NA (2 μM) and relaxed following washout with aCSF. Neither of these vessels, however, dilated in response to the application of glutamate (0.5 mM) in the presence of NA (2 μM), and one vessel from this patient showed no clear response to the application of noradrenaline or glutamate. There was insufficient tissue from this patient to send it for histopathological examination.

In summary, constriction to noradrenaline and dilation to glutamate were seen both in patients with and without glioma infiltration of the tissue studied. However, responses were rather variable to both neurotransmitters. A similar variability was reported for rodent tissue by Peppiatt et al. (2006), and may reflect some pericytes not having contractile processes around the capillary.

3.3.4 Pericytes constrict in response to endothelin

To investigate whether pericytes constrict rodent capillaries in response to endothelin, I applied ET-1 (10 nM) either alone (Fig. 3.4a, b) or with a blocker of its type A or type B receptors. ET-1 evoked a strong pericyte-mediated constriction of capillaries (by 67±0.04%, $p=2x10^{-12}$), which was

blocked by the type A receptor blocker BQ123 (1 μM, $p=2.6x10^{-11}$), but not by the type B receptor blocker BQ788 (1 μM, p=0.91, Fig. 3.4b).

Arterioles are also known to constrict in response to endothelin (Brain, 1989), but an interesting difference was observed when the response of penetrating arterioles and of capillaries was compared (Fig. 3.5a-c): Arterioles constricted far more slowly in response to endothelin than capillaries, taking 31.3±4.3min (n=10) vs 7.1±1.0min (n=10) to constrict by 25% of the resting diameter ($p=3.44x10^{-5}$), respectively. Furthermore, arterioles often showed an initial dilation to endothelin, before a more severe constriction, suggesting that endothelin might be having two opposing effects via its different receptors. Blocking type B endothelin receptors with BQ788 abolished the initial dilation and greatly speeded the onset of the contractile response in arterioles, while blocking type A receptors with BQ123 abolished arteriolar constriction (Fig. 3.5b). Blocking nitric oxide synthase with N-nitroarginine (1 mM) had an effect similar to BQ788 on the time course of arteriole constriction (Fig. 3.5c), suggesting that endothelin's dilating action via ET_B receptors is mediated by NO production, possibly in endothelial cells although unpublished transcriptome data from the Barres group indicate that the highest level expression of the ET_B receptor is in astrocytes. In contrast, N-nitroarginine did not affect the pericyte response to endothelin (Fig 3.5c), suggesting that the ET_A receptor dominates in generating the capillary response to endothelin. The Barres' group transcriptome data show that ET_A receptors are highly expressed in pericytes, but also in astrocytes. Interestingly, a recent paper also reported that NO production plays a significant role in the generation of arteriole dilation by neuronal activity, but

not in the generation of capillary dilation (Mishra et al., 2016).

3.3.5 Pericytes labelled by Neurotrace have contractile ability

A notable feature of the response of capillaries to endothelin was that essentially all capillaries seemed to show a contraction or deformation in response to the drug. To examine whether this included mid-capillary bed pericytes that could be labelled with NeuroTrace (Damisah et al., 2017), I applied NeuroTrace to label these pericytes in live P21 rat brain slices (for methods, see section 3.2) and then applied ET-1 (10 nM).

I found that NeuroTrace-labelled pericytes were able to constrict capillaries in response to ET-1 under bright field plus fluorescent imaging (Fig. 3.6). Performing the same experiments with 2-photon imaging allowed clear visualisation of pericytes somata and their processes, and demonstrated that pericytes with longitudinally extensive processes are contractile *in vitro*, and retract their processes towards the soma, with the length of processes decreasing by 32±5% (n=4) over 20 mins in response to endothelin (ET 10 nM) (Fig. 3.7a, b). The implications of this are considered below.

3.4 Discussion

Though recently challenged (Damisah et al., 2016; Hill et al., 2014; Wei et al., 2016), the prevailing view is that subgroups of contractile pericytes contribute to regulation of capillary diameter and CNS blood flow (Biesecker et al., 2016; Dai et al., 2009; Kisler et al., 2017; Peppiatt et al., 2006; Fernández-Klett et al., 2010; Fernández-Klett & Priller, 2015; Hall et al., 2014; Mishra et al., 2016). Here I have shown that human cortical capillary

pericytes display a similar ‘bump on a log’ morphology to rodent pericytes and populate the capillary bed with a similar frequency to rodent cortical capillary pericytes (Hall et al., 2014). Like rodent cortical pericytes, human cortical pericytes express PDGFRβ, and approximately a third of them could be labelled for α-smooth muscle actin. Human pericytes also constricted and relaxed cortical capillaries following application of noradrenaline and glutamate respectively, with a magnitude and variability comparable to that of rodent capillary pericytes (Hall et al., 2014; Peppiatt et al., 2006). These findings - that a subgroup of human cortical capillary pericytes possess contractile apparatus and are capable of altering capillary diameter - suggest pericytes are capable of controlling human cerebral blood flow.

Endothelin is a potent vasoconstrictor and has been shown to constrict capillaries by acting on pericytes in the retina (Chakravarthy et al., 1992; Kawamura et al., 2002), the kidney (Kennedy-Lydon et al., 2015; Pallone & Silldorff, 2001) and the ureter (Borysova et al., 2013). I have now shown that endothelin acting through ET_A (and not ET_B) receptors is also a potent and highly reliable vasoconstrictor of cortical capillaries. Interestingly, cortical capillaries were found to constrict far more rapidly than cortical arteriloles (which initially dilated) in response to endothelin. This observation was shown to be due to endothelin acting on arteriolar ET_B receptors leading to release of vasodilatory NO. These findings raise the possibility that endothelin-mediated cortical capillary constriction plays an important role (perhaps more important than arteriolear constriction) in disease states thought to involve pathological endothelin release, such as subarachnoid haemorrhage (Bertsch et al., 2001; Pluta et al., 1997) and Alzheimer’s disease (Deane et al., 2003;

Thomas et al., 2016: see Chapter 5 for further work on the role of endothelin in Alzheimer's disease).

NeuroTrace has recently been shown to label only non-α smooth muscle containing pericytes *in vivo* (Damisah et al., 2017), but I found that NeuroTrace-labelled pericytes in live P21 rat brain slices are contractile and able to constrict capillaries in response to ET1 (10 nM, under bright field plus fluorescent imaging: Fig. 3.7a). Performing the same experiments with 2-photon imaging allowed clear visualisation of pericytes' somata and their processes, and demonstrated that pericytes with longitudinally extensive processes are contractile *in vitro*, and appear to retract their processes towards the soma in response to ET1 (10 nM, Fig. 3.7b).

These findings argue against those who have proposed that pericytes are not contractile (Damisah et al., 2017; Hill et al., 2015; Wei et al., 2016): Against long-standing convention, some researchers have re-defined spatially isolated, α smooth muscle- containing (contractile) cells, with a bump on a log morphology and circumferential processes wrapping (up to 4th branch order) capillaries, to be smooth muscle cells rather than pericytes (Damisah et al., 2017; Hill et al., 2015). In doing so they have also redefined what they term pericytes, as being all other spatially isolated, non-α-smooth muscle containing (and therefore non-contractile) cells with longitudinally extending processes wrapping the capillary bed. This has generated debate about what precisely defines pericytes (particularly at a molecular level), given that a specific pericyte-defining marker has yet to be discovered (Attwell et al., 2016).

Setting aside these semantic arguments, the branch-order level of the capillary bed where capillary diameter and cerebral blood flow are controlled by pericytes remains to be determined. Do pericytes control cerebral blood flow throughout the entire capillary bed, or just at the arteriole end of the bed where dilatory responses and smooth muscle actin expression are seen in up to the 4th branching order of capillaries from the arteriole (Hall et al, 2014; Hill et al., 2015)? Whilst it is clear that α-smooth muscle containing pericytes (with circumferential processes) are capable of contracting and reducing capillary diameter (Hall et al, 2014; Hill et al., 2015), it is not known whether pericytes which do not reliably label for α-smooth muscle actin, and possess longitudinally extensive processes, are able to alter capillary diameter and/ or contribute to controlling cerebral blood flow. Recently, it has been demonstrated that cardiac pericytes, which label for β-actin and γ-actin in addition to α- smooth muscle actin, contribute significantly to the post-ischaemic no-reflow phenomenon in the heart by constricting cardiac capillaries (O'Farrell et al., 2017). Potentially, therefore, capillary pericytes in the brain, which do not label for α-smooth muscle actin, may also use β and/γ actin as their mechanical substrate for contraction. Furthermore, as I have demonstrated, pericytes with processes extending longitudinally might also be contractile and thereby alter the compliance of the capillary wall to passing red blood cells, thus providing a mechanism for regulating blood flow that differs from the notion of increasing resistance by decreasing capillary diameter (see Chapter 6 for suggested further work relating to these findings).

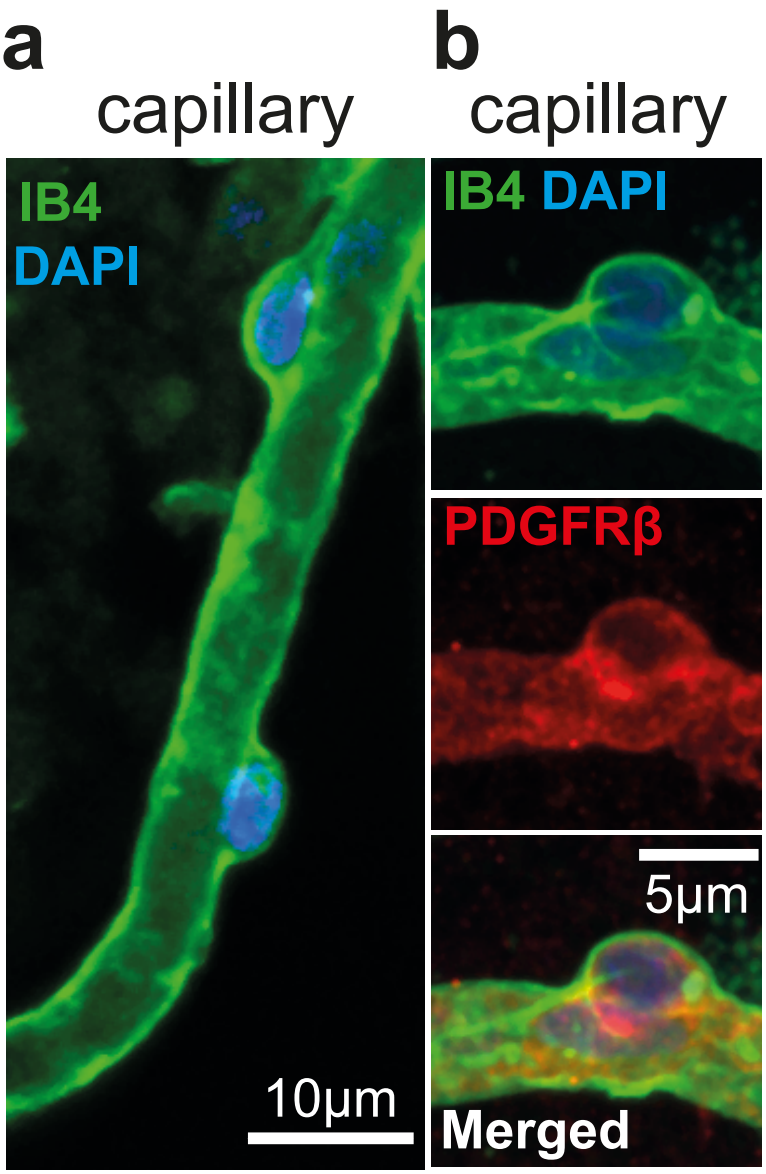

Figure 3.1 Human pericyte morphology. (a) Isolectin B_4 (green) labelled capillary in a cortical slice, with two pericyte somata (arrowheads) outlined by their basement membrane. DAPI (blue) labels nuclei. (**b**) Pericyte labelled with antibody to PDGFRβ (red).

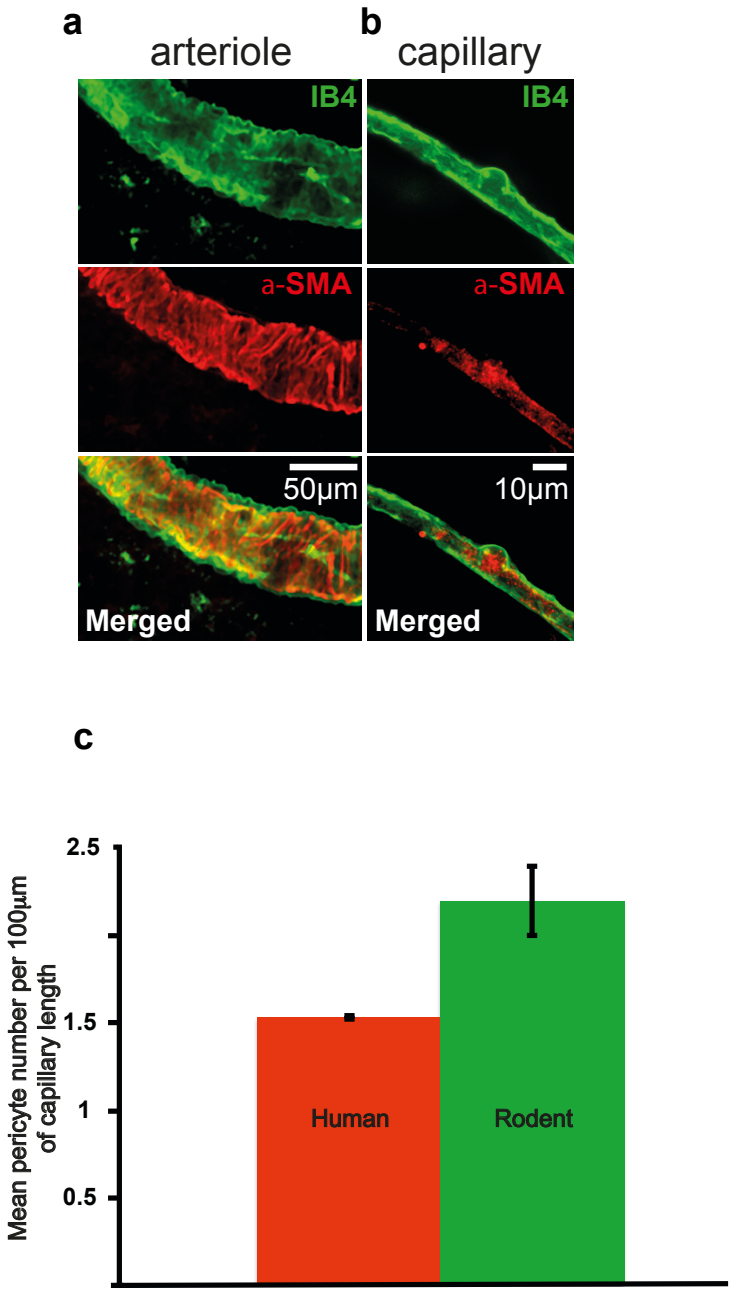

Figure 3.2 Actin expression by human pericytes and pericyte number. Labelling of an arteriole (**a**) and a pericyte (**b**) with antibody to α-smooth muscle actin (red) in a human brain slice labelled with isolectin B4 (green) to outline the basement membrane of the vessels and pericytes. (**c**) Mean number of pericytes per 100 µm length of human and rodent (data taken from Hall et al, 2014) cortical capillaries.

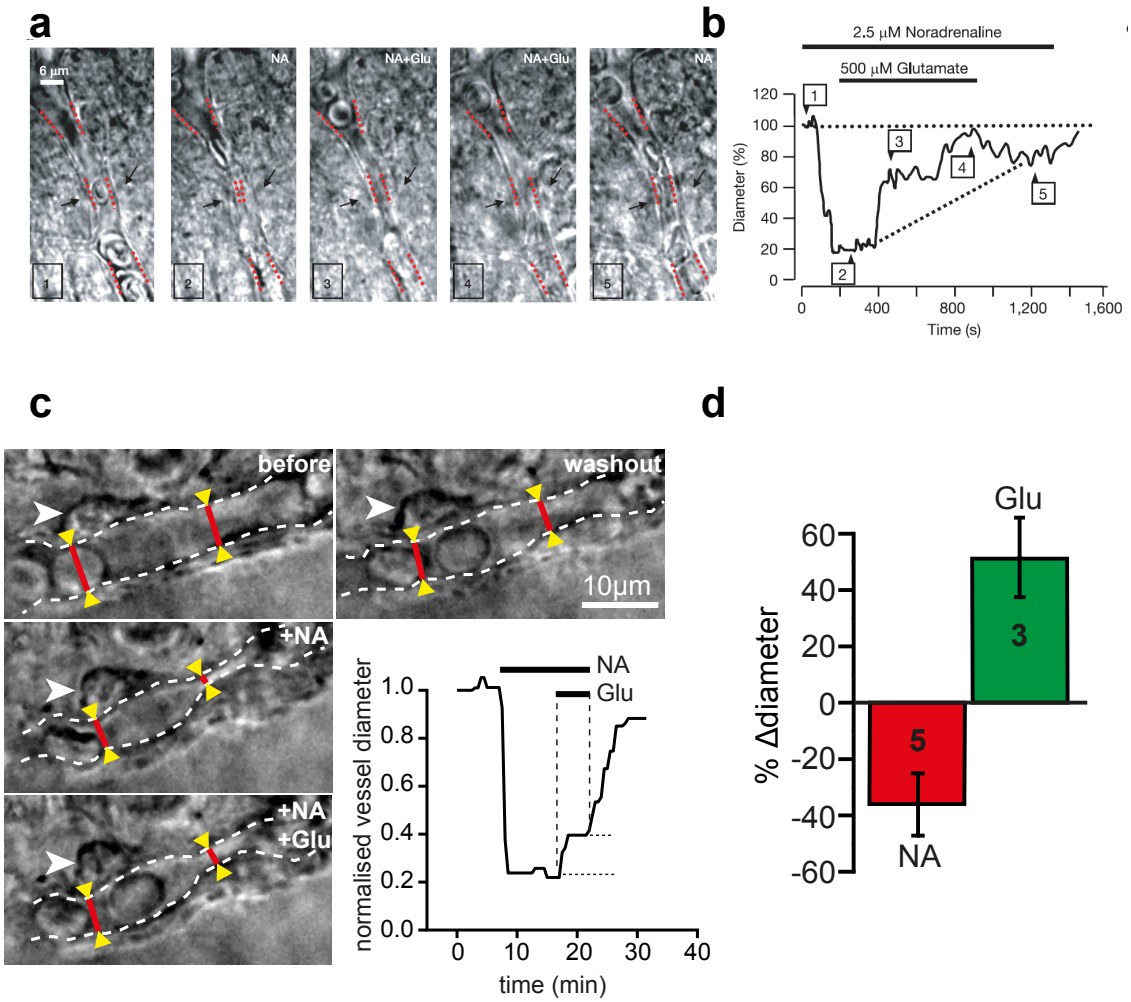

Figure 3.3 Human cortical pericytes constrict and dilate capillaries in response to noradrenaline and glutamate, respectively. (a) Images, and (b) quantification of diameter, in response to superfusion of 2 µM noradrenaline and 0.5 mM glutamate for a pericyte in a rat cerebellar slice (from Peppiatt et al., 2006). **(c)** Images of a capillary (dashed lines indicate wall) and pericyte soma (arrowhead) in a live human brain slice before drug application (*before*), in the presence of 2 µM superfused noradrenaline (+NA), with 2 µM NA and 500 µM glutamate superfused (+NA +Glu), and after stopping drug superfusion (*washout*). Graph shows time course of capillary diameter at right red line throughout the experiment. **(d)** Mean glutamate-evoked dilation and noradrenaline-evoked constriction in experiments as in (c) (change in diameter quantified relative to that before application of each drug; relative to the pre-noradrenaline diameter the glutamate-evoked dilation was 26.8±7.7%).

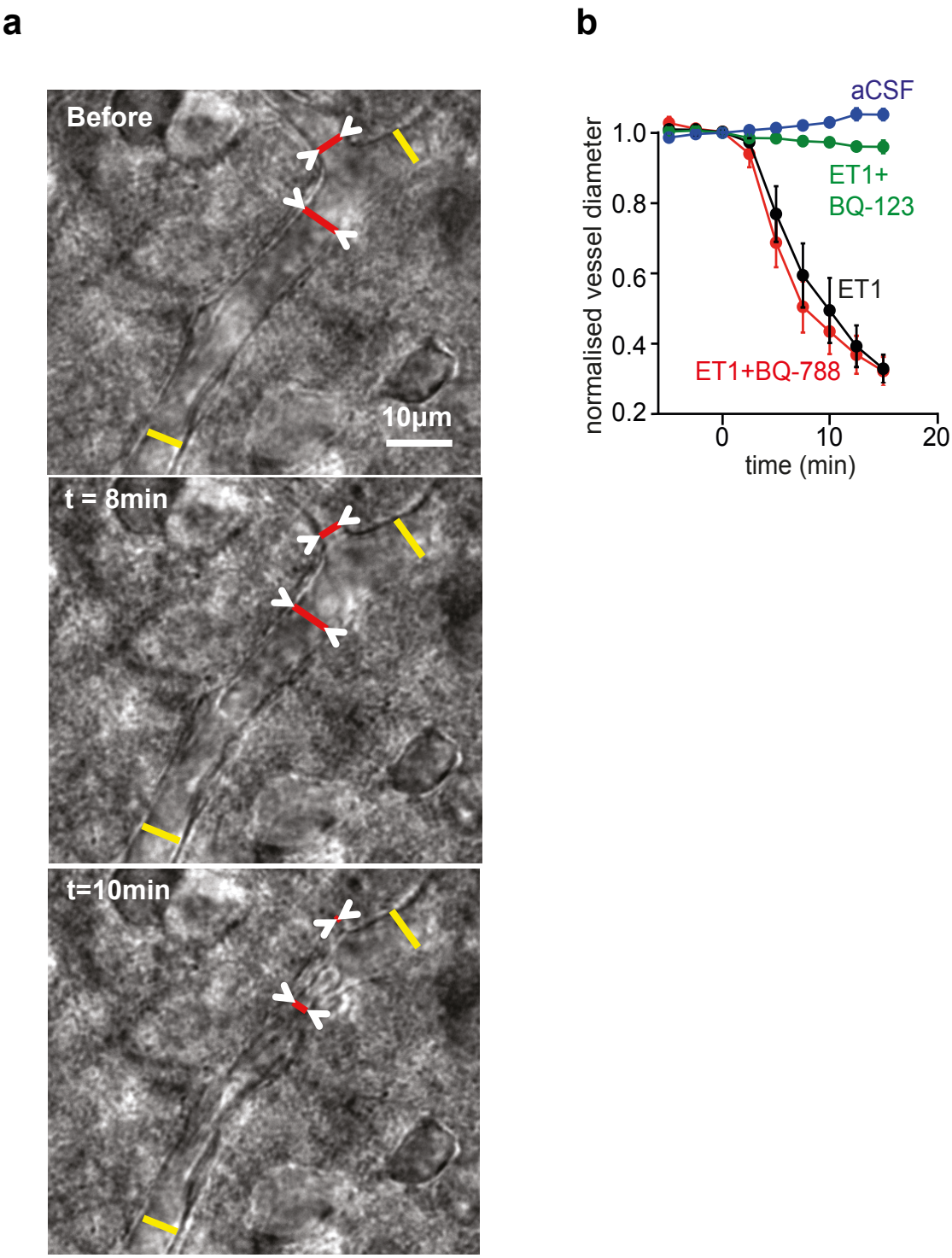

Fig. 3.4 Endothelin constricts cortical capillaries. (a) Bright field images showing ET (10 nM) evoked focal constriction of a cortical capillary **(b)** Mean time course of normalised capillary diameter during superfusion with aCSF (n=10), ET1 alone (10 nM, n=10), or ET1 in the presence of the ET-A receptor blocker BQ-123 (1 nM, n=10) or the ET-B receptor blocker BQ-788 (1 μM, n=12).

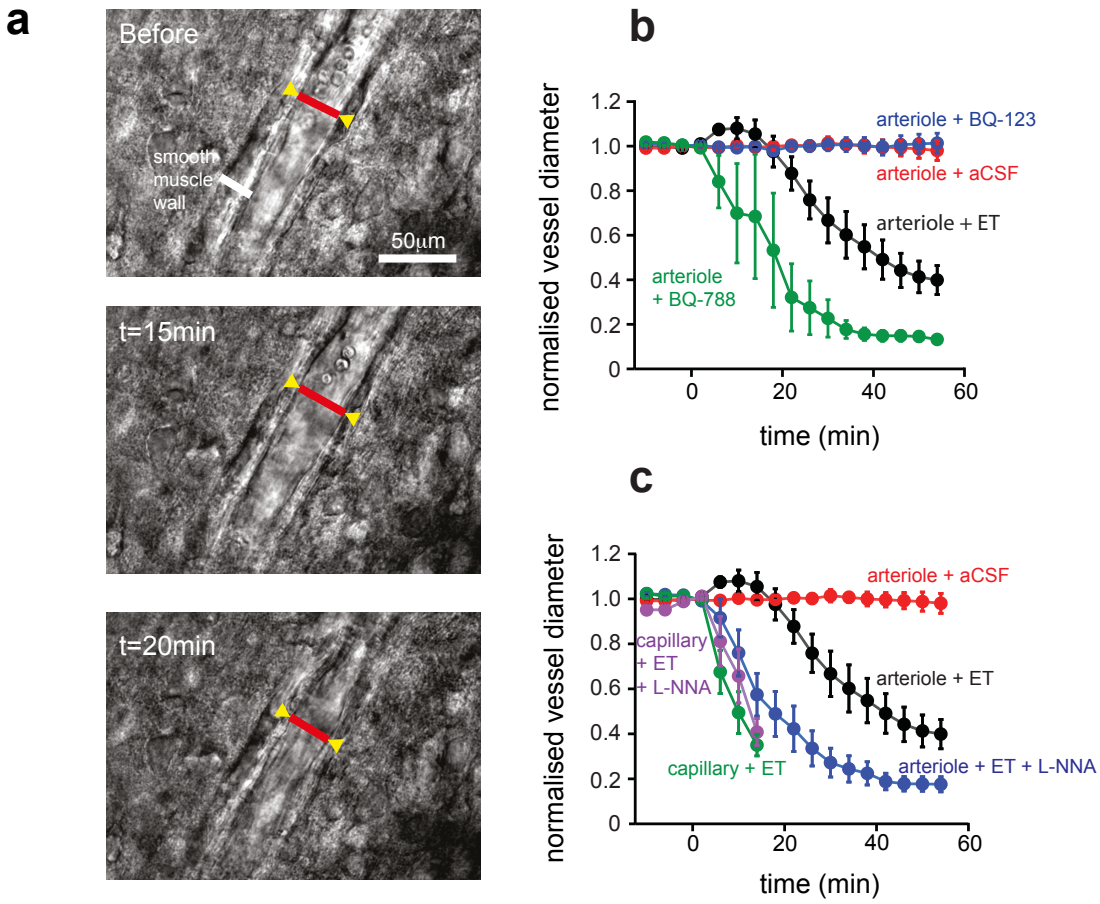

Figure 3.5 Capillaries constrict faster than arterioles in response to endothelin. (a) Bright field images showing ET (10 nM) evoked constriction of a cortical arteriole (white line highlights wall of smooth muscle). **(b)** Time course of normalised arteriole diameter during superfusion with aCSF (n=8), ET1 alone (10 nM, n=10), or ET1 in the presence of the ET-A receptor blocker BQ-123 (1 nM, n=11) or the ET-B receptor blocker BQ-788 (1 μM, n=6). **(c)** Time course of normalised arteriole diameter during superfusion with aCSF (n=8), ET1 alone (10 nM, n=10), or ET1 in the presence of the NO blocker L-NNA (1 mM, n=12) together with time course of normalised capillary diameter during superfusion with ET1 alone (10 nM, n=10) or ET1 in the presence of NO blocker L-NNA (1 mM, n=9).

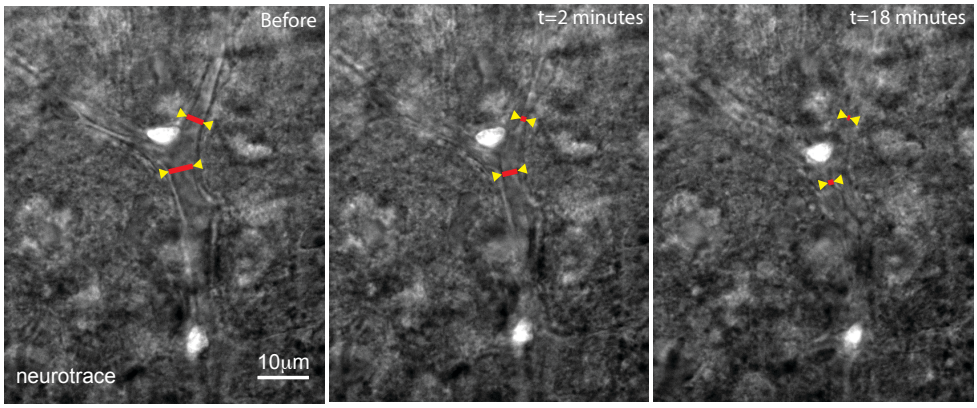

Figure 3.6 NeuroTrace-labelled pericytes constrict capillaries in response to endothelin. Brightfield plus fluorescent imaging of (NeuroTrace-labelled) pericyte-mediated constriction of a cortical capillary imaged at different times (shown in the pictures) before and after the application of ET (10 nM).

a

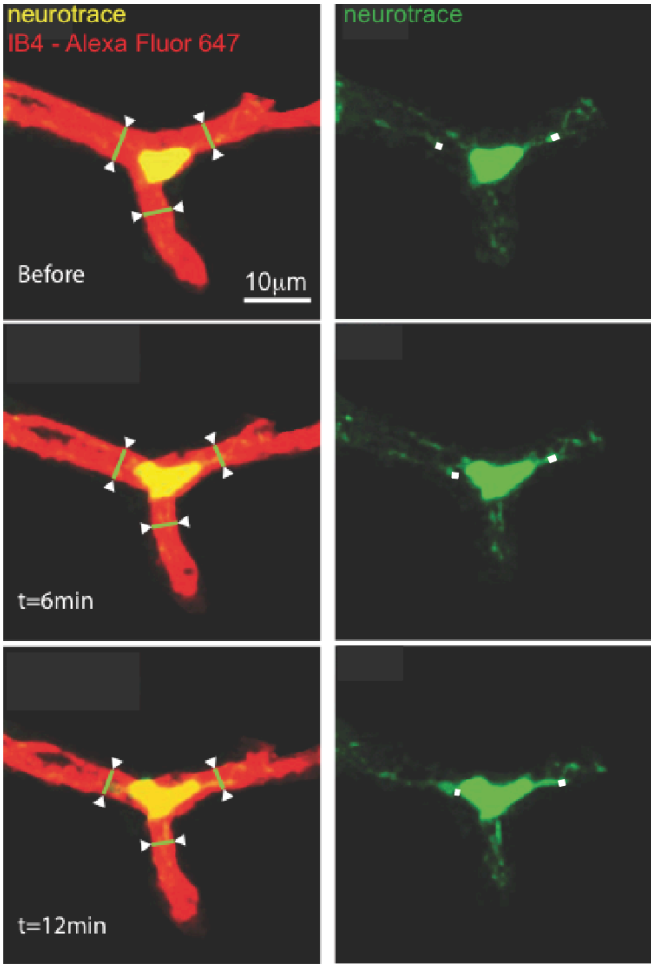

b

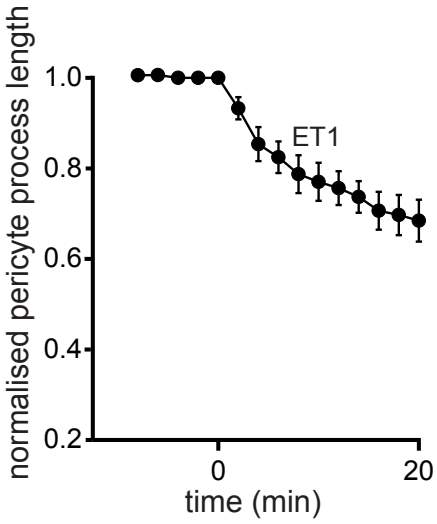

Figure 3.7 Pericytes processes retract towards the soma whilst constricting capillaries in response to endothelin. (a) Left panels, top-bottom: 2-photon images of IB_4 (red) and NeuroTrace (yellow) fluorescence of a capillary and pericyte respectively, in rat cortical slices in normal aCSF and after superfusion with ET (10 nM) (at the time points given), showing focal capillary constrictions next to the pericyte soma. **Right panel top-bottom:** 2-photon images of the same pericyte displaying NeuroTrace fluorescence alone (green) highlighting pericyte processes (white marker) and their retraction towards the soma following superfusion with ET. **(b)** Graph shows mean change of process length of 4 pericyte processes (2 processes from each of 2 pericytes) following exposure to ET (10nM).

Chapter 4: Preventing pericyte constriction of brain capillaries and death in rigor during simulated ischaemia

4.1 Introduction

Ischaemic stroke is a leading cause of adult disability in the United Kingdom and United States, with many survivors left dependent on others for activities of daily living (Royal College of Physicians National Sentinal Stroke Clinical Audit (2011)). In experimental models of stroke, both the duration and the severity of ischaemia have been shown to determine whether irreversible damage occurs (Lo et al., 2003). Treatment of patients with intravenous tissue plasminogen activator (rt-PA) within 4.5 hours of stroke onset increases the probability of a favourable outcome (Emberson et al., 2014). However, more than half of patients treated with rt-PA show a lack of recovery, which may be attributable to inadequate reperfusion or reperfusion occurring too late to prevent tissue infarction (von Kummer, 2009; Wechsler, 2011). Indeed, it has been demonstrated that even after re-opening of a blocked artery there is a long-lasting decrease in blood flow (the 'no-reflow' phenomenon) which may be due to pericytes constricting capillaries and subsequently dying in rigor following cerebral ischaemia (reviewed by O'Farrell & Attwell, 2014). During simulated ischaemia in brain slices, it has been demonstrated that neocortical grey matter and cerebellar white matter capillaries are constricted by pericytes within ~15 minutes and pericytes die in rigor within ~40 minutes, while *in vivo* pericytes die following 90 min of middle cerebral artery occlusion (MCAO) (Hall et al., 2014). An increase in pericyte [Ca^{2+}], following ion pump inhibition by ATP depletion, may partly explain why

pericytes constrict in ischaemia (see section 1.2.16). Indeed, removal of external calcium significantly reduced pericyte death (Hall et al., 2014).

Based on the premise that, during ischaemia, calcium-evoked pericyte constriction and death in rigor leads to a long-lasting capillary constriction (which will decrease effective reperfusion of ischaemic brain tissue, even following thrombolysis), pericytes represent an attractive therapeutic target in the treatment of acute stroke. It seems reasonable to propose therefore, that a treatment that prevents pericyte constriction and death in ischaemia would have a beneficial effect in acute stroke.

Against this background, I assessed whether blockade of particular ion channels and receptors involved in pathways leading to constriction of the cerebral microvasculature would prevent pericyte constriction of capillaries and reduce pericyte death during simulated ischaemia. I studied blockage of

(i) L-type Ca^{2+} channels (with nimodipine)

(ii) endothelin A receptors (with BQ-123)

and

(iii) thromboxane A_2 receptors (with ICI-192605)

for the following reasons:

4.1.1 L-type Ca^{2+} channel blockade

L-type Ca^{2+} channels may exist in one of three distinct states, termed modes. In mode 0, the channel does not open in response to a depolarisation. In mode 1, depolarisation produces a low opening probability, and if opening does occur, it is brief. In mode 2, depolarization results in a

very high chance of opening probability, and single openings are prolonged (Hess et al., 1984). Nimodipine is a diyhydropyridine class of Ca^{2+} entry blocker (partly selective for the cerebral vasculature (Kazda and Towart, 1982), which binds specifically to the α_1 subunit of the L-type calcium channel and affects its function by selectively binding to and maintaining channels in mode 0, thus preventing channel opening and reducing Ca^{2+} entry (Hess et al., 1984; Rang et al., 2016). Nimodipine may be administered orally or intravenously, and is well absorbed from the gastrointestinal tract. It has few idiosyncratic adverse effects and is usually well tolerated, but it may cause flushing and headache because of its vasodilatory action (Katz & Leach, 1987). Given that Ca^{2+} entry into pericytes is necessary for pericyte contraction (Sakagami et al., 2001), and that uncontrolled calcium entry overload during ischaemia is likely to be responsible for their death (Hall et al., 2014), I investigated whether blockade of L-type Ca^{2+} channels with nimodipine may help prevent unwanted pericyte constriction and death during ischaemia.

4.1.2 ET_A receptor blockade

Endothelin (ET), a potent vasoconstrictor with a long-lasting effect, is thought to act in a paracrine rather than a systemic manner (Clozel et al., 1993; Hickey et al., 1985; Yanagisawa et al., 1986) and is expressed in 3 isoforms: ET-1 (the only ET present in vascular endothelial cells) is expressed in many tissues, ET-2 is present only in the gut and kidneys, and ET-3 is present in the brain, lung, intestine and adrenal gland. ET-1 and ET-2 act on 2 types of receptor, ET_A and ET_B receptors, both of which are G-protein coupled, while ET-3 acts mainly on ET-B receptors. Activation of ET_A

receptors produces vasoconstriction, whilst activation of ET_B receptors leads to vasodilation. ET_A-mediated vasoconstriction is believed occur via the G-protein controlled-phospholipase C/inositol trisphosphate (IP_3/diacylglycerol (DAG) second messenger pathway raising $[Ca^{2+}]_i$, where receptor activation triggers phospholipase C catalysed production of IP_3 (and DAG), which then acts to release cytosolic Ca^{2+} from intracellular stores to trigger smooth muscle contraction. ET_B receptors evoke dilation by stimulating NO production (Liu et al., 2003).

Endothelin is released during ischaemia and subarachnoid haemorrhage (Pluta et al., 1997; Dawson et al., 1999; Bertsch et al., 2001; Lampl et al., 1997) and blockade of ET receptors has been shown in animal models to prevent post-ischaemic vasoconstriction (Patel et al., 1996). Additonally, ET receptor blockade was shown to prevent the decrease in cerebral blood flow that occurs following subarachnoid haemorrhage, and to improve brain blood flow following cerebral ischaemia (Brunner and Opie, 1998; Clozel et al., 1993; Dawson et al., 1999; Galiuto et al., 1998; Rodríguez, 2011; Schaller, 2008; Ziv et al., 1992). Furthermore, ET can raise the intracellular Ca^{2+} level within, and cause contraction of, cultured retinal pericytes (at a concentration of 0.1 nM: Chakravati et al., 1992) as well as producing contraction of pericytes in rodent kidney slices (Kennedy-Lydon et al., 2015). Notably, ET has also been demonstated to contribute to cerebral post-ischaemic hypoperfusion (Spatz et al., 1996). Furthermore (as detailed in Chapter 3), I have now shown that endothelin acting through ET_A (and not ET_B) receptors is also a potent and highly reliable vasoconstrictor of cortical capillaries. Thus, it seems reasonable to propose that blockade of ET_A

receptors during simulated ischaemia would reduce pericyte constriction.

4.1.3 TXA_2 receptor blockade

Thromboxane A_2 (TXA_2) is a vasoconstrictor and pro-thrombotic prostanoid, which acts on thromboxane prostanoid (TP) receptors (a type of G-protein coupled receptor) found on monocytes/macrophages, platelets, endothelial cells and vascular smooth muscle cells (Capra et al., 2013). It is produced (mainly by platelets, but also by microglia) from the metabolism of the eicosanoid precursor, arachidonic acid, by cyclo-oxygenase (COX)-1, COX-2 and TXA_2 synthase (TXA_2), and its synthesis is increased and it is released during acute (cerebral) ischaemia (Shohami et al., 1987); Koudstaal et al., 1993; Nakahata, 2008). Of note, this agent evokes pericyte contraction (Dodge et al., 1991; Fernandez-Klett et al., 2010; Mishra et al., 2016). I therefore investigated whether blocking TXA_2 receptors would have an effect on pericyte constriction during simulated ischaemia.

4.2 Methods

4.2.1 Animals and preparations

The experiments described in this chapter were performed on live 300 µm cortical slices from P21 Sprague-Dawley rats of either sex, prepared on a vibratome in ice-cold NMDG-based slicing solution and stored at room temperature in recovery solution (as described in section 2.2.1)

4.2.2 Brightfield imaging of capillaries during ischaemia

Brightfield imaging was performed of cortical capillary responses to superfusion with aCSF (control), ischaemic solution and ischaemic solution with the following drugs added: 3 µM nimodipine, 1 µM BQ-123 (an ET_A

receptor blocker), 1 μM ICI192605 (a TXA_2 receptor blocker) and 7.5 μM prodidium iodide (PI) (to label cells with membranes that had become non-specifically permeable which were presumed to be dying). During simulated ischaemia experiments, slices were superfused with aCSF prior to superfusion of ischaemic solution (prepared as in section 2.1), whilst capillaries were being located. Only capillaries with at least 30 μm of vessel wall along the length of the capillary in focus within a single plane were selected for imaging. The microscope objective was continually adjusted during experiments to ensure that the selected portion of the vessel remained in sharp focus throughout. For the first 10 minutes of imaging, slices were perfused with aCSF (to ensure the selected vessel had a stable baseline diameter) before switching to perfusion with ischaemic solution or ischaemic solution with drugs for 60 minutes (for further detail see section 2.3).

4.2.3 Fluorescent imaging during ischaemia

The number of dead pericytes per 100 μm of capillary following 60 minutes of simulated ischaemia was measured during live imaging by identifying PI labelled cells with pericyte morphology (using fluorescence microscopy) which also had pericyte morphology on corresponding brightfield imaging. As stated in section 1.2.15, pericytes produce a characteristic ‘bump on a log’ appearance as they wrap around endothelial cells (EC) on the outside of the capillary and are completely surrounded by the basal lamina. They can be distinguished from ECs, which have elongated, cigar-shaped nuclei, by their prominent round nuclei (Dore-Duffy and Cleary, 2012). Fluorescent images were obtained (with an epifluorescent xenon lamp and appropriate filters) every 5 minutes with an exposure time of 2.5 sec (for

further detail see section 2.3).

4.2.4 Analysis and Statistics

Capillary internal diameters were measured as described in Section 2.3.4. Statistical analysis was performed as described in section 2.7.

4.3 Results

4.3.1 Ischaemia induces a constriction of pericytes

The internal diameter of a neocortical capillary did not decrease when perfused with aCSF for 60 minutes (Figure 4.1a, c) replicating previous data from this laboratory (Hall et al., 2014). However, capillaries were seen to constrict vigorously within ~15-20 minutes when perfused with ischaemic solution, with the mean capillary internal diameter decreasing by 69.6% (n=5) ($p=3.4x10^{-6}$ vs control), following 20 minutes of perfusion with ischaemic solution (Figure 4.1b, c).

4.3.2 Nimodipine slows pericyte-evoked capillary constriction in ischaemia

In comparison to perfusion with ischaemic solution alone, pericyte constriction was inhibited by the presence of nimodipine, with the capillary internal diameter decreasing by only 27.6±11% (n=6) following 20 minutes of simulated ischaemia plus nimodipine ($p=0.028$ compared with no nimodipine) (Fig. 4.2a). With prolonged ischaemia (> 25 minutes), the inhibitory effect of nimodipine on pericyte constriction lessened to being just outside statistical significance, with a mean normalised capillary diameter at 45 min reducing to 19±3% (n=7) and 45±11% (n=7) ($p=0.066$) for simulated ischaemia and

simulated ischaemia plus nimodipine respectively (Fig. 4.2a).

4.3.3 Endothelin A receptor block does not affect pericyte constriction in ischaemia

There was no difference in pericyte constriction during simulated ischaemia at 20 minutes with or without the presence of an ET_A receptor blocker (BQ123, 1 μM). The internal capillary diameter decreased in ischaemia by 65±13% (n=5) with, and by 64±5% (n=4) without the ET_A receptor blocker present (Fig. 4.2b). These data were not significantly different (p=0.97).

4.3.4 Constriction of pericytes in ischaemia is unaffected by the presence of the thromboxane A_2 receptor blocker ICI-192605

I investigated capillary constriction by pericytes during simulated ischaemia for at least 20 minutes with and without the presence of the TXA_2 receptor blocker ICI-192605 (1 μM). The mean capillary diameter decreased in ischaemia by 57±10% (n=5) and by 45±14% (n=6) for ischaemia with and without ICI-192605, respectively (Fig 4.2c, not significantly different, p=0.5). Pericyte induced capillary constriction during ischaemia does not therefore appear to be affected by blockade of TXA_2 receptors.

4.3.5 Ischaemia leads to pericyte death

In accordance with data previously published by this laboratory (Hall et al., 2014), after capillaries are constricted by pericytes during simulated ischaemia, applying propidium iodide revealed that pericytes die approximately 30 to 40 minutes (Fig. 4.3a, b). The presence of nimodipine showed a tendency to delay, (by approximately 5 min), but not prevent,

pericyte death in the early stage of ischaemia, although this result did not reach statistical significance (p=0.9, Kolmogarov-Smirnov test on the entire time course of death, Fig. 4.3b). For example, with simulated ischaemia, at 30 minutes the mean number of dead pericytes/100 μm of capillary was 0.85±0.52 (n=5 capillaries) whilst with simulated ischaemia plus nimodipine, the mean number of dead pericytes/100 μm capillary was 0.25±0.16 (n=5 capillaries, p=0.31 compared with no nimodipine).

4.4 Discussion

In vitro, it has been shown that removing extracellular Ca^{2+} inhibits pericyte constriction to electrical stimuli and decreases pericyte death in simulated ischaemia (Peppiatt et al., 2006; Hall et al., 2014). I therefore tested the hypothesis that reducing Ca^{2+} entry into pericytes by blocking L-type voltage gated Ca^{2+} channels would reduce pericyte constriction and death in ischaemia.

I demonstrated that, in simulated ischaemia, pericytes constrict neocortical capillaries within ~15 minutes and then die in rigor within ~40 minutes (replicating previous data from this laboratory: Hall et al., 2014). I then showed that the L-type Ca^{2+} channel blocker nimodipine, when present throughout the ischaemia, significantly delayed pericyte-mediated constriction of capillaries, and showed a possible trend towards prolonging pericyte survival in the early stage of ischaemia. I assume that nimodipine exerted these effects by acting directly on pericyte L-type Ca^{2+} channels, although an indirect action cannot be ruled out.

With ongoing ischaemia (>30 min), the inhibitory effect of nimodipine on

pericyte constriction waned and pericyte death was not prevented. This is expected because reperfusion was not mimicked by removing the ischaemic conditions, and furthermore the block of ATP production by iodoacetate and antimycin, used to inhibit glycolysis and oxidative phosphorylation respectively, is irreversible. Therefore, an experimental model using instead oxygen-glucose deprivation to simulate ischaemia (without iodoacetate and antimycin), followed by re-application of the oxygen and glucose to simulate reperfusion, may model better the extent to which nimodipine would inhibit ischaemia-induced pericyte constriction and death. Of course an *in vivo* experimental model of stroke (MCAO occlusion) would provide the most robust model in which to examine the effect of nimodipine on pericyte constriction and death in ischaemia (see Chapter 6 – suggestions for future work). Indeed, unpublished work by other members of the Attwell group has shown that nimodipine reduces pericyte death after oxygen-glucose deprivation of cortical slices, see Fig. 6.1 below).

The data I have presented above may help to explain why nimodipine can be used therapeutically to treat subarachnoid haemorrhage (SAH). Nimodipine has been shown in clinical trials to be the only pharmacological treatment to improve outcome in patients with SAH produced by aneurysm rupture (Feigin et al., 1998; Dorhourt et al., 2007). Aneurysmal rupturing of blood into the subarachnoid space, and less often the brain parenchyma and ventricles, has two main consequences. Firstly, it causes early brain injury from a combination of the direct effects of intracranial blood itself, a mass effect (causing compression of vital structures, raised intracranial pressure and reduced cerebral perfusion), the development of hydrocephalus and

acute global ischaemia. These effects will perturb fluid and ion balance, activate the sympathetic nervous system and pro-inflammatory pathways, and may lead to further, serious complications such as neurogenic pulmonary oedema and acute cardiomyopathy (Macdonald, 2014). Secondly, SAH may cause delayed cerebral ischaemia (DCI), a clinical syndrome of focal neurological and/or cognitive deficit that occurs unpredictably in around 30% of patients 3-14 days post SAH (Vergouwen, 2010). DCI is now the main factor associated with poor outcome following survival of the initial subarachnoid bleed and aneurysm treatment (Kassell, 1990). The pathogenesis of DCI is poorly understood, but angiographically-visible vasospasm, cortical spreading ischaemia, microthrombosis, microcirculation constriction and delayed effects of early brain injury have been implicated as possible factors (Macdonald, 2014). The link between angiographic vasospasm and the development of DCI, however, has been called into question because it has been shown that successful reduction of angiographic vasospasm does not improve patient outcome (Etminan, 2011). It has also been found that only 50% of patients with angiographic vasospasm develop DCI (Fisher, 2011; Crowley, 2011). Moreover, treatment with nimodipine significantly reduces the risk of developing DCI, but does not, in most clinical trials, lead to a reduction of angiographic vasospasm (Petruk et al., 1998).

My data suggest that nimodipine reduces pericyte constriction of cortical capillaries and may also reduce pericyte death in rigor under ischaemic conditions. Conceivably, capillary constriction by pericytes and subsequent death in rigor may be a factor in the development of DCI and explain the

mechanism by which nimodipine protects against DCI. Indeed, it has been suggested that following SAH, haemoglobin, and its breakdown products and other vasoactive substances, come into contact with pericytes when these substances are cleared from the CSF along the perivascular spaces (adjoining the basement membranes of arterioles and capillaries) to drain to the cervical lymph nodes, and that these substances could trigger pericyte constriction by mechanisms involving oxidative stress, superoxide formation and NO depletion (Ostergaard et al., 2013).

Nimodipine has not been conclusively shown to be of benefit in treating stroke patients (Zhang et al., 2012; Horn and Limburg, 2001). However, clinical trials investigating the efficacy of nimodpine as a treatment for ischaemic stroke were performed in the pre-thrombolyis era. My data suggest that nimodipine warrants further investigation as a potential treatment to be given soon after stroke onset (to delay pericyte constriction and possibly death), in combination with or perhaps before rt-PA is administered. Ideally nimodipine could be administered via a catheter placed near the occluding thrombus, in order to minimise its action in other vascular beds of the body.

In contrast to blockade of L-type Ca^{2+} channels with nimodipine, ET_A receptor blockade and TXA_2 receptor blockade did not delay capillary constriction by pericytes, suggesting that neither ET-1, nor TXA_2 have a crucial role to play in the mechanism generating capillary constriction during ischaemia. The lack of effect of ET_A block is surprising since this has previously been found to reduce the no-reflow phenomenon after ischaemia (Dawson et al., 1999): conceivably this effect reflects an action on arterioles or arteries upstream of the capillaries that I have studied here. The lack of

effect of TXA_2 receptor block is consistent with previous data showing that block of its synthesis did not prevent the lack of reperfusion that occurs after ischaemia (Prough et al., 1986), although Tokiyoshi et al. (1991) found that it was effective after subarachnoid haemorrhage. However, as stated above, the use of iodoacetate and antimycin, to simulate tissue ischaemia in brain slices (by completely inhibiting ATP generation by glycolysis and oxidative phosphorylation, respectively) may perhaps be too toxic to the brain tissue for prevention of ET_A and TXA_2 effects to demonstrate any beneficial effect. Therefore, an experimental model using oxygen-glucose deprivation only to simulate ischaemia (without iodoacetate and antimycin) followed by re-application of the oxygen and glucose, or MCAO *in vivo*, may determine better whether ET_A and/or TXA_2 blockade reduces ischaemia-induced pericyte constriction and death (see below – Chapter 6, suggestions for future work).

a

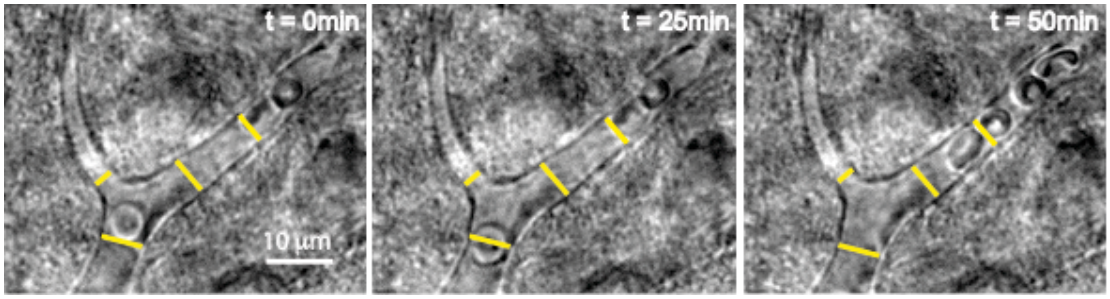

b

c

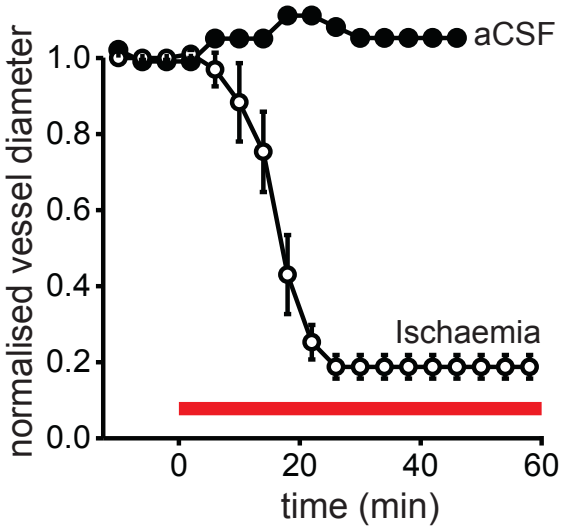

Figure 4.1 Constriction of pericytes in response to simulated ischaemia. **(a)** Repeated images of a slice superfused with control solution show no change of diameter. **(b)** Focal capillary constriction in simulated ischaemia Times on images are times in control or ischaemic solution. (**c**) Mean capillary diameter as a function of time in control solution (n=2) and in ischaemia (n=6).

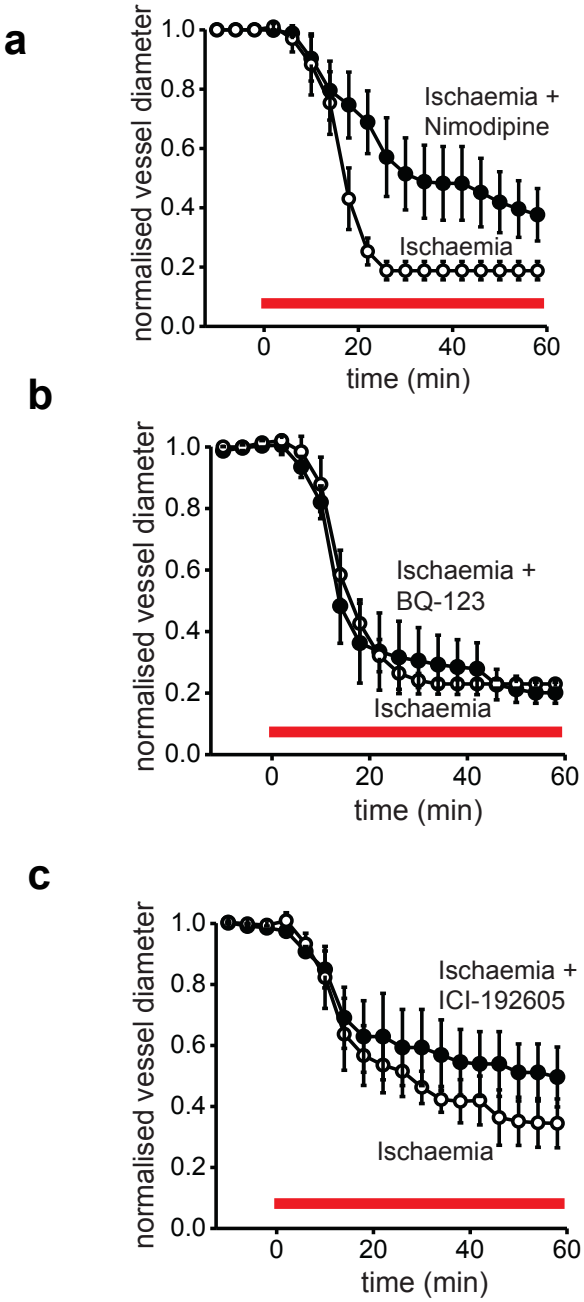

Figure 4.2 Constriction of pericytes in response to simulated ischaemia in the presence and absence of nimodipine, an endothelin A receptor blocker and a thromboxane A_2 receptor blocker. (a) Mean capillary diameter as a function of time with simulated ischaemia alone (n=6, data from Fig. 4.1) or simulated ischaemia in the presence of nimodipine (n=7) (**b)** Pericyte constriction was not significantly different in the presence (n=5) or absence (n=4) of the thromboxane A_2 receptor blocker BQ123 (1 μM) during ischaemia. (**c**) Pericyte constriction was not significantly different in the presence (n=6) or absence (n=5) of the endothelin A receptor blocker ICI-192605 (1 μM) during ischaemia (n=5).

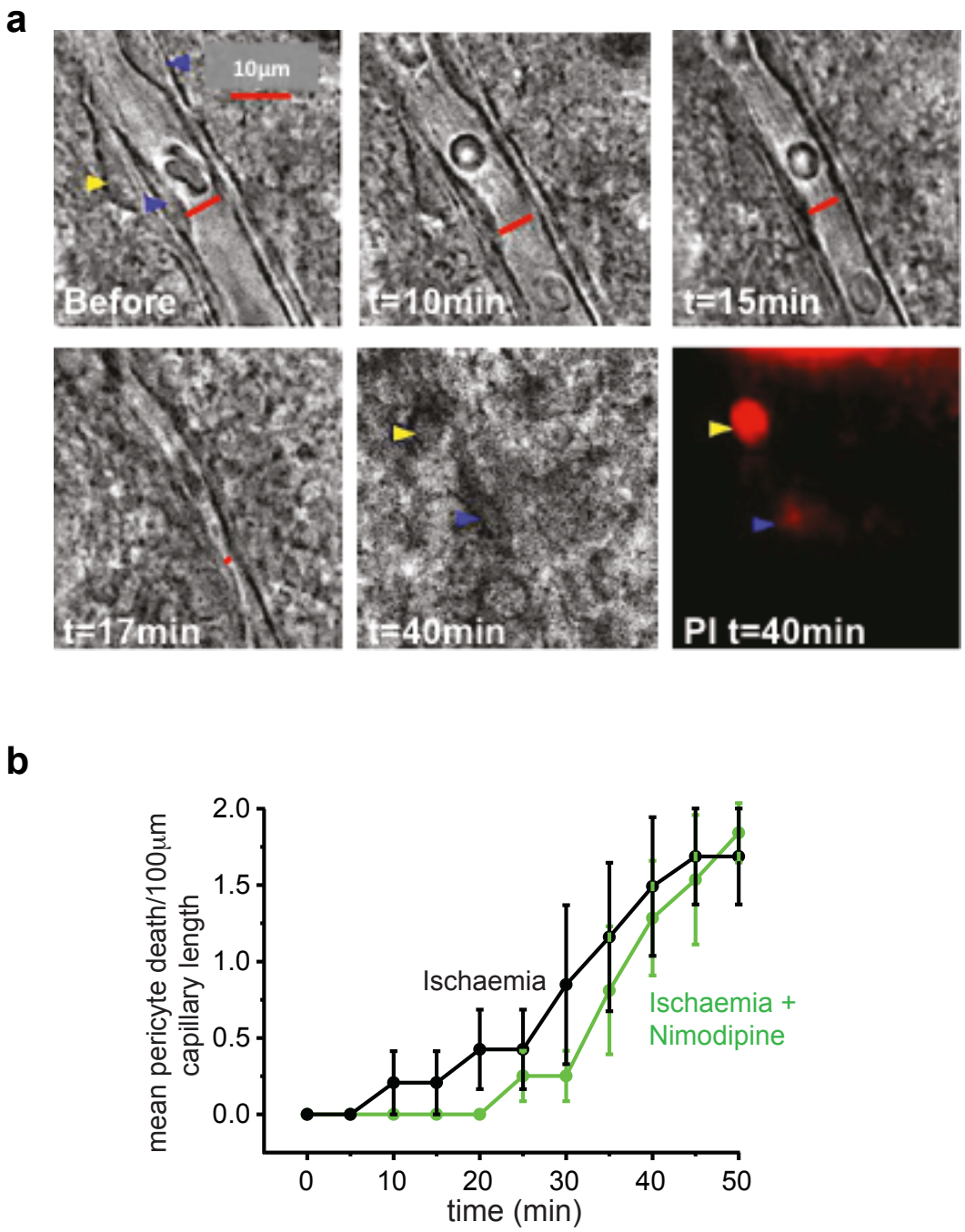

Figure 4.3 Pericyte constriction followed by death in rigor, and the effect of nimodipine on pericyte death, in ischaemia. (a) Focal constriction of a capillary imaged at different times (shown on the pictures) and pericyte death induced by simulated ischaemia (bottom right: fluorescence image of propidium iodide labelling: yellow arrowhead = pericyte; blue arrowhead = endothelial cell; red fluorescence = propidium iodide (PI) labelling of dead cells). Some movement of the slice, was induced by the ischaemia. (**b**) Effect of nimodipine on pericyte death in simulated ischaemia as a function of time (n=5 pericyes for ischaemia alone and n= 5 pericytes for ischaemia in nimodipine.

Chapter 5: Effect of amyloid β oligomers on capillary pericytes

5.1 Introduction

AD is characterised neuropathologically by (Aβ-laden) senile plaques, neurofibrillary tangles (comprised of phosphorylated tau), and synaptic and neuronal loss (Braak and Braak, 1991). Accompanying these pathological hallmarks in most patients with AD (Love and Miners, 2016), however, are a range of pathological vascular changes including, notably, cerebral amyloid angiopathy (CAA) (Attems et al., 2005). In this condition, $A\beta_{1-42}$ (the predominant species of Aβ in arterial/arteriolar and capillary CAA in AD (Attems & Jellinger, 2005; Attems et al., 2004; Roher et al., 1993)) accumulates in the vessel walls and perivascular spaces. This compromises vessel integrity and increases the risk of haemorrhage, microinfarction and cerebral hypoperfusion.

In addition there are morphological changes to capillaries, which appear to occur independently of CAA. Indeed, around the time that the amyloid hypothesis for AD was first proposed (Hardy and Allsop, 1991; Kang et al., 1987; Selkoe, 1991), it was reported that capillaries in the brains of AD patients showed an abnormal focally-constricted morphology (Hashimura et al., 1991; Kimura et al., 1991), similar to that produced by pericyte contraction (Hall et al., 2014; Peppiatt et al., 2006). Others too have reported significant changes in the capillary bed in AD, including a reduction in capillary length, diameter and density, as well as documenting the presence of thin 'string vessels', postulated to represent degenerated capillaries devoid of endothelial cells and pericytes (Buee et al., 1994; Bouras et al., 2006;

Kitaguchi et al., Fischer et al., 1990; Bell & Ball, 1981; Hunter et al., 2012; Meyer et al., 2008; Smith & Greenberg, 2009).

Following the publication of the amyloid hypothesis for AD, much succeeding work focused on Aβ- and tau-evoked damage to neurons, though increasing evidence suggests a role for vascular disturbance in the onset of AD, an idea formalised in 1993 (de la Torre & Mussivand, 1993; Thomas et al., 1996). This concept is supported by observations of reduced cerebral blood flow early in the development of the disease (Iturria-Medina et al., 2016) and by the fact that reduced cerebral blood flow increases Aβ production (Sun et al., 2006; Zhang et al., 2007). Investigations into the vasoactive effects of Aβ in AD have tended to focus on arteries and arterioles (Deane et al., 2003; Dietrich et al., 2010; Niwa et al., 2001; Thomas et al., 1996), but in the CNS the majority of the vascular resistance is located in capillaries (Gould et al., 2017), suggesting that the cause of the AD-associated reduction in blood flow may lie here.

As discussed above, a subset of pericytes on capillary walls is contractile and can alter cerebral blood flow by adjusting their contractile tone (Hall et al., 2014; Peppiatt et al., 2006) (section 1.2.16). Furthermore, in a rodent model of AD there is disrupted control of capillary blood flow (Gutiérrez-Jiménez et al., 2017). I therefore investigated how pericytes were affected by $A\beta_{1\text{-}42}$ oligomers, the molecular species believed to be responsible for Aβ's toxic effects in AD (Attems et al., 2004; Benilova et al., 2012; Klein et al., 2001). To maximise the relevance to human disease, I used living human brain slices derived from neurosurgically-resected brain tissue (removed to access tumours) to study acute responses to Aβ, and

rapidly-fixed human brain biopsy tissue (with or without Aβ deposition) to assess pericyte responses to long-term accumulation of Aβ in human AD. The mechanisms of the effects seen in human tissue were then defined in rodent brain slices.

5.2 Methods (for detailed methods see the relevant sections in Chapter 2)

5.2.1 Species and preparation

The experiments described in this chapter were performed on live human cortical tissue, human cortical biopsy tissue rapidly fixed in 4% paraformaldehyde, and live cortical tissue from P21 Sprague-Dawley rats of either sex. Human and rodent tissue was obtained, processed and stored as described in Section 2.2. The general condition of human neocortical tissue slices used for live imaging was inferior to that of P21 rat neocortical slices. This is probably due to a combination of factors, including the relatively traumatic means by which the tissue must be obtained, the unavoidable time delay during transportation of the tissue to the lab (15 mins) and the increased difficulty encountered with slicing heavily myelinated live adult human cortical brain tissue.

5.2.2 Extracellular solution

For live imaging experiments, human and rodent cortical slices were superfused with aCSF extracellular fluid with or without drugs as described in Sections 2.1.1 – 2.1.2.

5.2.3 Oligomerising Aβ and assessing the form and concentration of Aβ applied

Aβ was oligomerised as described in Section 2.4.1. Quantification of Aβ

peptide concentration following oligomerisation (see Section 2.4.1) showed that the amount of the molecule remaining as soluble monomers and oligomers was 28.7±2.9% (n=4) of the total concentration added for $A\beta_{1-42}$, 39.9±1.5% (n=3) for $A\beta_{1-40}$, and 43.6±2.3% for scrambled $A\beta_{1-42}$. Concentrations stated in the results section below have been corrected for these factors. Assessment of the degree of aggregation of the Aβ isoforms following oligomerisation (see Section 2.4.1) showed that the predominant species produced (other than monomers) for $A\beta_{1-42}$ and $A\beta_{1-40}$ had a molecular weight of 4 to 5 times that of monomers, whereas scrambled $A\beta_{1-42}$ formed mainly monomers (Fig. 5.1).

5.2.4 Imaging capillaries

As described in detail in section 2.3, healthy capillaries (<10 μm in diameter, mean diameter 5.61±0.03 μm (n=299) in rat, and 5.08±0.33 μm (n=12) in human, with no rings of arteriolar smooth muscle around them) were selected as previously described (Mishra et al., 2014). Regions of them were imaged which were in focus in a single image plane over at least 30 μm along the length of a capillary, and exhibited a candidate pericyte with a bump-on-a-log morphology (shown in Figs. 5.2a and 5.3a below). A CCD camera was then used to capture images 100 μm square during superfusion of drugs. Capillary diameter was measured from the resulting movies, by an analyst blinded to the time and identity of drug application, by placing a line across the lumen on magnified images. In some experiments pericytes were explicitly identified prior to imaging by incubating slices for 30 min in 10 μg/ml isolectin B_4 conjugated to Alexa 488, which binds to α-D-galactose residues

in the basement membrane secreted by pericytes and endothelial cells, and outlines pericytes (Mishra et al., 2014). This allowed 2-photon imaging (using a Zeiss LSM710 microscope, excitation wavelength 800 nm) of the endothelial tube and the pericytes on it (shown in Fig. 5.3b below).

5.2.5 Assessing pericyte death

As described in detail in section 2.3.6, P21 Sprague-Dawley rat brain slices (250 μm thick) were incubated in a multi-well plate, with oxygen blown gently at the surface, in aCSF, or aCSF with oligomerised $A\beta_{1\text{-}42}$ or ET-1 added. All extracellular solutions contained isolectin B_4 to label the microvasculature basement membrane and 7.5 μM propidium iodide to label cells with membranes that had become non-specifically permeable (Hall et al., 2014) and were thus deemed to be dead cells (Fig. 5.6). After 3 hours incubation, slices were fixed in 4% paraformaldehyde, and imaged on a Zeiss LSM700 confocal microscope. To avoid counting cells killed by the slicing procedure, quantification of the percentage of pericytes that were dead excluded cells within 20 μm of the slice surface.

5.2.6 Immunohistochemistry of human tissue

This was performed as described in detail in section 2.5

5.2.7 Human biopsy data

As described in section 2.6. fixed human tissue from patients with cognitive decline was obtained from diagnostic brain biopsies, performed as part of routine clinical investigations at the National Hospital for Neurology and Neurosurgery, Queen Square, London.

5.2.8 Statistical analysis

This was performed as described in detail in section 2.7.

5.3 Results

5.3.1 Oligomeric Aβ constricts human cortical capillaries

Aβ was oligomerised (see Section 2.4.1), and silver staining of SDS-PAGE gels was used to assess the degree of aggregation of the Aβ isoforms. The predominant species produced (other than monomers) for $A\beta_{1-42}$ and $A\beta_{1-40}$ had a molecular weight of 4 to 5 times that of monomers, whereas scrambled $A\beta_{1-42}$ formed mainly monomers (Fig. 5.1a). Applying soluble oligomeric $A\beta_{1-42}$ (oligomers + monomers, 72 nM after correction for loss of material in the oligomerisation process: see Section 2.4.1) to human brain slices evoked a slowly developing constriction of capillaries that reduced their diameter by ~25% ($p=0.01$) after 40 mins (Fig. 5.2a, b). For a fixed pressure across the capillary bed, a focal constriction of this magnitude at pericyte somata is predicted to reduce cerebral blood flow by 45% if it occurred throughout the capillary network (see section 2.7.2).

Tissue obtained for these experiments came from the following patients: a 40-year old female with a glioma, a 46-year old male with a glioma, a 35-year old with a glioblastoma multiforme (grade IV glioma) and a 38-year old male with a glioma. Tissue sent for histopathological examination from these four patients showed no evidence of tumour invasion.

5.3.2 Amyloid β oligomers constrict rodent capillaries

As the limited availability of live human tissue precludes detailed analysis of the mechanism underlying the Aβ-evoked constriction, I carried out experiments on cortical slices from 21 day-old rats to investigate this.

As for human capillaries, $A\beta_{1-42}$ and also $A\beta_{1-40}$ evoked a constriction of rat capillaries near pericyte locations that was visible using either bright field illumination or 2-photon fluorescence imaging of isolectin B_4 (Fig. 5.3a, b). The time course of the Aβ-evoked constriction was similar to that in human cortex (Fig. 5.3c), reaching ~16% after 1 hour ($p=0.006$ for $A\beta_{1-42}$ and 0.048 for $A\beta_{1-40}$). Capillaries monitored for an hour without applying Aβ, or those to which a version of $A\beta_{1-42}$ with a scrambled sequence was applied (prepared as for the Aβ oligomers), showed no significant diameter change (Fig. 5.3c). Scrambled $A\beta_{1-42}$ does not form oligomers (Fig. 5.1), unlike $A\beta_{1-42}$ and $A\beta_{1-40}$, which may indicate oligomer formation is obligatory for an effect on pericytes. The pericyte-mediated constriction evoked by $A\beta_{1-42}$ showed a Michaelis-Menten dependence on Aβ concentration, with an EC_{50} of 4.7 nM (Fig. 5.3d) - a concentration similar to that of soluble Aβ oligomers in the brains of AD patients (~6 nM, from the TBS fraction in Table 1 of Roberts et al., 2017).

5.3.3 Aβ oligomers constrict capillaries via endothelin signalling to pericytes

The $A\beta_{1-42}$-evoked capillary constriction in rat cortical slices was blocked by the endothelin-1 (ET-1) type A receptor blocker BQ123 (1 μM, $p=0.008$), or by application of superoxide dismutase 1 (SOD1, 150 units/ml, $p=3.7\times10^{-6}$)

which scavenges reactive superoxide generated when Aβ activates NADPH oxidase in immune cells (Fig. 5.4), as previously reported for the effect of Aβ on arteries and isolated penetrating arterioles (Deane et al., 2003; Dietrich et al., 2010; Niwa et al., 2001). Neither of these agents alone affected capillary diameter: BQ123 evoked a -0.7±5.2% dilation in 13 vessels, while SOD1 evoked a 3.4±5.8% dilation in 9 vessels). Unlike for $A\beta_{1-40}$ effects on blood flow *in vivo* (Deane et al., 2003), blocking binding of Aβ to the receptor for advanced glycation endproducts (RAGE) using FPS-ZM1 (1 μM) had no effect on the pericyte constriction (p=0.34, Fig. 5.4), reflecting the fact that we applied Aβ in the extracellular fluid, while RAGE is only needed to transport Aβ into the brain from the blood (Deane et al., 2003).

I showed in Chapter 3 that pericytes constrict in response to application of ET-1 and that this constriction was blocked by the type A receptor blocker BQ123, but not by the type B receptor blocker BQ788. Figure 5.5a and c show that generating reactive oxygen species with H_2O_2 also evokes a pericyte-mediated constriction of pericytes. Interestingly, ET-1 still evoked a constriction in the presence of the ROS scavenger SOD1 ($p=1.3x10^{-8}$, Fig. 5.5b) implying that, when Aβ is applied, ET-1 acts downstream of superoxide. In contrast, the constriction evoked by reactive oxygen species generating using H_2O_2 was reduced by BQ123 (p=0.03, Fig. 5.5c), suggesting that H_2O_2 constricts pericytes, at least in part, via endothelin receptor activation. These data establish $A\beta_{1-42}$–evoked generation of reactive oxygen species, presumably by resident microglia (Bianca et al., 1995) or perivascular macrophages (Park et al., 2017), as being upstream of the elevated level (Luo & Grammas, 2010; Palmer et al., 2012) (or potentiated

effect: Paris et al., 2003) of endothelin, which makes pericytes constrict capillaries.

5.3.4 Acute exposure to Aβ oligomers or endothelin does not lead to pericyte death

In profound ischaemia, pericyte-evoked constriction of capillaries is followed by the pericytes dying in rigor, probably because of an excessive rise of $[Ca^{2+}]_i$, thus maintaining a decreased capillary diameter and a long-lasting decrease of blood flow (Hall et al., 2014). Pericytes also die after accumulating Aβ in AD (reviewed by Hamilton et al., 2010). We assessed whether exposure to 1.4 μM $Aβ_{1–42}$ or 100 nM ET-1 for 3 hours had a similar effect on pericyte health, by applying propidium iodide to label cells with membranes that had become non-specifically permeable (Hall et al., 2014) (Fig. 5.6a). These procedures did not significantly increase pericyte death on this time scale (Fig. 5.6b, p=0.85 for $Aβ_{1-42}$ and 0.59 for ET-1).

5.3.5 Chronic effect of amyloid β on human capillary pericytes

Since acute exposure to Aβ cannot mimic the slow increase which occurs over decades in human AD patients, I studied rapidly-fixed brain cortical biopsy tissue from patients being investigated for cognitive decline of unknown cause. Tissue sections were labelled with antibodies to Aβ (recognising residues 8-17 of Aβ), PDGFRβ (to label pericytes) and phosphorylated tau. Of 13 patients (for demographics, see Section 2.6), 7 turned out to have Aβ deposition while 6 did not. Specimen images of their vessels and Aβ labelling are shown in Fig. 5.7a, b. Pericytes were readily identifiable from their PDGFRβ labelling.

Averaging over 120-140 adjacent fields of view (400 μm square in size, randomly placed on each section as a 5x4 grid of squares) in tissue from the two types of patient, it was found that the mean capillary diameter was reduced by 8.1% ($p=0.0007$) in the patients with Aβ deposition (5121 diameters measured) compared to those without Aβ deposition (3921 diameters measured: Fig. 5.7c). I was blinded to the patients' condition while doing this analysis.

To assess whether this diameter reduction was a non-specific effect of AD, or was pericyte-related, I plotted the capillary diameter measurements as a function of the distance from the nearest PDGFRβ-labelled pericyte soma (see Section 2.6). In patients with no detectable Aβ deposition the capillary diameter increased at locations near pericyte somata compared to at locations far from the soma (~25% larger, the slope of the line is significantly less than zero, $p=3.7\times10^{-7}$ for 813 data points from 6 such patients, Fig 5.7d). A similar increase in capillary diameter near pericyte somata has previously been found in rodent brain capillaries *in vivo* (Hall et al., 2014), and attributed to the presence of the soma inducing more growth of the endothelial tube. In contrast, in patients with Aβ deposition, the capillary diameter was significantly reduced near the pericyte somata compared to locations distant from the somata (Fig. 5.7d; ~30% smaller, slope of line is significantly greater than zero, $p=1.6\times10^{-20}$ for 1313 data points from 7 patients), as expected if pericytes cause the capillary constriction by contracting their circumferential processes which are mainly located near their somata. Mathematical modelling indicates that this constriction is predicted to reduce flow by ~50% compared to if there were no constriction (see Section 2.7.2).

The subjects were classified by neuropathologists assessing the Aβ-labelled biopsies as having either “no Aβ deposition”, “moderate Aβ deposition” or “severe Aβ deposition” in the parenchyma (as diffuse deposits and/or as plaques with central amyloid cores, Fig. 5.8a). The mean slope from graphs like those in Fig. 5.7d, for 6 patients with no Aβ deposition, 3 patients with moderate deposition and 4 patients with severe Aβ deposition, showed a progressive change from negative (implying a larger capillary diameter at the soma) to positive (implying a smaller diameter at the soma) as the severity of the Aβ deposition increased (Fig. 5.8b, $p=0.003$ compared with a relationship with zero slope), supporting further the idea that Aβ is the cause of the capillary constriction. Plotting similar graphs for the slope against the neuropathologist-assessed degree of cerebral amyloid angiopathy or phosphorylated tau labelling (see Fig. 5.9a, b), gave a broadly similar trend with disease severity, but with a higher p value (0.013 and 0.007 respectively).

To quantify Aβ level more rigorously, we measured light absorption by the peroxidase product generated by the Aβ antibody, in the region where the vessel diameters were measured in each biopsy (see section 2.6: although this measure of Aβ may largely reflect the presence of plaques, it is likely that the soluble Aβ concentration is maintained by, and correlates with, the presence of the plaques). Plotting the slopes of the graphs of capillary diameter against distance from pericyte soma for each biopsy, against the amount of Aβ deposition, again showed a monotonic progression from a negative slope to a positive slope as Aβ deposition increased, but with the change of slope occurring more strongly at low levels of Aβ deposition (Fig.

5.8c). Similarly, plotting the extrapolated value of the capillary diameter at the pericyte soma for each biopsy as a function of Aβ deposition showed that the diameter was reduced more strongly by low levels of Aβ, with less further constriction as deposition increased (Fig. 5.8d).

5.4 Discussion

My data demonstrate that, at low nanomolar concentrations, soluble $A\beta_{1-42}$ oligomers evoke a constriction of human cortical capillaries, mediated by pericytes. Capillaries are the site in the cortical vasculature where most of the resistance to flow is located (Gould et al., 2017), and so are the site where diameter changes will reduce blood flow most (although arteries (Niwa et al., 2001) and arterioles (Dietrich et al., 2010) are also reported to be constricted by Aβ). In rodents I have shown that this constriction is the result of reactive oxygen species generation activating endothelin signalling, via ET_A receptors, which makes pericytes constrict the capillaries. The EC_{50} for Aβ's action, 4.7 nM, is comparable to the concentration of soluble Aβ found in the brain (6 nM, from the TBS fraction in Table 1 of Roberts et al. (2017)) and two factors indicate that the effects seen are pathologically relevant. First, analysing the diameter of capillaries in human patients with cognitive decline, who either showed or lacked deposition of Aβ, shows that Alzheimer's pathology leads to capillary constriction specifically at pericytes (Fig. 5.7d), with a magnitude that is estimated to reduce blood flow by a factor of at least 2. Second, the magnitude of the capillary constriction in dementia patients increases with the severity of Aβ deposition (Fig. 5.8d).

Both the reduction of basal blood flow produced by Aβ, and a reduction in the blood flow increase normally produced by neuronal activity (Park et al., 2004), which may also reflect the action of Aβ on pericytes (Hall et al., 2014), will decrease the energy supply to the brain. This is turn increases Aβ production by upregulating β-amyloid converting enzyme (β-secretase 1, BACE1: Sun et al., 2006; Zhang et al., 2007). Consequently, the regulation of pericyte-mediated capillary constriction by Aβ may act as an amplifying mechanism in a positive feedback loop (Fig. 5.10), increasing the level of Aβ and tau aggregation which ultimately lead to the loss of synapses and neurons.

5.5 Conclusion

Aβ oligomers constrict brain capillaries via ROS- and endothelin-mediated signalling to pericytes, an effect that probably explains the early cerebral blood flow disturbances seen in AD. The data in this thesis chapter suggest several potential therapeutic approaches for early AD, based on the mechanisms generating pericyte constriction. Aβ-evoked generation of reactive oxygen species (ROS) might be targeted, but this would require resolving whether these are generated by resident microglia (Bianca et al., 1999) or perivascular macrophages (Park et al., 2017), and ROS may play important signalling roles in pathways other than the one controlling endothelin effects. A more promising approach, therefore, might be to try to reduce endothelin release (which is presumably from microglia or endothelial cells, the brain cells expressing endothelin strongly: Zhang et al., 2014) or the effects of endothelin specifically on its type A receptors located on CNS pericytes. This could be achieved, for example, by generating an endothelin

receptor blocker which also binds to another target protein on pericytes, such as the PDGF receptor β or the proteoglycan NG2. This concept raises the question of whether Aβ also evokes constriction of capillaries in other vascular beds by acting through pericytes, in which case drugs might be usefully targeted at all pericytes, and not just those in the brain.

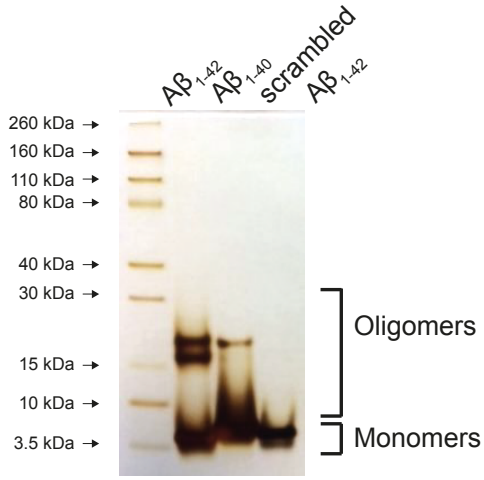

Figure 5.1 Oligomerisation of Aβ.

Silver staining of an SDS-PAGE gel for solutions of $A\beta_{1-42}$, $A\beta_{1-40}$, and scrambled $A\beta_{1-42}$. Scrambled $A\beta_{1-42}$ forms only monomers, while $A\beta_{1-42}$, and $A\beta_{1-40}$ also form low molecular weight oligomers.

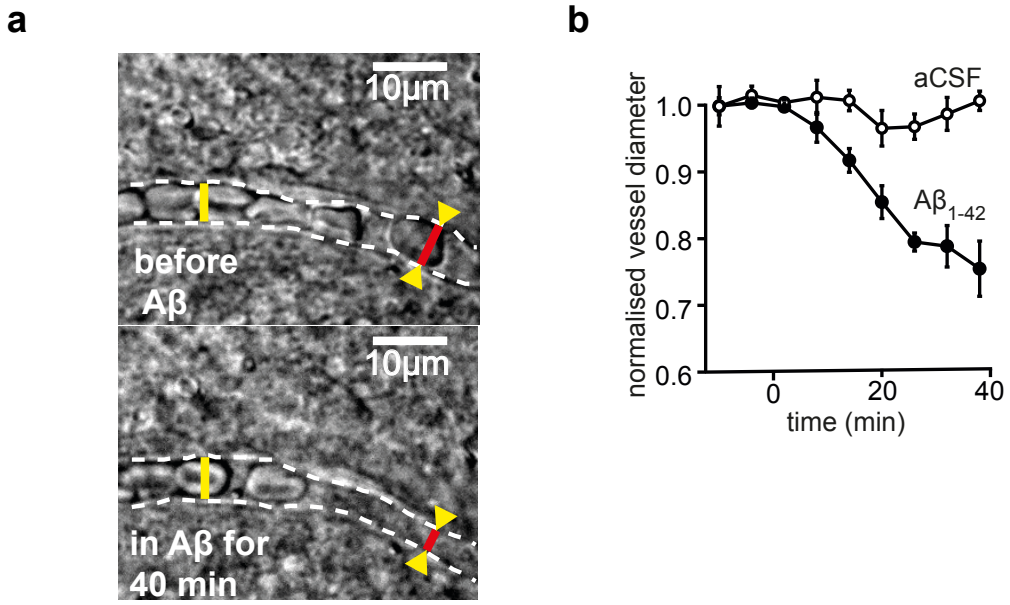

Figure 5.2 Oligomeric Aβ acts on pericytes to constrict capillaries in human brain slices. (a) Bright field images of a capillary before and after superfusion of 70 nM $A\beta_{1-42}$ (dashed lines indicate wall), showing one region (red line) being constricted by pericytes and one region (yellow line) that is not constricted. (**b**) Graph shows mean diameter change at 4 pericyte locations from 3 slices treated with Aβ and 3 pericyte locations from 3 slices treated with aCSF.

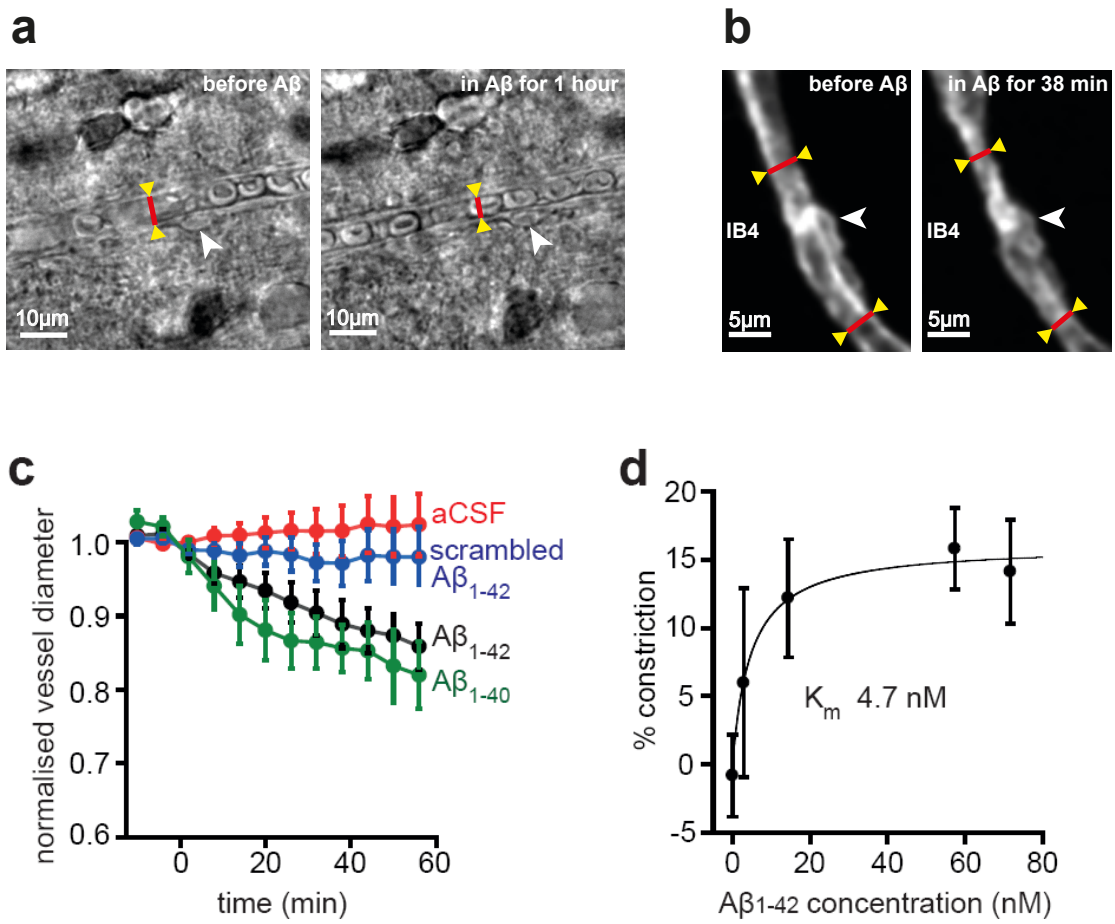

Figure 5.3 Aβ acts to constrict rat capillaries via a high affinity binding site. **(a-b)** Bright field images **(a)** and 2-photon images of IB_4 fluoresence **(b)** of capillaries in rat cortical slices in normal aCSF and after superfusion with 70 nM $Aβ_{1-42}$ for 1 hour, showing capillary constriction near pericytes. **(c)** Mean time course of normalised capillary diameter during superfusion with aCSF (n=51 vessels), scrambled $Aβ_{1-42}$ (109 nM, n=32), $Aβ_{1-42}$ (70 nM, n=20) or $Aβ_{1-40}$ (100 nM, n=6). **(d)** Constriction produced after 1 hour by different concentrations of $Aβ_{1-42}$ (n=51, 11, 10, 19 and 20 for 0, 2.9, 14, 57 and 70 nM). Curve through the points is a Michaelis-Menten relation with a best-fit K_m of 4.7 nM.

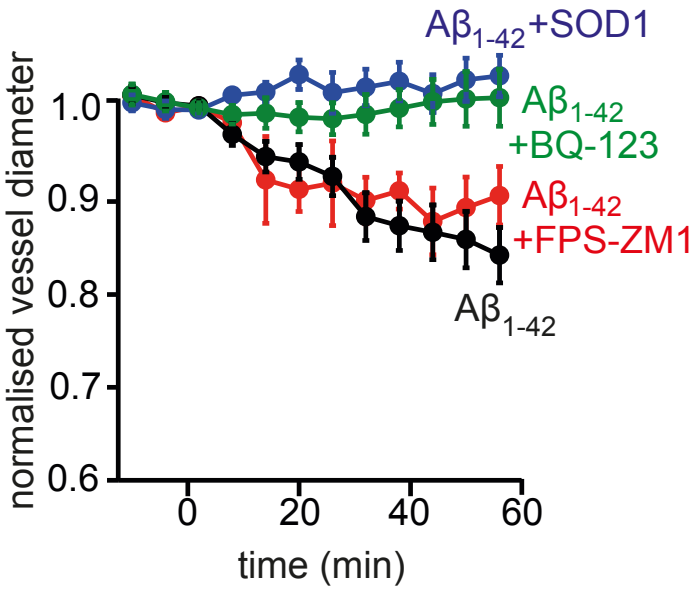

Figure 5.4 Aβ acts via reactive oxygen species and endothelin type A receptors. Mean time course of normalised capillary diameter during superfusion with 57 nM $A\beta_{1-42}$ alone (n=19), or in the presence of superoxide dismutase 1 (SOD1, 150 units/ml, n=19), the ET-A receptor blocker BQ123 (1 μM, n=14), or the RAGE blocker FPS-ZM1 (1 μM, n=8).

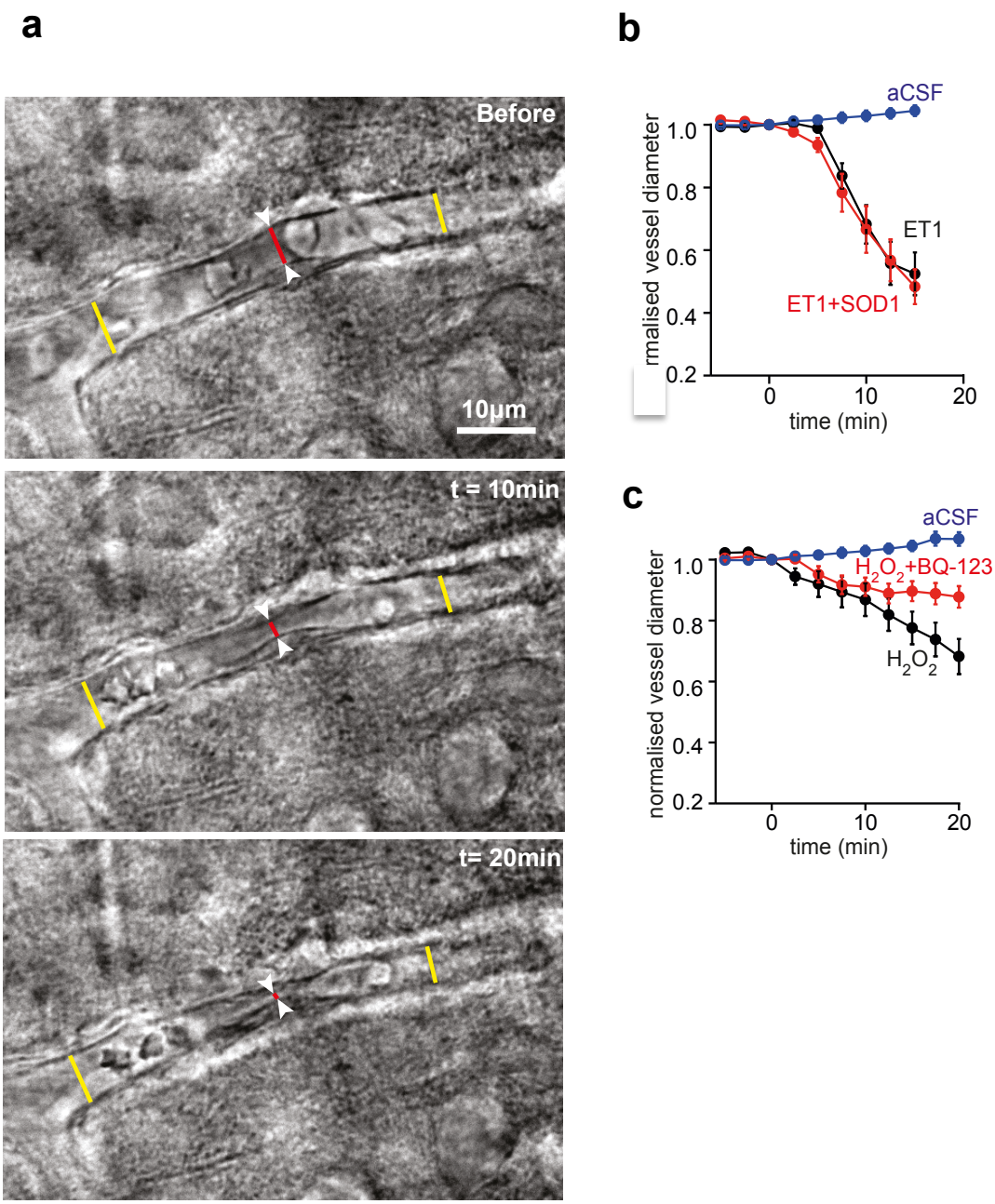

Figure 5.5 Endothelin type A receptor blockade attenuates reactive oxygen species mediated capillary constriction. (a) Bright field images showing that H_2O_2 (1 mM) evokes a focal capillary constriction (times shown on images, with application starting at t=0 min). (**b**) SOD1 (150 U/ml, n=8) does not block the constriction evoked by endothelin (ET-1, 5 nM, n=12),. (**c**) The reactive oxygen species generator H_2O_2 (1 mM, n=9) evokes capillary constriction which is reduced by the ET-A receptor blocker BQ123 (1 µM, n=11).

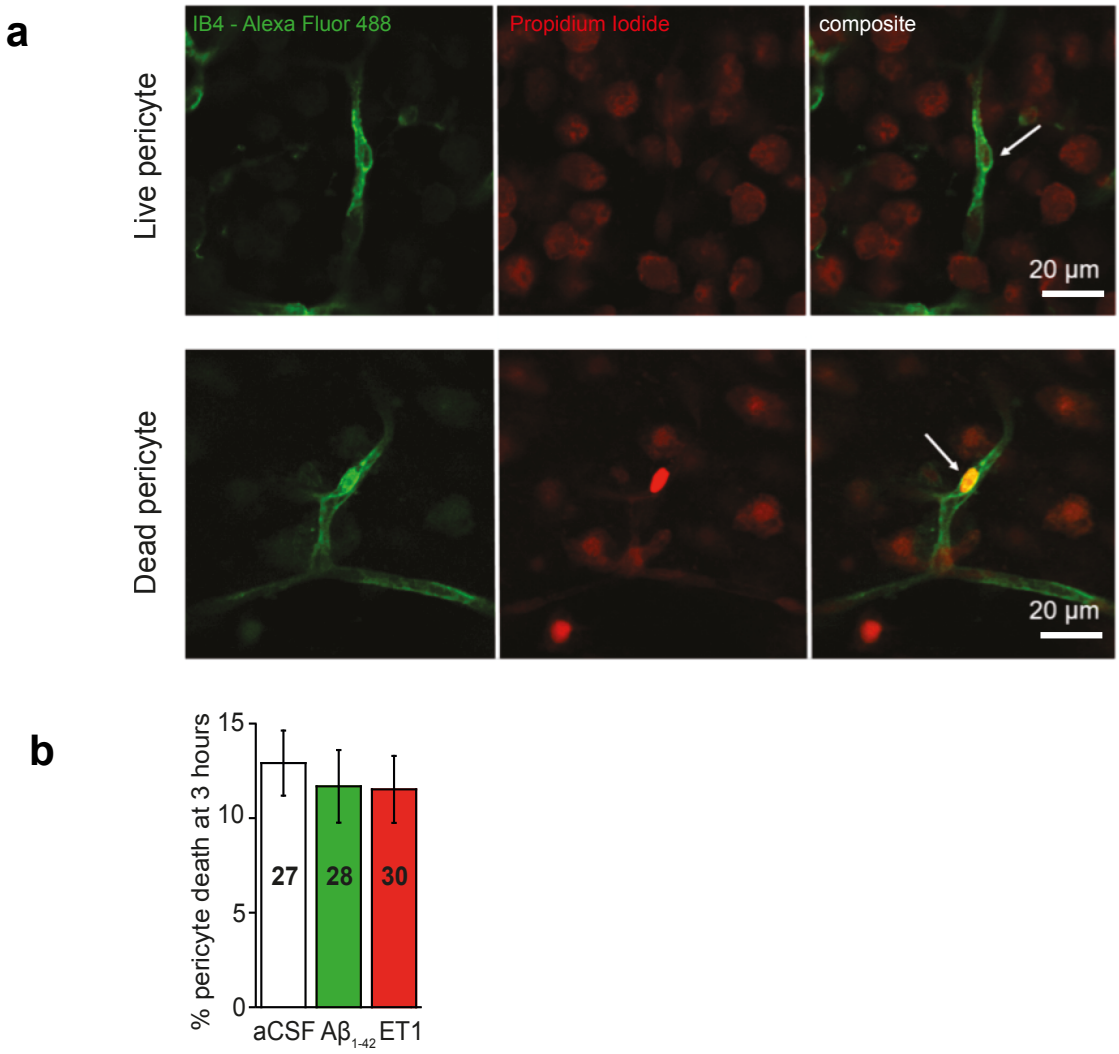

Figure 5.6 Acute exposure to Aβ oligomers or endothelin does not lead to pericyte death. (a) Top panels, left to right: Identifying 'live' pericytes by 'bump-on-a-log' morphology and absence of PI-labelling (white arrow). **Bottom panels, left to right:** Identifying dead pericytes labelled with PI (white arrows). **(b)** Incubating rat brain slices in solution containing $A\beta_{1\text{-}42}$ oligomers (1.4 μM, n=28) or ET1 (100 nM, n=30) for 3 hours does not increase pericyte death over that seen when incubating for the same period in aCSF (n=27).

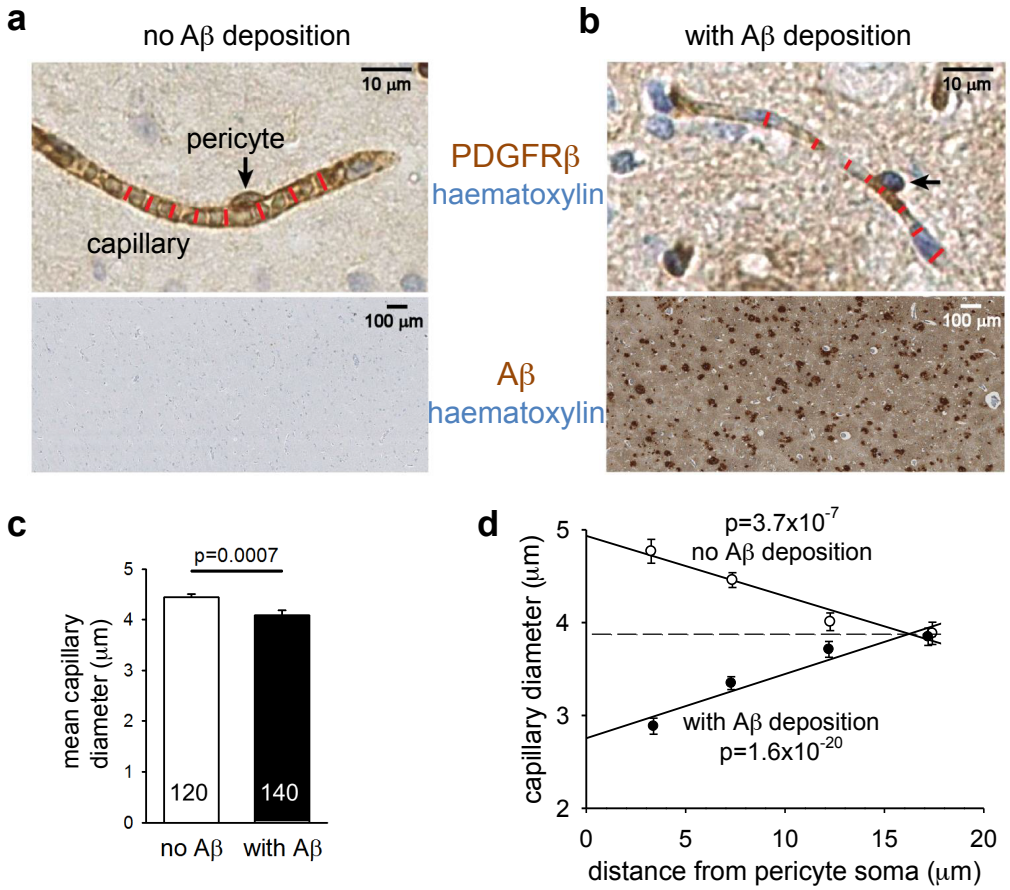

Figure 5.7 Pericyte-mediated capillary constriction occurs in humans with Aβ deposits. (**a-b**) Sample images of human cortical biopsies, labelled for PDGFRβ to show pericytes (arrows), from patients lacking (**a**) or exhibiting (**b**) Aβ deposits (immunostaining brown, haematoxylin counterstain blue). Red lines indicate capillary diameter. (**c**) Mean diameter of capillaries in patients lacking (3921 diameters measured) or exhibiting (5121 diameters measured) Aβ deposits (number of images measured shown on bars). (**d**) Dependence of capillary diameter on distance (in 5 μm bins, from 0-5, 5-10, 10-15 and 15-20 μm) from a visible pericyte soma for patients lacking or exhibiting (pooling moderate and severe Aβ deposition) Aβ deposits. P values assess whether slope of regression line is significantly different from zero.

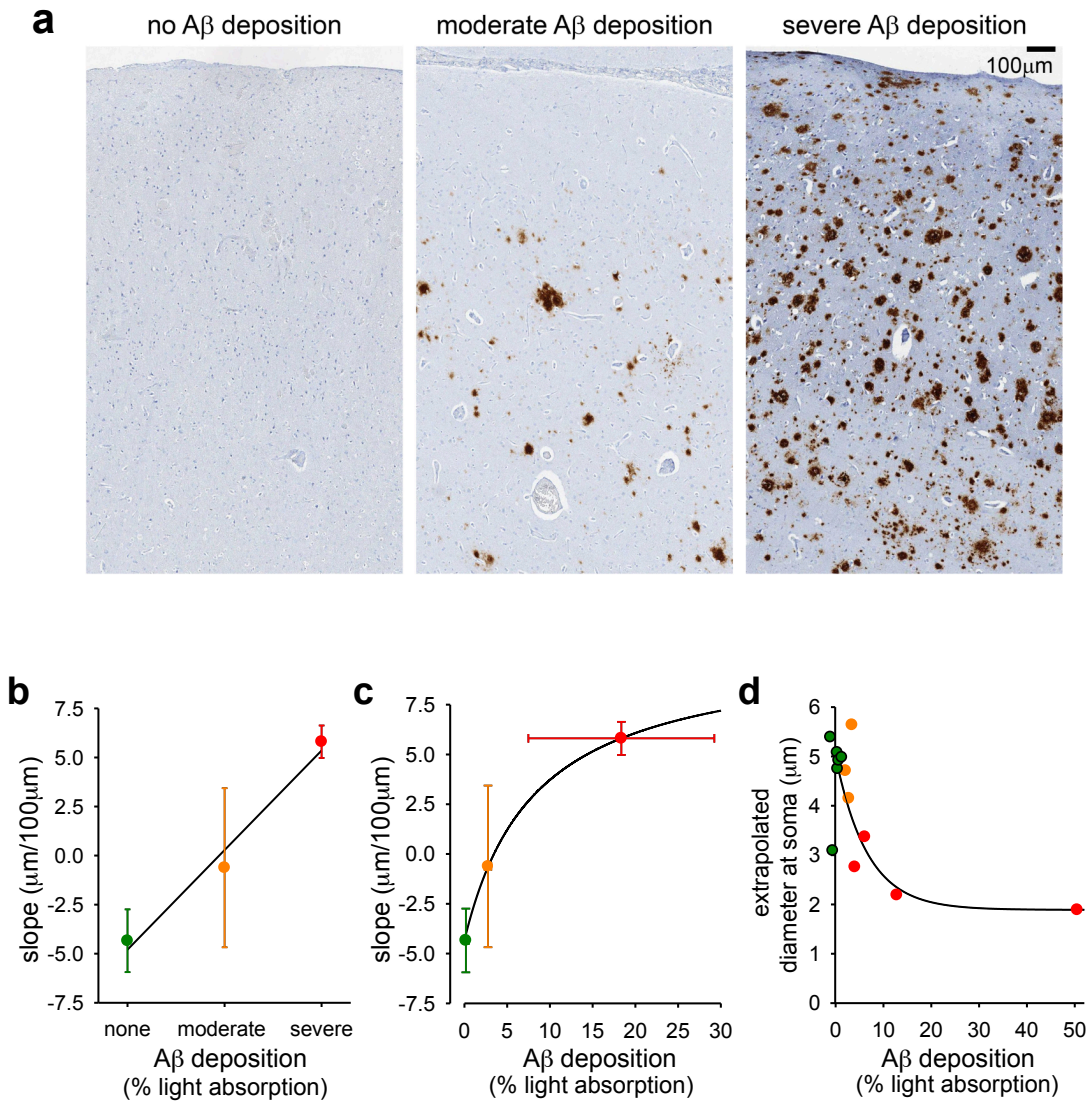

Figure 5.8 Magnitude of the capillary constriction in dementia patients increases with the severity of Aβ deposition. (**a**) Examples of Aβ labelling assessed by the neuropathologist as absent, moderate or severe. (**b**) Slope of regression lines (averaged over patients), as in Fig. 5.7d, as a function of parenchymal Aβ load as rated by neuropathologist. (**c**) Slope of regression lines as in Fig. 5.7d as a function of the severity of Aβ deposition measured optically, with subjects grouped by colour (defined in b) as classified by neuropathologist. (**d**) Dependence of extrapolated diameter at the pericyte soma (as in Fig. 5.7d) on severity of Aβ deposition measured optically, with subjects grouped as classified by the neuropathologist. Lines through data in b-d are to show the trends in the data.

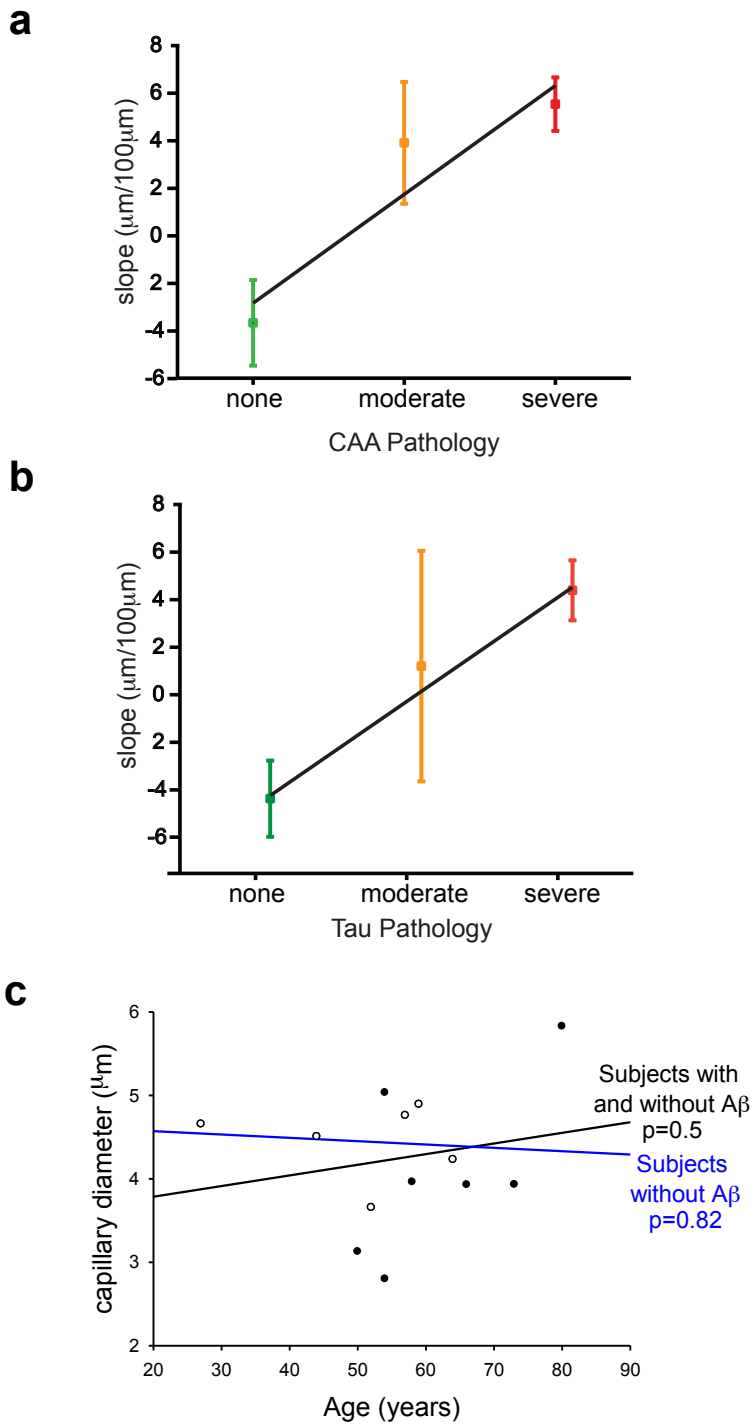

Figure 5.9 Magnitude of the capillary constriction in dementia patients increases with the severity of Tau and CAA pathology. Slope of regression lines (averaged over patients), as in Fig. 5.7d, as a function of **(a)** parenchymal tau load and **(b)** severity of CAA pathology as rated by neuropathologist. **(c)** Regressing mean capillary diameter against age from all patients or from the patients lacking Aβ deposition showed that there was no significant dependence on age.

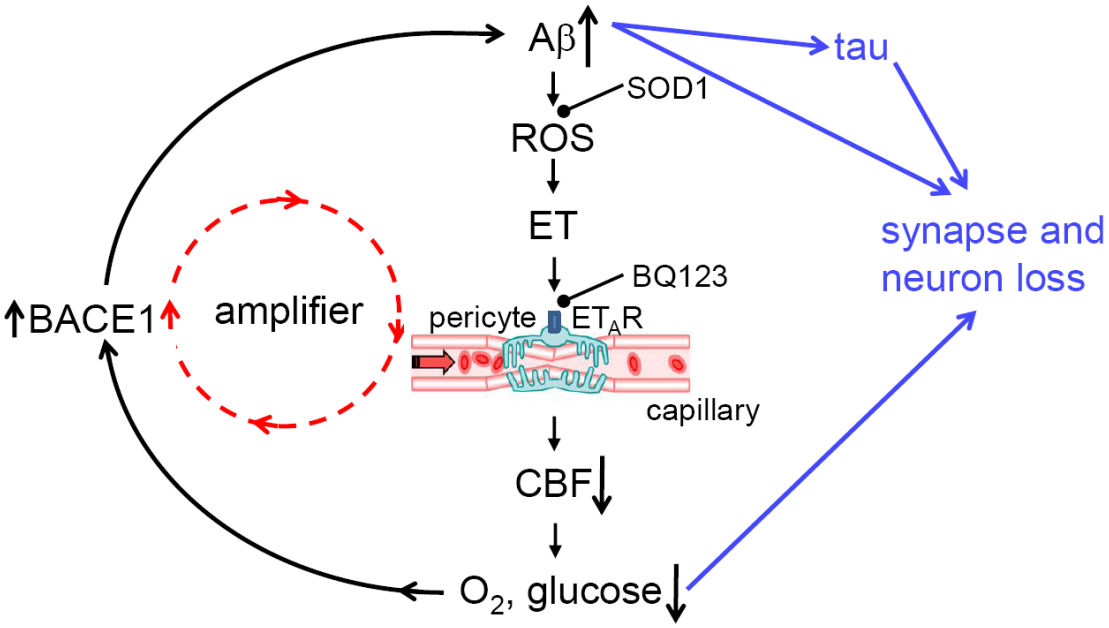

Figure 5.10 Aβ effects on capillaries may amplify the onset of AD.

Amyloid β oligomers activate NADPH oxidase in immune cells (Bianca et al., 1999; Park et al., 2017) to generate reactive oxidative species (ROS). These in turn release, or potentiate the constricting effects of endothelin, which acts via ET_A receptors on pericytes on capillaries - the locus (Gould et al., 2017) of the largest component of vascular resistance within the brain parenchyma. Capillary constriction decreases cerebral blood flow and hence the supply of oxygen and glucose to the brain, which increases the production of Aβ, in part by upregulating (Sun et al., 2006; Zhang et al., 2007) expression of β-amyloid converting enzyme (β-secretase 1, BACE1), thus forming an amplifying positive feedback loop. Either directly, or via tau production, or via the decrease in oxygen and glucose supply that it produces, a rise in Aβ concentration leads to the loss of synapses and neurons. Potential sites for therapeutic intervention are highlighted at the stages of ROS (SOD1) and endothelin receptors (BQ123).

Chapter 6: Suggestions for future work and final conclusion

In this chapter I will suggest further experiments that could be done to advance the research described in Chapters 3-5.

6.1 Reducing pericyte constriction of capillaries and death in ischaemia

In order to further examine whether nimodipine (and other candidate drugs) can prevent pericyte constriction and death in cerebral ischaemia (based on my data), other members of the Attwell lab are performing experiments *in vitro,* using oxygen-glucose deprivation (OGD) (without antimycin and iodoacetate) to simulate tissue ischaemia in incubated rodent cortical slices, in tandem with in *vivo* experiments, employing a rodent middle cerebral artery occlusion (MCAO) stroke model.

The *in vitro* work has already yielded promising results for the effect of nimodipine on pericyte death during ischaemia with re-oxygenation, whilst work in the MCAO stroke model is ongoing. The method used for the *in vitro* OGD ischaemia experiments has been previously described (Hall et al., 2014). Nimodipine was found to significantly reduce pericye death following ischaemia with re-oxygentation (see Fig. 6.1): reoxygenation after OGD led to 70.1±6.7% of pericytes dying but with OGD+nimodipine, this was reduced to 42.2±5.4% (n=6 each, p=0.018). Nimodipine did not however, have a significant effect in reducing pericyte death in ischaemia without re-oxygenation (p=0.32 vs control).

6.2 Using NeuroTrace and ET1 *in vivo* to determine the contractility of subdivisions of the capillary bed according to pericyte morphology

Following on from the work in Chapter 3, it needs to be determined whether NeuroTrace-labelled pericytes in live brain slices are using α or other forms of smooth muscle actin as their contractile apparatus, and whether pericytes with longitudinally extensive processes are contractile *in vivo*. This could be achieved by introducing ET1 to the immediate locality of NeuroTrace-labelled pericytes with a glass patch-clamp pipette, whilst performing 2-photon imaging through a cranial window in an anaesthetised rodent (with FITC dextran introduced intravenously to outline the cerebral vasculature).

Further work is also required to determine whether in pathological conditions when ET and other vasoactive substances are released (e.g. Alzheimer's disease, subarachnoid haemorrhage (Vergouwen et al., 2012)), the capillary bed constricts more readily in response to the released ET than does the arteriolar network.

6.3 Using an Alzheimer's mouse model to test potential treatments for Aβ- meditated capillary constriction

As stated in Chapter 5, targeting pericyte ET_A receptors may be a therapeutic option for preventing Aβ-mediated capillary constriction in AD. Initial work towards this goal will require determining whether or not Aβ-mediated constriction of the capillary bed develops in an AD mouse model. Our laboratory has therefore obtained knock-in AD model mice (harbouring Swedish and Beyereuthian/Iberian mutations ± APP Artic mutation) that

overproduce $A\beta_{1-42}$ without overproducing APP (Saito et al., 2014), and crossed them with the NG2-DsRedC56BL/6J mice, in which pericytes express the fluorescent protein DsRed under the control of the promoter for the proteoglycan NG2. These mice develop typical Aβ pathology, neuroinflammation and memory impairment in an age–dependent manner (Saito et al., 2014). We plan to perform *in-vivo* 2-photon imaging of FITC outlined cortical capillaries in these ADmodel/DsRed crossed mice, to determine whether there is progressive, age-dependent constriction of the capillary bed compared to litter-mate wild-type/DsRed controls. If AD model/DsRed crossed mice do show evidence of progressive capillary constriction, it would be interesting to see if this occurs prior to the development of Aβ plaques (typically at 3 months of age: Saito et al., 2014) and to determine whether capillary constriction can be prevented with drug treatment.

6.4 Final Conclusion

The human brain contains approximately 640 km of blood vessels that supply brain cells with oxygen and glucose and remove carbon dioxide and other metabolic waste products from the brain to the systemic circulation (Kisler et al., 2017; Sweeney et al., 2018; Zlokovic, 2008;). Although representing only 2% of total body mass, the brain consumes ~20% of the body's glucose and oxygen and is capable of rapidly increasing blood flow and oxygen delivery to its activated regions (a process known as neurovascular coupling) (Iadecola, 2013; Kisler et al., 2017; Sweeney et al., 2018). Capillaries are the smallest cerebral blood vessels but account for ~85% of cerebral vessel length (Zlokovic, 2008), are the locus of the largest

component of vascular resistance within the brain parenchyma (Gould et al., 2017) and are a major site of the BBB (Zlokovic, 2008).

In the human brain, pericytes are present at 65 μm intervals along blood vessels (Hall et al., 2014) and thus constitute a significant cell population; yet pericytes are the subject of less than 1 in 1000 papers published on the brain in Pubmed. These bibliographic data suggest that despite recent advances, our ignorance of the role of pericytes in health and disease implies missed therapeutic opportunities.

Numerous studies have shown that pericytes play an important part in disparate CNS disorders including, epilepsy (Leal-Campanario et al., 2017), spinal cord injury (Li et al., 2017), Huntington's disease (HD) (Drouin-Ouellet et al., 2015), multiple sclerosis (MS) (Rustenhoven et al., 2017), glioma (Svensson et al., 2015), radiation necrosis (Lee et al., 2017), motor neuron disease (Winkler et al., 2013) and cortical spreading depression (a wave of profound neuronal depolarization triggered by brain trauma, epilepsy or during migraine attacks) (Khennouf, et al 2018). It was also recently shown that pericytes have an important role in white-matter health and disease: pericyte degeneration leads to phenotypic changes in mice similar to those described in the white-matter disease associated with small-vessel disease contributing to dementia in humans (Montagne et al., 2018). Pericyte degeneration disrupted white-matter microcirculation, resulting in the accumulation of toxic blood-derived fibrin(ogen) deposits and blood-flow reductions, which triggered a loss of myelin, axons and oligodendrocytes. This disrupted brain circuits, leading to white-matter functional deficits before neuronal loss occurred. Other neurological disorders associated with

cognitive impairment, cerebrovascular dysfunction and white matter lesions, including AD (Baloyannis & Boloyannis, 2012; Farkas & Luiten, 2001; Halliday et al., 2016; Miners et al., 2017; Sengillo et al., 2013), mild dementia (Montagne et al., 2015), stroke (Hall et al., 2014; Peppiatt et al., 2006) and CADASIL (the most common genetic ischemic small-vessel disease associated with cognitive impairment) (Ghosh et al., 2015), also exhibit pericyte degeneration, including loss of pericyte coverage in the white matter (Montagne et al., 2018).

The detrimental role of pericytes in neurological disorders seem to occur through distinct, themed responses: pericyte constriction of CNS capillaries to reduce basal cerebral blood flow and disrupt neurovascular coupling, death of pericytes or their decreased expression of PDGFRβ leading to a breakdown of BBB function, their role in glial scar formation and vasculogenesis, and their regulation of immune cell entry in to the CNS (Cheng et al., 2018).

In this thesis, I focused primarily on investigating deleterious constriction of cortical capillaries by pericytes in stroke and AD, and determining whether human cortical capillaries are morphologically and functionally similar to rodent capillaries. I have now shown that human cortical capillary pericytes have a similar morphology and are able to constrict and relax capillaries in the same way as has been shown for rodent cortical capillary pericytes. I found that endothelin is a powerful vasoconstrictor of the cortical capillary bed and has a more rapid constricting effect on cortical capillaries than cortical arterioles. Futhermore, using endothelin and NeuroTrace-labelling, I was able to demonstrate that capillaries with longitudinally processes (which are found in the middle of the capillary bed) are contractile, raising the possibility that

pericytes are capable of controlling blood flow throughout the capillary network using contractile apparatus other than α smooth muscle actin (e.g. β or γ actin).

In further work using live brain slices, I found that ischaemia-driven constriction of pericytes may be delayed by pharmacological intervention with nimodipine, which spurred further experiments demonstrating that pericyte death can be prevented by treatment with the same drug during ischaemia followed by re-oxygenation. These findings suggest that nimodipine warrants further investigation as a potential treatment (to delay pericyte constriction and death to prevent no reflow) to be given at the same time as, or perhaps before, thrombolysis/ mechanical thrombectomy.

Considering that pericytes have recently been shown to play a role in the pathogensis of subcortical vascular dementia (a disease for which there are currently no licenced treatments) (Montagne et al., 2018), and that nimodipine inhibits pericyte mediated constriction of brain capillaries and subsequent death in rigor during ischaemia, it will be intesting to see the outcome of an ongoing randomised controlled trial of calcium channel blockade with 'Amlodipine For the treatment oF subcortical ischaEmic vasCular demenTia' (AFFECT; Greenan et al., 2016). This trial is based on the hypothesis that treatment with amlodipine can improve outcomes for patients with subcortical ischaemic vascular dementia in a phase IIb, multi-centre, double-blind, placebo-controlled randomised trial. Of course, if any beneficial outcomes are found, it will be difficult to determine whether these are in any part attributable to the action of calcium channel blockers on pericytes.

Moving from investigations relevant to the role played by pericytes in acute disturbances of cortical blood flow, I focused on the role of pericytes in Alzheimer's disease, where chronic blood flow changes may play an early, important role in its pathogenesis. Here, I found that Aβ oligomers constrict human cortical capillaries at low nanomolar concentrations and that this effect is mediated by generation of reactive oxygen species, which activates endothelin signalling via ET_A receptors. Furthermore, by analysing the diameter of capillaries in human patients with cognitive decline, who either showed or lacked deposition of Aβ, I demonstrated that Alzheimer's pathology leads to capillary constriction specifically at pericytes, with a magnitude that is estimated to reduce blood flow by a factor of at least 2, and that the magnitude of the capillary constriction in dementia patients increases with the severity of Aβ deposition.

These novel data on Aβ induced pericyte capillary constriction likely explain the recent findings by Østergaard's group of increased capillary transit time heterogeneity in an aged AD mouse model and patients with Alzheimer's disease AD and that cognitive decline over time in AD patients was associated with increasing whole brain relative transit time heterogeneity (Gutiérrez-Jiménez et al., 2017; Nielsen et al., 2017). Moreover, these data suggest several potential therapeutic approaches for early AD, the most promising of which perhaps is to try to reduce endothelin release or the effects of endothelin specifically on its type A receptors located on CNS pericytes, by generating an endothelin receptor blocker which also binds to another target protein on pericytes, such as PDGFRβ or the proteoglycan NG2.

In light of the findings of this thesis, it seems conceivable that signaling pathways upstream of pericyte Ca^{2+}, or operating in parallel with pericyte Ca^{2+} (such as oxidative stress in ischaemia; Yemisci, 2009, or amyloid deposition in capillary walls in Type 1 CAA; Smith & Greenberg, 2009) which promote pericyte constriction are involved in CNS disorders and neurodegenerative diseases other than stroke and AD (Cheng et al., 2018). Diseases in which such pathways might exist include Parkinson's disease (Padel et al., 2016), and HIV-associated dementia (Niu et al., 2014), where other forms pericyte dysfunction have previously been shown to play pathogenic roles. These signaling pathways could be targeted to relieve to capillary constriction by pericytes, which may contributing to the pathogenesis of these diseases.

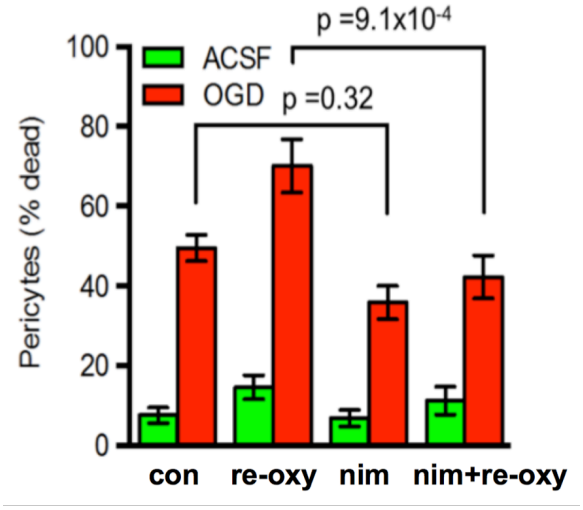

Figure 6.1 Nimodipine reduces pericyte death in oxygen and glucose deprivation followed by re-supply of oxygen and glucose. Nimodipine (3 μM) significantly reduced pericyte death for OGD followed by reoxygenation (p values from one-way ANOVA with Holm-Bonferroni corrected post-hoc t-tests): 49.5±3.3% of pericytes died in OGD and 35.8±4.2% died in OGD+nimodipine (n=6 each, p=0.029); reoxygenation after OGD led to 70.1±6.7% of pericytes dying but with OGD+nimodipine this was reduced to 42.2±5.4% (n=6 each, p=0.018). Work carried out by Fergus O'Farrell in the Attwell lab.

Bibliography

Adams, H.P. Jr, Bendixen, B.H., Kappelle, L.J. et al. Classification of subtype of acute ischemic stroke. Definitions for use in a multicenter clinical trial. TOAST. Trial of Org 10172 in Acute Stroke Treatment. Stroke 24, 35–41 (1993).

Agarwal, A., Wu, P.H., Hughes, E.G., Fukaya, M., Tischfield, M.A., Langseth, A.J., Wirtz, D., Bergles, D.E. Transient opening of the mitochondrial permeability transition pore induces microdomain calcium transients in astrocyte processes. Neuron 93, 587-605 (2017).

Ahmed, M., Davis, J., Aucoin, D., Sato, T., Ahuja, S., Aimoto, S., Elliot, J.I., Van Nostrand, W.E., Smith, S.O. Structural conversion of neurotoxic amyloid-beta$_{1-42}$ oligomers to fibrils. Nat Struct Molecular Biol. 17(5), 561-7 (2010).

Allen, N. J., Karadottir, R. & Attwell, D. A preferential role for glycolysis in preventing the anoxic depolarization of rat hippocampal area CA1 pyramidal cells. J Neurosci. 25(4), 848-59 (2005).

Alzheimer, A. Über einen eigenartigen schweren Erkrankungsprozeβ der Hirnrincle. Neurol Central. 25, 1134 (1906).

András, I.E., Deli, M.A., Veszelka, S. et al. The NMDA and AMPA/KA receptors are involved in glutamate-induced alterations of occludin expression and phosphorylation in brain endothelial cells. J Cereb Blood Flow Metab 27, 1431–1443 (2007).

Ames A. III, Wright, R.L., Kowada, M., Thurston, J.M., Majno, G. Cerebral

Ischaemia II. The no-reflow phenomenon. Am J Pathol. 52, 437-453 (1968).

Amarenco, P., Bogousslavsky, J., Caplan, L.R., Donnan, G.A., Wolf, M.E., Hennerici, M.G. The ASCOD phenotyping of ischemic stroke (Updated ASCO Phenotyping). Cerebrovasc Dis. 36, 1–5 (2013).

Armulik, A., Abramsson, A., Betsholtz, C. Endothelial/Pericyte Interactions. Circ. Res. 97, 512-23 (2005).

Armulik, A., Genové, G., Betsholtz, C. Pericytes: Developemental, physiological and pathological perspectives, problems and promises. Developmental Cell 21, 193-215 (2011).

Armulik, A., Genové, G., Mäe, M., Nisancioglu, M.H., Wallgard, E., Niaudet, C., He, L., Norlin, J., Lindblom, P., Strittmatter, K., Johansson, B.R., Betsholtz. C. Pericytes regulate the blood-brain barrier. Nature 468, 557-61 (2010).

Arriagada, P. V., Growdon, J. H., Hedley-Whyte, E. T., Hyman, B. T. Neurofibrillary tangles but not senile plaques parallel duration and severity of Alzheimer's disease. Neurology 42, 631–639 (1992).

Attems J, Jellinger KA. Only cerebral capillary amyloid angiopathy correlates with Alzheimer pathology--a pilot study. Acta Neuropathol. 107, 83–90 (2004).

Attems, J., Lintner, F., Jellinger, K.A. Amyloid β peptide 1-42 highly correlates with capillary cerebral amyloid angiopathy and Alzheimer disease pathology. Acta Neuropathol. 107, 283-291 (2004).

Attems, J., Jellinger, K.A., Lintner, F. Alzheimer's disease pathology influences severity and topographical distribution of cerebral amyloid angiopathy. Acta Neuropathol. 10, 222– 231 (2005).

Attwell, D., Buchan, A., Charpak, S., Lauritzen, M., MacVicar, B.A., Newman, E.A. Glial and neuronal control of blood flow. Nature 468, 232-243 (2010).

Attwell, D., Iadecola, C. The neural basis of functional brain imaging signals. Trends Neurosci. 25, 621–-625 (2002).

Attwell, D., Laughlin, S. B. An energy budget for signalling in the grey matter of the brain. J. Cereb Blood Flow Metab. 21, 113-1145 (2001).

Attwell, D., Mishra, A., Hall, C.N., O'Farrell, F.M., Dalkara, T. What is a pericyte? J. Cereb. Blood Flow Metab. 36, 451-455 (2016).

Ay, H., Benner, T., Arsava, E.M. et al. A computerized algorithm for etiologic classification of ischemic stroke: the Causative Classification of Stroke System. Stroke 38, 2979–84 (2007).

Badhiwala, J.H., Nassiri, F., Alhazzani, W. et al. Endovascular thrombectomy for acute ischemic stroke: a meta-analysis. JAMA 314, 1832–43 (2015).

Bak, L.K., Schousboe, A. Misconceptions regarding basic thermodynamics and enzyme kinetics have led to erroneous conclusions regarding the metabolic importance of lactate dehydrogenase isoenzyme expression. J Neurosci Res doi: 10.1002/jnr.23994. [Epub ahead of print] (2017).

Baloyannis, S.J. & Baloyannis, I.S. The vascular factor in Alzheimer's disease: a study in Golgi technique and electron microscopy. J. Neurol. Sci. 322, 117–121 (2012).

Bandopadhyay, R., Orte, C., Lawrenson, J. G., Reid, A. R., De, S. S., Allt, G. Contractile proteins in pericytes at the blood-brain and blood-retinal barriers. J. Neurocytol. 30, 35–44 (2001).

Barnes, D.E., Yaffe, K. The projected effect of risk factor reduction on Alzheimer's disease prevalence. Lancet Neurology 10 (9), 819-28 (2011).

Bateman, R.J., Xiong, C., Benzinger, T.L. et al. Clinical and biomarker changes in dominantly inherited Alzheimer's Disease. NEJM 367 (9), 795-804 (2012).

Bazargani, N., Attwell, D., Astrocyte calcium signalling: the third wave. Nat Neurosci 19, 182-189 (2016).

Bell, M.A., Ball, M.J. Morphometric comparison of hippocampal microvasculature in ageing and demented people: diameters and densities. Acta Neuropathol. 53, 299–318 (1981).

Bell, R.D., Winkler, E.A., Singh, I. et al. Apolipoprotein E controls cerebrovascular intergrity via cyclophilin A. Nature 485, 512-16 (2012).

Bell, R.D., Winkler, E.A., Sagare, A.P., Singh, I., LaRue, B., Deane, R., Zlokovic, B.V. Pericytes control key neurovascular functions and neuronal phenotype in the adult brain and during ageing. Neuron 68 (3), 409-27 (2010).

Benedictus, M.R., Goos, J.D.C., Binnewijzend, M.A.A., Muller, M., Barkhof, F., Scheltens, P., Prins, N.D., and van der Flier, W.M. Specific risk factors for microbleeds and white matter hyperintensities in Alzheimer's disease. Neurobiol. Aging 34, 2488–2494 (2013).

Benilova, I., Karran, E., De Strooper, B. The toxic Aβ oligomer and Alzheimer's disease: an emperor in need of clothes. Nat Neurosci. 15, 349-357 (2012).

Berkhemer O.A., Fransen P.S.S., Beumer D. et al. A randomized trial of intraarterial treatment for acute ischemic stroke. N Engl J Med 372, 11-20 (2015).

Bertram, L., McQueen, M.B., Mullin, K., Blacker, D., Tanzi, R.E. Systematic meta-analyses of Alzheimer disease genetic association studies: the AlzGene database. Nat Genet 39(1), 17-23 (2007)

Bertsch, T., Kuehl, S., Muehlhauser, F. et al. Source of endothelin-1 in subarachnoid haemorrhage. Clin Chem Lab Med. 39, 341-345 (2001).

Bettens, K., Sleegers, K., Van Broeckhoven, C. Genetic insights in Alzheimer's disease. Lancet Neurol. 12 (1), 92-104 (2013).

Bianca, V.D., Dusi, S., Bianchini, E., Dal Prà, I., Rossi, F. β-amyloid activates the O_2 forming NADPH oxidase in microglia, monocytes, and neutrophils. A possible inflammatory mechanism of neuronal damage in Alzheimer's disease. J. Biol. Chem. 274,15493-15499. (1999).

Biesecker, K.R., Srienc, A.I., Shimoda A,M., Agarwal, A., Bergles, D.E., Kofuji, P., Newman, E.A. Glial cell calcium signalling mediated capillary regulation of blood flow in the retina. J Neurosci. 36, 9435-9445 (2016).

Biesold, D., Inanami, O., Sato, A., Sato, Y. Stimulation of nucleus basilis of Meynert increases cerebral cortical blood flow in rats. Neurosci Lett 13, 39-44 (1989).

Biffi, A., Sonni, A., Anderson, C.D., et al. Variants at APOE influence risk of deep and lobar intracerebral hemorrhage. Ann Neurol 68, 934–43 (2010).

Blinder P, Tsai PS, Kaufhold JP, Knutsen PM, Suhl H, Kleinfeld D. The cortical angiome: an interconnected vascular network with noncolumnar patterns of blood flow. Nat Neurosci. 16:889-897 (2013).

Bouras C, Kovari E, Herrmann FR, Rivara CB, Bailey TL, von Gunten A, Hof PR, Giannakopoulos P. Stereologic analysis of microvascular morphology in the elderly: Alzheimer disease pathology and cognitive status. J Neuropathol Exp Neurol. 65, 235–244 (2006).

Borysova, L., Wray, S., Eisner, D.A., Burdyga, T. How calcium signals in myocytes and pericytes are integrated across in situ microvascular netwroks and control microvascular tone. Cell Calcium 54, 163-174 (2013).

Braak, H., Braak, E. Neuropathological staging of Alzheimer-related changes. Acta Neuropathol. 82, 239–59 (1991).

Brain, S.D. The direct observation of arteriolar constriction induced by endothelin in vivo. Eur J Pharmacol 160, 401-3 (1989).

Bramlett, H.M., Dietrich, W.D. Pathophysiology of cerebral ischaemia and brain trauma: Similarities and differences. J. Cereb Blood Flow Metab. 24, 133-150 (2004).

Brandner S. Histopathology of cerebral microbleeds. In: Werring DJ, ed. Cerebral microbleeds: pathophysiology to clinical practice. Cambridge: Cambridge University Press, 2011:49e64.

Brecht, W. J., Harris, F.M., Chang, S. et al. Neuron-specific apolipoprotein e4 proteolysis is associated with increased tau phosphorylation in brains of transgenic mice. J. Neurosci. 24, 2527–2534 (2004).

Brenman, J.E., Chao, D.S., Gee, S.H. Interaction of nitric oxide synthase with postsynaptic density protein PSD-95 and α1-Syntrophin Mediated by PDZ domains. Cell 84, 757-767 (1996).

Broughton, B.R., Reutens, D.C., Sobey, C.G. Apoptotic Mechanisms After Cerebral Ischemia. Stroke 40, e331-e339 (2009)

Brunner, F., Opie, L.H. Role of Endothelin-A recptors in ischaemic contracture and reperfusion injury. Circulation 97, 391-8 (1998)

Buee, L., Hof, P.R., Bouras, C., Delacourte, A., Perl, D.P., Morrison, J.H., Fillit, H.M. Pathological alterations of the cerebral microvasculature in Alzheimer's disease and related dementing disorders. Acta Neuropathol. 87, 469–480 (1994).

Butryn, R.K., Ruan, H., Hull, C.M., Frank, R.N. Vasoactive agonists do not change the calibre of retinal capillaries of the rat. Microvasc Res. 50, 80-93 (1995).

Campbell, B.C.V., Mitchell, P.J., Kleinig, T.J. et al. Endovascular therapy for ischemic stroke with perfusion-imaging selection. N Engl J Med 372, 1009-18 (2015).

Capra, V., Bäck, M., Barbieri, S.S. Camera, M., Tremoli, E., Rovati, G.E. Eicosanoids and their drugs in cardiovascular diseases: focus on atherosclerosis and stroke. Med. Res. Rev. 33, 364-438 (2013).

Caughey, B., Lansbury, P.T. Protofibrils, pores, fibrils, and neurodegeneration: separating the responsible protein aggregates from the innocent bystanders. Annu. Rev. Neurosci. 26, 267–298 (2003).

Cauli, B., Hamel, E. Revisiting the role of neurons in neurovascular coupling. Front. Neuroenergetics *2*, 9 (2010).

Chakravarthy, U., Gardiner, T.A., Anderson, P., Archer, D.B., Trimble, E.R. The effect of endothelin-1 on the retinal microvascular pericyte. Microvasc Res. 43, 241-254 (1992).

Charidimou, A., Gang, Q., and Werring, D.J. Sporadic cerebral amyloid angiopathy revisited: recent insights into pathophysiology and clinical spectrum. J. Neurol. Neurosurg. Psychiatry *83*, 124–137 (2011).

Chen, B. R., Kozberg, M.G., Bouchard, M.B., Shaik, M.A. Hillman, E.M. A critical role for the vascular endothelium in functional neurovascular coupling in the brain. J Am Heart Assoc. 3, e000787 (2014).

Cheng, J., Korte, N., Nortley, R. et al. Targeting pericytes for therapeutic approaches to neurological disorders. Acta Neuropathol. 136, 507-523 (2018)

Cipolla, M.J. Integrated Systems Physiology: From Molecule to Function (Morgan & Claypool Life Sciences) (2010)

Cleary, J. P., Walsh, D.M. Hofmeister, J.J., Shankar, G.M., Kuskowski, M.A., Selkoe, D.J., Ashe, K.H. Natural oligomers of the amyloid-β protein specifically disrupt cognitive function. Nat Neurosci. 8, 79–84 (2005).

Clozel, M., Breu, V., Burri, K., Cassal, J., Fischli, W., Gray, G. A., Hirth, G., Löffler, B., Müller, M., Neidhart, W., Ramuz, H. Pathophysiological role of endothelin revealed by the first orally active endothelin receptor antagonist. Nature 365, 759-761 (1993).

Cohen, Z., Bonvento, G., Lacombe, P., Hamel, E. Serotonin in the regulation of brain microcirculation. Prog. Neurobiol. *50*, 335–362 (1996).

Cohen, Z., Molinatti, G., Hamel, E. Astroglial and vascular interactions of noradrenaline terminals in the rat cerebral cortex. J. Cereb. Blood Flow Metab. 17, 894-904 (1997).

Crowell, J. W., Sharpe, G.P., Lambright, R.L., Read W.L. Mechanism of death after resuscitation following acute circulatory arrest. Surgery 38, 696-702 (1955).

Crowley, R. W., Medel, R., Dumont, A.S. et al. Angiographic vasospasm is strongly correlated with cerebral infarction after subarachnoid haemorrhage. Stroke 42, 919-23 (2011).

Dai, M., Nuttall, A., Yang, Y., Shi, X. Visualization and contractile activity of cochlear pericytes in the capillaries of the spiral ligament. Hear. Res. 254, 100–107 (2009).

Dalkara, T., Gursoy-Ozdemir, Y., Yemisci, M. Brain microvascular pericytes in health and disease. Acta Neuropathol. 122, 1–9 (2011).

Damisah, E.C., Hill, R.A., Tong, L., Murray, K.N., Grutzendler, J. Nat Neurosci. 20, 1023-1032 (2017).

Daneman, R., Zhou, L., Kebede, A.A., Barres, B.A. Pericytes are required for blood-brain barrier integrity during embryogenesis. Nature 468, 562-566 (2010).

Dawson, D.A., Sugano, H., McCarron, R.M., Hallenbeck, J.M., Spatz, M. Endothelin receptor antagonist preserves microvascular perfusion and reduces ischemic brain damage following permanent focal ischemia. Neurochem Res. 24, 1499-1505 (1999).

Deane, R., Du Yan, S., Submamaryan, R.K. et al. RAGE mediates amyloid-β peptide transport across the blood-brain barrier and accumulation in brain. Nat Med. 9 (7), 907-13 (2003).

de la Torre, J.C., Mussivand, T. Can disturbed brain microcirculation cause Alzheimer's disease? Neurol. Res. 15, 146-153 (1993)

Deming, Y., Li, Z., Kapoor, M. et al. Genome-wide association study identifies four novel loci associated with Alzheimer's endophenotypes and disease modifiers. Acta Neuropathol. 133, 839–856 (2017).

DeNofrio, D., Hoock, T.C., Herman, I. Functional sorting of actin isoforms in microvascular pericytes. J Cell Biol. 109, 191-202 (1989).

Derouiche, A., Haseleu, J., Korf, H.W. Fine astrocyte processes contain very small mitochondria: glial ooxidative metabolism may fuel transmitter metabolism. Neurochem Res 40:2402-2413 (2015).

Dietrich, H.H., Xiang, C., Han, B.H., Zipfel, G.J., Holtzman D.M. Soluble amyloid-beta, effect on cerebral arteriolar regulation and vascular cells. Mol. Neurodegener. 5, 15 (2010).

Dodge, A.B., Hechtman, H.B., Sherpo, D. Microvascular endothelial-derived

autocoids regulate pericyte contractility. Cell Motil Cytoskeleton 18, 180-188 (1991).

Doody, R.S., Raman, R., Farlow, M. et al., A Phase 3 trial of semagacestat for treatment of Alzheimer's disease. N Engl J Med, 369, 341-350 (2013)

Doody, R.S., Thomas, R.G., Farlow, M. et al . Phase 3 trials of solanezumab for mild-to-moderate Alzheimer's disease. N Engl J Med, 370, 311-321 (2014).

Dore-Duffy, P., Cleary, K. Morphology and properties of pericytes. Methods Mol Biol. 686, 49-68 (2011).

Dore-Duffy, P., Katychev, A., Wang, X., Van Buren, E. CNS microvascular pericytes exhibit multipotential stem cell activity. J. Cereb. Blood Flow Metab. 26, 613-24 (2006).

Dorhourt Mees S.M., Rinkel, G. J. E., Feigin, V. L., Algra, A., van den Bergh, W. M., Vermeulen, M., van Gijn, J. Calcium antagonists for aneurysmal subarachnoid haemorrhage. Cochrane database Syst Rev. 3, Art. No: CD000277 (2007).

Drouin-Ouellet, J., Sawiak S.J., Cisbani, G. et al. Cerebrovascular and blood-brain barrier impairments in Huntington's disease: potential implications for its pathophysiol- ogy. Ann Neurol 78, 160–177 (2015).

Duvernoy, H.M., Delon, S., Vannson, J.L. Cortical blood vessels of the human brain. Brain Res Bull. 7(5), 519-79 (1981)

Eberth, C.J. Handbuch der Lehre von der Gewegen des Menschen und der Tiere. 1 (1871)

Egan, M.F., Kost, J., Tariot, P.N. et al. Randomised Trial of Verubecestat for Mild-Moderate Alzheimer's disease. N Engl J Med 378, 1691-1703 (2018)

Elahi, F.M., Miller, B.L. A clinicopathological approach to the diagnosis of dementia. Nat Rev Neurol 13, 457-476 (2017).

Emberson, J., Lees, K.R., Lyden, P. et al., for the Stroke Thrombolysis Trialists' Collaborative Group. Effect of treatment delay, age, and stroke severity on the effects of intravenous thrombolysis with alteplase for acute ischaemic stroke: a meta-analysis of individual patient data from randomised trials. Lancet 384, 1929–35 (2014).

Etminan, N., Vergouwen, M. D., Ilodigwe, D., Macdonald, R. L. Effect of pharmaceutical treatment on vasospasm, delayed cerebral ischaemia and clinical outcome in patients with aneurysmal subarachnoid haemorrhage: a systematic review and meta-analysis. J Cereb. Blood flow Metab. 31, 1443-51 (2011)

Fa, M., Orozco, I.J., Francis, Y.I., Saeed, F., Gong, Y., Arancio, O. Preparation of oligomeric beta-amyloid 1-42 and induction of synaptic plasticity on hippocampal slices. J Vis Exp. 41, 1-3 (2010).

Farkas, E. & Luiten, P.G. Cerebral microvascular pathology in aging and Alzheimer's disease. Prog. Neurobiol. 64, 575–611 (2001).

Feigin, V.L., Forouzanfar, M.H., Krishnamurthi, R. et al. Global and regional burden of stroke during 1990-2010: findings from the global burden of disease study 2010. Lancet 383, 245-55 (2014).

Feigin, V. L., Rinkel, Algra, A., Vermeulen, M., van Gijn, J. Calcium channel antagonists in patients with aneurysmal subarachnoid hemorrhage: A systematic review. Neurology 50, 876-83 (1998).

Fernández-Klett, F., Offenhauser, N., Dirnagl, U., Priller, J., Lindauer, U. Pericytes in capillaries are contractile in vivo, but arterioles mediate functional hyperemia in the mousebrain. Proc. Natl. Acad. Sci. U.S.A. 107, 22290-22295 (2010).

Fernandez-Klett, F., Priller, J. Diverse functions of pericytes in cerebral blood flow regulation and ischemia. J. Cereb. Blood Flow Metab. 35, 883-887 (2015).

Ferri, CP., Prince, M., Brayne, C. et al. Alzheimer's disease International. Global prevalence of dementia: a Delphi consensus study. Lancet 366, 2112–17 (2005).

Filosa, J.A., Bonev, A.D., Straub, S.V., Meredith, A.L., Wilkerson, M.K., Aldrich, R.W., Nelson, M.T. Local potassium signalling couples neuronal activity to vasodilation in the brain. Nat Neurosci. 9, 1397-1403 (2006).

Fisher M. Characterising the target of acute stroke therapy. Stroke. 28, 886-72 (1997)

Fisher, C. M., Kistler, J. P., Davis, J. M. Relation of cerebral vasospasm to subarachnoid haemorrhage visualized by computerized tomographic scanning. Neurosurgery 6, 1-9 (1980).

Fischer, V.W., Siddiqi, A., Yusufaly, Y. Altered angioarchitecture in selected areas of brains with Alzheimer's disease. Acta Neuropathol. 79, 672–679 (1990).

Fitzgerald, M.J.T., Gruener, G., Mtui, E. Clinical Neuroanatomy and Neuroscience, 5th edn Elselvier Saunders (2007).

Flores, J., DiBona, D.R., Beck, C.H., et al. The role of cell swelling in ischemic renal damage and the protective effect of hypertonic solute. J Clin Invest. 51,118–126 (1972).

Freeman, R.D., Li, B. Neural-metabolic coupling in the central visual pathway. Philos. Trans. R. Soc. Lond. B Biol. Sci. *371*, 20150357 (2016).

Galiuto, L., DeMaria, A.N., May-Newman, K. et al. Evaluation of dynamic changes in microvascular flow during ischaemia-reperfusion by myocardial contrast echocardiography. J Am Coll Cardiol. 32(4), 1096-1101 (1998).

Ghika, J.A., Bogousslavsky, J., Regli, F. Deep perforators from the carotid system. Template of vascular territories. Arch Neurol. 47, 1097-1100 (1990).

Ghosh, M. et al. Pericytes are involved in the pathogenesis of cerebral autosomal dominant arteriopathy with subcortical infarcts and leukoencephalopathy. Ann. Neurol. 78, 887–900 (2015).

Glabe, C.G. Common mechanisms of amyloid oligomer pathogenesis in degenerative disease. Neurobiol. Aging 27, 570–575 (2006).

Globus, M.Y., Busto, R., Martinez, E. et al. Comparative effect of transient global ischaemia on extracellular levels of glutamate, glycine, and gamma-aminobutyric acid in vunerable and non-vunerable brain regions in the rat. J Neurochem. 57, 470-478 (1991).

Gordon, G.R., Choi, H.B., Rungta, R.L., Ellis-Davies, G.C., MacVicar, B.A. Brain metabolism dictates the polarity of astrocyte control over arterioles. Nature 456, 745-749 (2008).

Göritz, C., Dias, D.O., Tomilin, N., Barbacid, M., Shupliakov, O., Frisén, J. A pericyte origin of spinal cord scar tissue. Science 333, 238-42 (2011).

Götz, J. & Ittner, L.M. Animal models of Alzheimer's disease and frontotemporal dementia. Nat. Rev. Neurosci. 9, 532–544 (2008).

Gould, I.G., Tsai, P., Kleinfeld, D., Linninger, A. The capillary bed offers the largest hemodynamic resistance to the cortical blood supply. J. Cereb. Blood Flow Metab. 37, 52-68 (2017).

Goyal, M., Demchuk, A.M., Menon, B.K. et al. Randomized assessment of rapid endovascular treatment of ischemic stroke. N Engl J Med 372, 1019-30 (2015).

Goyal, M., Menon B.K., van Zwam, W.H. et al., for the HERMES collaborators. Endovascular thrombectomy after large-vessel ischaemic stroke: a meta-analysis of individual patient data from five randomised trials. Lancet 387, 1723–31 (2016).

Grant, R. I. Hartmann, D.A., Underly, R.G. et al. Organizational hierarchy and structural diversity of microvascular pericytes in adult mouse cortex. J Cereb Blood Flow and Metab. 017 Jan 1:271678X17732229 (2017).

Greenan, C. et al. A randomised controlled trial of calcium channel blockade (CCB) with Amlodipine For the treatment oF subcortical ischaEmic vasCular demenTia (AFFECT): study protocol. Trials. Jul 18;17(1):324. doi: 10.1186/s13063-016-1449-3 (2016)

Greenberg S.M., Briggs, M.E., Hyman, B.T., et al. Apolipoprotein E epsilon 4 is associated with the presence and earlier onset of hemorrhage in cerebral amyloid angiopathy. Stroke 27, 1333–1337 (1996).

Greenberg S.M., Rebeck, G.W., Vonsattel J.P., et al. Apolipoprotein E epsilon 4 and cerebral hemorrhage associated with amyloid angiopathy. Ann Neurol 38, 254–259 (1995).

Greenberg, S,M., Vonsattel, J.P., Segal, A.Z., et al. Association of apolipoprotein E epsilon2 and vasculopathy in cerebral amyloid angiopathy. Neurology 50, 961–965 (1998)

Grinberg, L. T. et al. Prevalence of dementia subtypes in a developing country: a clinicopathological study. Clinics (Sao Paulo) 68, 1140–1145 (2013).

Gutiérrez-Jiménez, E., Angleys, H., Rasmussen, P.M., West, M.J., Catalini, L., Iversen, N.K., Jensen, M.S., Frische, S., Østergaard L. Disturbances in the control of capillary flow in an aged APPswe/PS1ΔE9 model of Alzheimer's disease. Neurobiol. Aging 62, 82-94 (2017).

Hacke, W., Kaste, M., Eluhmki, E. et al. Thrombolysis with alteplase 3 to 4.5 hours after acute ischaemic stroke. N Engl J Med. 359, 1317-29 (2008).

Halim, N.D., Mcfate, T., Mohyeldin, A. et al. Phosphorylation status of pyruvate dehydrogenase distinguishes metabolic phenotypes of cultured rat brain astrocytes and neurons. Glia 58:1168-1176 (2010).

Hall, C.N., Reynell, C., Gesslein, B., Hamilton, N. B., Mishra, A., Sutherland, B. A., O'Farrell, F. M., Buchan, A. M., Lauritzen, M., Attwell, D. Capillary pericytes regulate cerebral blood flow in health and disease. Nature 508, 55–60 (2014).

Hall, C. N., Klein-Flugge, M. C., Howarth, C., Attwell, D. Oxidative phosphorylation, not glycolysis powers presynaptic and postsynaptic mechanisms underlying brain information processing. J Neurosci. 32, 8940-51 (2012).

Hall-Craggs, E.C.B. Anatomy as a basis of clinical medicine, 2nd edn Urban & Schwarzenberg, 1990.

Halliday, M.R. et al. Accelerated pericyte degeneration and blood-brain barrier breakdown in apolipoprotein E4 carriers with Alzheimer's disease. J.

Cereb. Blood Flow Metab. 36, 216–227. (2016).

Hamel, E. Perivascular nerves and the regulation of cerebrovascular tone. J. Appl. Physiol. *100*, 1059–1064 (2006).

Hamilton, N.B., Attwell, D., Hall, C.N. Pericyte-mediated regulation of capillary diameter: a component of neurovascular coupling in health and disease. *Front. Neuroenergetics* **2**, 5 (2010)

Hankey, G. Stroke. Lancet. 389, 641-654 (2016).

Hardy, J., Allsop, D. Amyloid deposition as the central event in the aetiology of Alzheimer's disease. Science. Trends Phamacol Sci 12 (10), 383-8 (1991).

Hardy, J.A., Higgins, G.A. Alzheimer's disease: The amyloid cascade hypothesis. Science 256, 184-85 (1992).

Harris, J.J., Jolivert, R., Attwell, D. Synaptic energy use and supply. Neuron 75 (5), 762-77 (2012).

Hart, R.G., Diener, H.C., Coutts, S.B. et al, and the Cryptogenic Stroke/ESUS International Working Group. Embolic strokes of undetermined source: the case for a new clinical construct. Lancet Neurol. 13, 429–38 (2014).

Hartmann, D.A., Underly, R.G., Grant, R.I. et al. Pericyte structure and distribution in the cerebral cortex revealed by high resolution imaging transgenic mice. Neurophotonics 2 (4), 1-13 (2015)

Hashimura, T., Kimura, T., Miyakawa, T. Morphological changes of blood vessels in the brain with Alzheimer's disease. Jap. J. Psychiatr. Neurol. 45, 661-665 (1991).

Hauck, E.F., Apostel, S., Hoffmann, J.F., Heimann, A., Kempski, O. Capillary flow and diameter changes during reperfusion after global cerebral ischemia studied by intravital video microscopy. J. Cereb. Blood Flow Metab. 24, 383-391 (2004).

Hecht, M., Krämer, L.M., von Arnim, C.A.F. et al. Capillary cerebral amyloid angiopathy in Alzheimer's disease: association with allocortical/hippocampal microinfarcts and cognitive decline. Acta Neuropathologica 135, 681–694 (2018).

Heneka, M.T., Kummer, M.P., Stutz, A. et al. NLRP3 is activated in Alzheimer's disease and contributes to pathology in APP/PS1 mice. Nature 493, 674–678 (2013).

Heneka, M.T., Carson, M.J., El Khoury, J. et al. Neuroinflammation in Alzheimer's disease. Lancet Neurol. 14, 388-405 (2015).

Heneka, M.T., Golenbock, D. T., Latz, E. Innate immunity in Alzheimer's disease. Nat. Immunol. 16, 229–236 (2015).

Herrero-Mendez, A., Almeida, A., Fernández, E., Maestre, C., Moncada, S., Bolaños, J.P. The bioenergetic and antioxidant status of neurons is controlled by continuous degradation of a key glycolytic enzyme by APC/C-Cdh1. Nat Cell Biol 11, 747-752 (2009).

Herrup, K. The case for rejecting the amyloid cascade hypothesis. Nat Neurosci. 794-799 (2015).

Hess, P., Lansman, Jeffry, B., Tsien, R.W. Different modes of Ca channel behaviour favoured by diydropyridine agonists and antagonists. Nature 311, 538-544 (1984).

Hickey, K.A., Rubanyi, G., Paul, R.J., Highsmith, R.F. Characterisation of coronary vasoconstrictor produced by cultured endothelial cells. Am J. Physiol. 248, C550-C556 (1985).

Hill, R.A., Tong, L., Yuan, P., Murikinati, S., Gupta, S., Grutzendler, J. Regional blood flow in the brain is controlled by arteriolar smooth muscle cell contractility and not by capillary pericytes. Neuron. 87, 1-16 (2015).

Hochgräfe, K., Sydow, A. & Mandelkow, E.M. Regulatable transgenic mouse models of Alzheimer disease: onset, reversibility and spreading of Tau pathology. FEBS J. 280, 4371–4381 (2013).

Hock, B.J. Jr. & Lamb, B.T. Transgenic mouse models of Alzheimer's disease. Trends Genet. 17, S7–S12 (2001).

Holmes, C. et al. Long-term effects of Aβ42 immunisation in Alzheimer's disease: follow-up of a randomised, placebo-controlled phase I trial. Lancet 372, 216–223 (2008).

Honig, L.S., Kukull, W., and Mayeux, R. Atherosclerosis and AD: analysis of data from the US National Alzheimer's Coordinating Center. Neurology 64, 494–500 (2005).

Horn, J., Limburg, M. Calcium antagonists for ischemic stroke: a systematic review. Stroke. 32, 570-6 (2001).

Howarth, C., Sutherland, B., Choi, H.B., Martin, C., Lind, B.L., Khennouf, L., LeDue, J.M., Pakan, J.M., Ko, R.W., Ellis-Davies, G. et al. A critical role for astrocytes in hypercapnic vasodilation in brain. J Neurosci. 37, 2403-2414 (2017).

http://www.alzgene.org

http://www.alzheimers.org.uk/site/scripts/documents_info.php?documentID=418

Huang, Y., Lennart Mucke, L. Alzheimer mechanism and therapeutic strategies. Cell 148, 1204-22 (2012).

Huang, F.J., You, W.K., Bonaldo, P., Seyfried, T.N., Pasquale, E.B., Stallcup, W.B. Pericyte deficiencies lead to aberrant tumor vascularization in the brain of NG2 null mouse. Dev. Biol. 344, 1035-46 (2010).

Iadecola, C. Regulation of the cerebral microcirculation during neural activity: is nitric oxide the missing link? Trends Neurosci. *16*, 206–214 (1993).

Iadecola, C. The pathobiology of vascular dementia. Neuron 80, 844-866 (2013).

Iadecola, C. Neurovascular regulation in the normal brain and in Alzheimer's disease. Nat Rev Neurosci. 5, 347-360 (2004).

Iadecola, C. The Neurovascular unit coming of age: A journey through neurovascular coupling in health and disease. Neuron 96, 17-42 (2017).

Iadecola, C., Zhang, F., Niwa, K. et al. SOD1 rescues cerebral endothelial dysfunction in mice overexpressing amyloid precursor protein. Nat Neurosci. 2, 157–161 (1999).

Iadecola, C., Yang, G., Ebner, T. J., Chen, G. Local and propergated vascular responses evoked by focal synaptic activity in cerebellar cortex. J. Neurophysiol. 78, 651-59 (1997).

Institoris, Á., Rosenegger, D.G., Gordon, G.R. Arteriole dilation to synaptic activation that is sub-threshold to astrocyte endfoot Ca^{2+} transients. J Cereb Blood Flow Metab 35, 1411-1415 (2015).

IST-3 collaborative group. The benefits and harms of intravenous thrombolysis with recombinant tissue plasminogen activator within 6 h of acute ischaemic stroke (the third international stroke trial [IST – 3]: a randomised controlled trial. Lancet. 9834, 2352-63 (2012).

Iturria-Medina, Y. Sotero, R.C., Toussaint, P.J. et al. Early role of vascular dysregulation on late-onset Alzheimer's disease based on multifactorial data-driven analysis. Nat Commun 7, 11934 (2016).

Iwamoto, R., Yamazaki, S., Asakura, M. et al. Heparin binding EGF-like growth factor and ErbB signaling is essential for heart function. Proc Natl. Acad. Sci. USA 100, 3221-26 (2003).

Jackson, J.G., O'Donnell, J.C., Takano, H., Coulter. D.A., Robinson, M.B. Neuronal activity and glutamate uptake decrease mitochondrial mobility in astrocytes and position mitochondria near glutamate transporters. J Neurosci 34, 1613-1624 (2014).

James, B. D., Bennett, D. A., Boyle, P. A., Leurgans, S. & Schneider, J. A. Dementia from Alzheimer disease and mixed pathologies in the oldest old. JAMA 307, 1798–1800 (2012).

Jan, A., Hartley, D.M., Lashuel, H.A. Preparation and characterization of toxic Aβ aggregates for structural and functional studies in Alzheimer's disease research. Nat Protoc. 5, 1186-1209 (2010).

Jellinger, K.A. Pathology and pathogenesis of vascular cognitive impairment-a critical update. Front Aging Neurosci *5*, 17 (2013.

Jones, E.G. On the mode of entry of blood vessels into the cerebral cortex. J. Anat. *106*, 507–520 (1970).

Jones, T. H., Morawetz, R. B., Cromwell, R. M. et al Thresholds of focal cerebral ischaemia in awake monkeys. J Neurosurg. 54, 773-82 (1981).

Josephs, K. A., Whitwell, J.L., Ahmed Z. et al. β-amyloid burden is not

associated with rates of brain atrophy. Ann. Neurol. 63, 204–212 (2008).

Jovin, T.G., Chamorro, A., Cobo, E. et al. Thrombectomy within 8 hours after symptom onset in ischemic stroke. N Engl J Med 372, 2296-306 (2015).

Juanmuktane, Z., Mead, S., Ellis, M. et al. Evidence for human transmission of amyloid-β pathology and cerebral amyloid angiopathy. Nature, 525, 247-250 (2015).

Kalaria, R. N. The role of cerebral ischemia in Alzheimer's disease. Neurobiol. Aging 21, 321–330 (2000).

Kamouchi, M., Kitazono, T., Ago, T., Wakisaka, M., Ooboshi, H., Ibayashi, S., Iida, M. Calcium influx pathways in rat CNS pericytes. Brain Res Mol Brain Res. 126, 114-20 (2004).

Kang, J., Lemaire, H.G., Unterbeck, A., Salbaum, J.M., Masters, C.L., Grzeschik, K.H., Multhaup, G., Beyreuther, K., Müller-Hill, B. The precursor of Alzheimer's disease amyloid A4 protein resembles a cell-surface receptor. Nature 325, 733-736 (1987).

Karch, C. M., Goate, A. M. Alzheimer's disease risk genes and mechanisms of disease pathogenesis. Biol Physchiatry 77, 43-51 (2015).

Kassell, N., Torney J., Clarke Haley, E. Jr., et al. The international cooperative study on the timing of aneurysm surgery. J Neurosug. 73, 18-36 (1990).

Katz, A.M. & Leach, N.M. Differential effects of 1,4-dihydropyridine calcium

channel blockers: therapeutic implications. J Clin Pharmacol. 825-34. (1987)

Kawamura, H., Oku, H., Li, Q., Sakagami, K., and Puro, D. G. (2002). Endothelin- induced changes in the physiology of retinal pericytes. *Invest Ophthalmol. Vis. Sci.* 43, 882–888.

Kazda, S., Towart, R. Nimodipine: a new calcium antagonistic drug with a preferential cerebrovascular action. Acta Neurochir. 63, 259-65 (1982).

Kennedy-Lydon, T., Carwford, C., Wildman, S.S., Peppiatt-Wildman, C.M. Nonsteroidal anti-inflammatory drugs alter vasa recta diameter via pericytes. Am J Physiol. 309, 648-657 (2015).

Khennouf, L., Gesslein, B., Brazhe, A., et al. Active role of capillary pericytes during stimulation-induced activity and spreading depolarisation. Brain 141, 2032-2046 (2018).

Kim, J. et al. Normal cognition in transgenic BRI2-Aβ mice. Mol. Neurodegener. 8, 15 (2013).

Kim K.J., Ramiro Diaz, J., Iddings, J.A., Filosa, J.A. Vasculo-neuronal coupling: retrograde vascular communication to brain neurons. J Neurosci. 36, 12624-12639 (2015).

Kimura, T., Hashimura, T., Miyakawa, T. Observations of microvessels in the brain with Alzheimer's disease by the scanning electron microscope. Jap. J. Psychiatr. Neurol. 45, 671-676 (1991).

Kisler, K., Nelson, A.R., Rege, S.V. et al. Pericyte degeneration leads to neurovascular uncoupling and limits oxygen supply to brain. Nat Neurosci 20, 406-416 (2017).

Kisler, K., Nelson, A.R., Montagne, A., Zlokovic, B.V. Cerebral blood flow regulaton and neurovascular dysfunction in Alzheimer disease. Nat Rev Neurosci. 18, 419-434 (2017).

Kitaguchi, H., Ihara, M., Saiki, H., Takahashi, R., Tomimoto, H. Capillary beds are decreased in Alzheimer's disease, but not in Binswanger's disease. Neurosci Lett. 417, 128–131 (2007).

Kitazawa, M., Medeiros, R. & Laferla, F.M. Transgenic mouse models of Alzheimer disease: developing a better model as a tool for therapeutic interventions. Curr. Pharm. Des. 18, 1131–1147 (2012).

Klein, W.L., Krafft, G.A., Finch, C.E. Targeting small Aβ oligomers: the solution to an Alzheimer's disease conundrum? Trends Neurosci. 24, 219-224 (2001).

Kloner, R.A., Ganote, C.E., Jennings, R.B. The "no-reflow" phenomenon after temporary coronary occlusion in the dog. J Clin Invest. 54, 1496–1508 (1974).

Klunk, W. et al. Amyloid imaging with PET in Alzheimer's disease, mild cognitive impairment, and clinically unimpaired subjects. in PET in the Evaluation of Alzheimer's Disease and Related Disorders (ed. Silverman, D.) 119–147 (Springer Science + Business Media LLC, 2009).

Ko, K.R., Ngai, A.C., Winn, H.R. Role of adenosine in regulation of regional cerebral blood flow in the sensory cortex. Am J Physiol. 259, 1703-1708 (1990).

Kogure, D. Matsuda, H., Ohnishi, T. et al. Longitudinal evaluation of early Alzheimer's disease using brain perfusion SPECT. J. Nucl. Med. 41, 1155–1162 (2000).

Koller, A., Toth, P. Contribution of flow-dependent vasomotor mechanisms to the autoregulation of cerebral blood flow. J. Vasc. Res. *49*, 375–389 (2012).

Korczyn, A. D. The complex nosological concept of vascular dementia. J. Neurol. Sci. 203–204, 3–6 (2002).

Kornau, H.C., Schenker, L.T., Kennedy, M.B., Seeburg, P.H. Domain interaction between NMDA receptor and the postsynaptic density protein PSD-95. Science 5231, 1737-1740 (1995).

Koudstaal, P.J., Ciabattoni, G., van Gijn, J., Nieuwenhuis, H.K., de Groot, P.G., Sixma, J.J., Patrono, C. Increased thromboxane biosynthesis in patients with acute cerebral ischaemia. Stroke 24, 219-23 (1993).

Kowada, M., Ames, A. III, Majno, G. et al. Cerebral ischemia. I. An improved experimental method for study; cardiovascular effects and demonstration of an early vascular lesion in the rabbit. J Neurosurg. 28, 150-157 (1968).

Krizbai, I. A., Deli, M.A., Pestenácz, A. Expression of glutamate receptors on cultured cerebral endothelial cells. J Neurosci Res 15, 814-819 (1998).

Krueger, M., Bechmann, I. CNS pericytes: concepts, misconceptions, and a way out. Glia *58*, 1–10 (2010).

Kunz, J., Krause, D., Kremer, M., Dermietzel, R. The 140-kDa protein of the blood-brain barrier associated with pericytes is identical to aminopeptidase. N. J. Neurochem. 6, 2375-86 (1994).

LaFerla, F.M. & Green, K.N. Animal models of Alzheimer disease. Cold Spring Harb. Perspect. Med. 2, a006320 (2012)

Lambert, M. P., Barlow, A.K., Chromy, B.A. et al. Diffusible, nonfibrillar ligands derived from Aβ1–42 are potent central nervous system neurotoxins. Proc. Natl Acad. Sci. *USA* 95, 6448–6453 (1998).

Lambert, M.P., Viola, K.L., Chromy, B.A. et al. Vaccination with soluble Ab oligomers generates toxicity-neutralizing antibodies. J Neurochem. 79, 595-605 (2001).

Lamont, R. E., Vu, W., Carter, A.D., Sertuca, F.C., MacRae, C.A., Childs, S.J. Hedgehog signaling via angiopoietin 1 is required for developmental vascular stability. Mech. Dev. 127, 159-68 (2010).

Lampl, Y., Fleminger, G., Gilad, R. Endothelin in cerebrospinal fluid and plasma of patients in the early stage of ischemic stroke. Stroke 28,1951-1955 (1997).

Leal-Campanario, R., Alarcon-Martinez, L., Rieiro, H. et al. Abnormal capillary vasodynamics contribute to ictal neurodegeneration in epilepsy. Sci Rep. 7:43276 doi: 10.1038/srep43276 (2017).

Lee, S.T., Seo, Y., Bae, J,Y. et al. Loss of pericytes in radia- 1121 tion necrosis after glioblastoma treatments. Mol Neurobiol 1122 55, 4918–4926 (2017).

Lee, Y., Morrison, B.M., Li, Y. et al. Oligodendroglia metabolically support axons and contribute to neurodegeneration. Nature 487, 443-448 (2012).

Levéen, P., Penky, M., Gebre-Medhin, S., Swolin, B., Larsson, E., Betcholz, C. Mice deficient for PDGFRβ show renal, cardiovascular and hematological abnormalities. Genes Dev. 8, 1875-87 (1994).

Li, Y., Lucas-Osma, A.M., Black, S. et al. Pericytes impair capillary blood flow and motor function after chronic spinal cord injury. Nature Medicine. 23, 733-741 (2017).

Lind, B.L., Brazhe, A.R., Jessen, S.B., Tan, F.C., Lauritzen, M.J. Rapid stimulus-evoked astrocyte Ca^{2+} elevations and hemodynamic responses in mouse somatosensory cortex in vivo. Proc Natl Acad Sci USA 110, E4678-E4687 (2013).

Lindahl, P., Johansson, B.R., Levéen, P., Betscholtz, C. Pericyte loss and microaneurysm formation in PDGFR-β-deficient mice. Science 277, 243-45 (1997).

Lipton, P. Ischemic cell death in brain neurons. Physiol Rev. 79, 1431-1568 (1999).

Liu, S., Premont, R.T., Kontos, C.D., Huang, J. & Rockey, D.C. Endothelin-1 activates endothelial cell nitric-oxide synthase via heterotrimeric G-protein betagamma subunit signaling to protein jinase B/Akt. J Biol Chem. 278, 49929-49935 (2003).

Livingston, G., Sommerlad, A., Orgeta, V. et al. Dementia prevention, intervention, and care. Lancet 390, 2673-2734 (2017).

Lo E.H., Dalkara T., Moskowitz, M. A. Mechanisms, challenges and opportunities in stroke. Nat Rev Neurosci. 4, 399-415 (2003).

Longden, T.A., Dabertrand, F., Koide, M. et al. Capillary K^+-sensing initiates retrograde hyperpolarization to increase local cerebral blood flow. Nat Neurosci 20, 717-726 (2017).

Love, S., Miners, J.S. Cerebrovascular disease in ageing and Alzheimer's disease. Acta Neuropathol. 131, 645-658 (2016).

Lu, A., Magupalli, V.G., Ruan, J. et al. Unified polymerization mechanism for the assembly of ASCdependent inflammasomes. Cell 156, 1193–1206 (2014).

Luengo-Fernandez, R., Paul, N.L., Gray, A.M. et al, for the Oxford Vascular Study. Population-based study of disability and institutionalization after transient ischemic attack and stroke: 10-year results of the Oxford Vascular

Study. Stroke. 44, 2854–61 (2013).

Luk, K.C., Kehm, V., Carroll, J. et al. Pathological α-synuclein transmission initiates Parkinson-like degeneration in nontransgenic mice. Science. 338, 949-53 (2012).

Lundgaard, I., Li, B., Xie, L. et al. Direct neuronal glucose uptake heralds activity-dependent increases in cerebral metabolism. Nat Comm 6, 6807 doi: 10.1038/ncomms7807 (2015).

Luo, J., Grammas, P. Endothelin-1 is elevated in Alzheimer's disease brain microvessels and is neuroprotective. J. Alzheimers Dis. 21, 887-896 (2010).

Lynch, M.A. Neuroinflammatory changes negatively impact on LTP: A focus on IL-1β. Brain Res. 1621, 197-204 (2015).

Macdonald, R. L. Delayed Neurological deterioration after subarachnoid haemorrhage. Nat. Rev. Neurol. 10, 44-58 (2014).

Majno, G., Ames, A III, Chiang, J., Wright, R.L. No reflow after cerebral ischaemia. The Lancet 290, 569-570 (1967).

Marcaggi, P., Attwell, D. Role of glial amino acid transporters in synaptic transmission and brain energetics. Glia 47, 217-225 (2004).

Masters, C.L., Bateman, R., Blennow, K. Alzheimer's disease. Nat. Rev. Dis. Primers 1, 1-18 (2015).

Masumoto, J., Taniguchi, S., Ayukawa, K. et al. ASC, a novel 22-kDa protein, aggregates during apoptosis of human promyelocytic leukemia HL-60 cells. J. Biol. Chem. 274, 33835–33838 (1999).

Mateo, C., Knutsen, P.M., Tsai, P.S., Shih, A.Y. Kleinfeld, D. Entrainment of arteriole vasomotor fluctuations by Neural Activity is a basis of blood-oxygenation-level-dependent 'resting-state' connectivity'. Neuron 96, 936-948 (2017).

Matsumura, S., Shinoda, K., Yamada, M. et al. Two distinct Amyloid β-protein (Aβ) assembly pathways leading to oligomers and fibrils identified by combined fluorescence correlation spectroscopy, morphology, and toxic aggregates. J Biol Chem 286, 11555-11562 (2011).

Mathiiesen, T.M., Lehre, K.P., Danbolt, N.C., Otterson, O.P. The perivascular astroglial sheath provides complete covering of the brain microvessels: an electron micrograpgh 3D reconstruction. Glia 58, 1094-1103 (2010).

McCarron, M.O., Nicoll, J.A., Stewart, J., et al. The apolipoprotein E epsilon2 allele and the pathological features in cerebral amyloid angiopathy-related hemorrhage. J Neuropathol Exp Neurol 58, 711–718 (1999).

McKenna, M.C., Stridh, M.H., McNair L.F., Sonnewald, U., Waagepetersen, H.S., Schousboe, A. Glutamate oxidation in astrocytes: Roles of glutamate dehydrogenase and aminotransferases. J Neurosci Res. 94, 1561-1571 (2016).

Mergenthaler, P., Lindauer, U., Dienel, G.A., Meisel, A. Sugar for the brain: the role of glucose in physiological and pathological brain function. Trends Neurosci. 36, 587-597 (2013).

Meyer, E.P., Ulmann-Schuler, A., Staufenbiel, M., Krucker, T. Altered morphology and 3D architecture of brain vasculature in a mouse model for Alzheimer's disease. Proc Natl Acad Sci U S A 105, 3587–3592 (2008).

Michels, L., Warnock, G., Buck, A. et al. Arterial spin labeling imaging reveals widespread and Aβ-independent reductions in cerebral blood flow in elderly apolipoprotein epsilon-4 carriers. J. Cereb. Blood Flow Metab. 36, 581–595 (2016).

Miklossy, J. Cerebral hypoperfusion induces cortical watershed microinfarcts which may further aggravate cognitive decline in Alzheimer's disease. Neurol. Res. *25*, 605–610 (2003).

Miners, J.S., Schulz, I., Love, S. Differing associations between Aβ accumulation, hypoperfusion, blood-brain barrier dysfunction and loss of PDGFRB pericyte marker in the precuneus and parietal white matter in Alzheimer's disease. J. Cereb. Blood Flow Metab. 38, 103–115 (2017).

Mink, J.W., Blumenschine, R.J., Adams, D.B. Ratio of central nervous system to body metabolism in vertebrates: its constancy and functional basis. Am J. Physiol 240, 203-12 (1981).

Mishra, A., O'Farrell, F. M., Reynell, C., Hamilton, N., Hall, C. N. and Attwell, D. Imaging pericytes and capillary diameter in brain slices and isolated retinae. Nat Protoc. 9, 323-36 (2014).

Mishra, A., Reynolds, J.P., Chen, Y., Gourine, A.V., Rusakov, D.A., Attwell, D. Astrocytes mediate neurovascular signalling to capillary pericytes but not to arterioles. Nat Neurosci.12, 1619-1627 (2016).

Molyneaux, B., Arlotta, P., Menezes, J.R., Macklis, J.D. Neuronal subtype specification in the cerebral cortex. Nat. Rev. Neurosci. 8, 427-437 (2007).

Montagne, A., Barnes, S.R., Sweeney, M.D. et al. Blood–brain barrier breakdown in the aging human hippocampus. Neuron 85, 296–302 (2015).

Montagne, A., Nation, D.A., Pa, J. et al. Brain imaging of neurovascular dysfunction in Alzheimer's disease. Acta Neuropathol. 131, 687–707 (2016).

Montagne, A., Nikolakopoulou, A. M., Zhoa, Z. et al. Pericyte degeneration causes white matter dysfunction in the mouse central nervous system. Nat Med 24, 326-337 (2018).

Montaner, J. Genetics of intracerebral haemorrhage: a tsunami effect of APOE varepsilon2 genotype on brain bleeding size? Lancet Neurol 10, 673–675 (2011).

Mortimer, J. A., van Duijn, C.M., Chandra, V. et al. Head Trauma as a risk factor for Alzheimer's disease: A collaborative re-Analysis of case-control studies. Int J Epidemiol 20 (Suppl. 2), S28-S35 (1991).

Mulligan, S.J., MacVicar, B.A. Calcium transients in astrocyte endfeet cause cerebrovascular constrictions. Nature 431, 195-199 (2004).

Musiek, E.S., Holtzman, D.M. Three dimensions of the amyloid hypothesis: time, space and ‘wingmen’. Nat Neurosci. 18(6), 800-6 (2015).

Nakahata, N. Thromboxane A_2: Physiology/pathophysiology, cellular signal transduction and pharmacology. Pharmacol Ther 118, 18-35 (2008).

Nanba, D., Kinugasa, Y., Morimoto, C. et al. Loss of HB-EGF in smooth muscle or endothelial cell lineages causes heart malformation. Biochem. Biphys. Res. Commun. 350, 315-21 (2006).

Nashmi, R. Velumian, A.A., Chung, I. et al. Patch clamp recordings from white matter glia in thin longitudinal slices of adult rat spinal cord. J Neurosci Methods. 117, 159-66 (2002).

Neely, W.A., Youmans, J.R. Anoxia of canine brain without damage. JAMA 183, 1085-1087 (1963).

Nehls, V., Drenckhahn, D. Heterogeneity of microvascular pericytes for smooth muscle type alpha-actin. J Cell Biol 113:147–154 (1991).

Nehls, V., Denzer, K., Drenckhahn, D. Pericyte involvement in capillary sprouting during angiogenesis in situ. Cell Tissue Res. 270, 469-74 (1992).

Nehls, V., Drenckhahn, D. The versatility of microvascular pericytes: from mesenchyme to smooth muscle? Histochemistry 99, 1-12 (1993).

Nelson, P.T., Schmitt, F.A., Lin, Y. et al. Hippocampal sclerosis in advanced age: clinical and pathological features. Brain 134, 1506-18 (2011).

Neurology Working Group of the Cohorts for Heart and Aging Research in Genomic Epidemiology (CHARGE) Consortium; Stroke Genetics Network (SiGN); International Stroke Genetics Consortium (ISGC). Identification of additional risk loci for stroke and small vessel disease: a meta-analysis of genome-wide association studies. Lancet Neurol. 15, 695–707 (2016).

Nicoll, J.A., Burnett, C., Love, S., et al. High frequency of apolipoprotein E epsilon 2 allele in hemorrhage due to cerebral amyloid angiopathy. Ann Neurol 41, 716–721 (1997).

Nielsen, R.B., Egefjord, L., Angleys, H. et al. Capillary dysfunction ins associated with symptom severity and neurodegeneration in Alzheimer's disease. Alzheimers Dement. 13, 1143-1153 (2017).

NINDS Stroke Genetics Network (SiGN) and International Stroke Genetics Consortium. Loci associated with ischaemic stroke and its subtypes (SiGN): a genome-wide association study. Lancet Neurol. 15: 174–84 (2016).

Nir, T. M., Jahanshad, N., Villalon-Reina, J.E. et al. Effectiveness of regional DTI measures in distinguishing Alzheimer's disease, MCI, and normal aging. Neuroimage Clin. 3, 180–195 (2013).

Niu, F., Yao, H., Zhang, W., et al. Tat 101-mediated enhancement of brain pericyte migration involves platelet-derived growth factor subunit B homodimer: implications for human immunodeficiency virus-associated neurocognitive disorders. J. Neurosci. 34, 11812–11825 (2014).

Niwa, K., Younkin, L., Ebeling, C. et al. Aβ1–40-related reduction in functional hyperemia in mouse neocortex during somatosensory activation. Proc. Natl Acad. Sci. USA 97, 9735–9740 (2000).

Niwa, K., Porter, V.A., Kazama, K., Cornfield, D., Carlson, G.A., Iadecola, C. Aβ-peptides enhance vasoconstriction in cerebral circulation. Am. J. Physiol. Heart Circ. Physiol. 281, H2417-2424 (2001).

Nizar, K., Uhlirova, H., Tian, P. et al. In vivo stimulus-induced vasodilation occurs without IP_3 receptor activation and may precede astrocytic calcium increase. J Neurosci 33, 8411-8422 (2013).

Ngai, A.C., Winn, H.R. Pial arteriole dilation during somatosensory stimulation is not mediated by an increase in CSF metabolites. Am. J. Physiol. Heart Circ. Physiol. *282*, H902–H907 (2002).

Nogueira, R.G., Jadhav, A.P., Haussen, D.C. et al. Thrombectomy 6 to 24 hours after stroke with a mismatch between deficit and infarct. N Engl J Med. DOI: 10.1056/NEJMoa1706442 (2017).

Noguchi, A., Matsumura, S., Dezawa, M. Isolation and characterization of patient-derived, toxic, high mass amyloid beta-protein (Abeta) assembly from Alzheimer disease brains. J Biol Chem 284, 32895-32905 (2009).

Norton, S., Matthews, F.E., Barnes, D.E., Yaffe, K., Brayne, C. Potential for primary prevention of Alzheimer's disease: an analysis of population-based data. Lancet Neurol 13, 788–94 (2014).

Nortley, R., Attwell, D. Control of brain energy supply by astrocytes. Curr Opin Neurobiol 47, 80-85 (2017).

O'Donnell, H.C., Rosand, J., Knudsen, K.A., et al. Apolipoprotein E genotype and the risk of recurrent lobar intracerebral hemorrhage. N Engl J Med 342 240–5 (2000).

O'Farrell, F.M., Attwell, D. A role for pericytes in coronary no-reflow. Nat Rev Cardiol. 11, 427-432 (2014).

O'Farrell, F.M., Mastitskaya, S. Hammond-Hayley, M. et al. Capillary pericytes mediate coronary no-reflow after myocardial ischaemia. eLife2017;6:e29280 DOI: 10.7554/eLife.29280

Orgogozo, J.M. et al. Subacute meningoencephalitis in a subset of patients with AD after Aβ42 immunization. Neurology 61, 46–54 (2003).

Ostergaard, L., Aamand, R., Karabegovic, S. et al. The role of the microcirculation in delayed cerebral ischaemia and chronic degenerative changes after subarachnoid hemorrhage. J Cereb. Blood flow Metab. 33, 1825-37 (2013).

Otsu, Y., Couchman, K., Lyons, D.G. et al. Calcium dynamics in astrocyte processes during neurovascular coupling. Nat Neurosci 18, 210-218 (2015).

Pallone T.L., Silldorff, E.P. Pericyte regulation of renal medullary blood flow. Exp Nephrol. 9 165-170 (2001).

Palmer, J.C., Barker, R., Kehoe, P.G., Love, S. Endothelin-1 is elevated in Alzheimer's disease and upregulated by amyloid-β. J. Alzheimers Dis. 29, 853-861 (2012).

Pantoni, L. Cerebral small vessel disease: from pathogenesis and clinical characteristics to therapeutic challenges. Lancet Neurol 9, 689-701 (2010).

Paris, D., Humphrey, J., Quadros, A. et al. Vasoactive effects of Aβ in isolated human cerebrovessels and in a transgenic mouse model of Alzheimer's disease: role of inflammation. Neurol. Res. 25, 642-651 (2003).

Park, L., Wang, G., Zhou, J. et al. Scavenger receptor CD36 is essential for the cerebrovascular oxidative stress and neurovascular dysfunction induced by amyloid-β. Proc. Natl Acad. Sci. USA 108, 5063–5068 (2011).

Park, L., Anrather, J., Zhou, P. et al. NADPH-oxidase-derived reactive oxygen species mediate the cerebrovascular dysfunction induced by the amyloid ß peptide. J. Neurosci. 25, 1769–1777 (2005).

Park, L., Uekawa, K., Garcia-Bonilla, L. et al. Brain perivascular macrophages initiate the neurovascular dysfunction of Alzheimer Aβ peptides. Circ. Res. 121, 258-269 (2017).

Park, L., Anrather, J., Forster, C., Kazama, K., Carlson, G.A. & Iadecola, C. Abeta-induced vascular oxidative stress and attenuation of functional hyperemia in mouse somatosensory cortex. J. Cereb. Blood Flow Metab. 24, 334-342 (2004).

Passman, J.N., Dong, X.R., Wu, S.P., Maguire, C.T., Hogan, K.A., Bautch, V.L., Majesky, M.W. A sonic hedgehog signalling domain in the arterial advenita supports resident Sca1+ smooth muscle progenitor cells. Proc Natl. Acad. Sci. USA 105, 9349-54 (2008).

Patel, T., Galbraith, S., Graham, D., Hallak, H., Doherty, A., McCulloch, J. Endothelin Receptor Antagonist Increases Cerebral Perfusion and Reduces Ischaemic Damage in Feline Focal Cerebral Ischaemia. J. Cereb Blood Flow Metab. 16, 950-958 (1996).

Pellerin L., Magistretti PJ. Sweet sixteen for ANLS. J. Cereb Blood Flow Metab. 32, 1152-1166 (2012).

Pendlebury, S. T. & Rothwell, P. M. Prevalence, incidence, and factors associated with pre-stroke and post-stroke dementia: a systematic review and metaanalysis. Lancet Neurol. 8, 1006–1018 (2009)

Peppiatt, C.M., Howarth, C., Mobbs, P., Attwell, D. Bidirectional control of CNS capillary diameter by pericytes. Nature 443, 700-04 (2006).

Petruk, K. C., West, M., Mohr, G. et al. Nimodipine treatment in poor grade aneurysm patients. Results of a multicenter double-blind placebo-controlled trial. J Neurosurg. 50, 876-83 (1988).

Pezzini, A., Padovani, A. Cerebral amyloid angiopathy-related hemorrhages. Neurol Sci. 29(Suppl 2), S260–263 (2008)

Phillis, J.W., Smith-Barbour, M., O'Regan, M.H. Changes in the extracellular

amino acid neurotransmitters and purines during and following ischemias of different durations in the rat cerebral cortex. Neuroschem Int. 29, 115-120 (1996).

Plassman, B. L., Havlik, R.J., Steffens, D.C. et al. Documented head injury in early adulthood and risk of Alzheimer's disease and other dementias. Neurology 55, 1158-1166 (2000).

Pluta, R.M., Boock, R.J., Afshar, J.K., Clouse, K., Bacic, M., Ehrenreich, H., Oldfield, E.H. Source and cause of endothelin-1 release into cerebrospinal fluid after subarachnoid hemorrhage. J. Neurosurg 87, 287-293 (1997).

Premkumar D.R., Cohen D.L., Hedera P., et al. Apolipoprotein E-epsilon4 alleles in cerebral amyloid angiopathy and cerebrovascular pathology associated with Alzheimer's disease. Am J Pathol 148, 2083–2095 (1996).

Pries, A.R., Secomb, T.W., Gaehtgens, P., Gross, J.F. Blood flow in microvascular networks. Experiments and simulation. Circ. Res. 67, 826-834 (1990).

Prince, M., Wimo, A., Guerchet, M., Ali, G.C., Wu, Y.T., Prina, M. World Alzheimer report 2015—the global impact of dementia: an analysis of prevalence, incidence, cost and trends. London: Alzheimer's Disease International, 2015.

Prough, D.S., Kong, D., Watkins, W.D., Stout, R., Stump, D.A. Beamer, W.C. Inhibition of thromboxane A2 production does not improve post-ischemic brain hypoperfusion in the dog. Stroke 17, 1272-1276 (1986).

Puro D.G. Physiology and pathobiology of the pericyte-containing retinal microvasculature: New developments. Microcirculation 14, 1-10 (2007).

Querfurth, H., LaFerla, F. Alzheimer's Disease. NEJM 362, 329-344 (2010).

Rang, H.P., Ritter, J.M., Flower, R.J., Henderson, G. Rang & Dale's Pharmacology. 8th edn. Elsevier Churchill Livingstone (2016).

Rakic, P. Evolution of the neocortex: a perspective from developmental biology. Nat Rev Neurosci. 10, 724-735 (2009).

Reeves, A.M., Shigetomi, E., Khakh, B.S. Bulk loading of calcium indicator dyes to study astrocyte physiology: key limitations and improvements using morphological maps. J Neurosci. 31, 9353-9358 (2011).

Reiman, E. M., Chen, K., Alexander, G.E. et al. Functional brain abnormalities in young adults at genetic risk for late-onset Alzheimer's dementia. Proc. Natl Acad. Sci. USA 101, 284–289 (2004).

Richardson, K., Stephan, B.C.M., Ince, P.G., et al. The neuropathology of vascular disease in the Medical Research Council Cognitive Function and Ageing Study (MRC CFAS). Curr. Alzheimer Res. 9, 687–696 (2012).

Roberts, B.R., Lind, M., Wagen, A.Z. et al. Biochemically-defined pools of amyloid-beta in sporadic Alzheimer's disease: correlation with amyloid PET. Brain 140, 1486-1498 (2017).

RodrÍguez-Pascual, F. Busnadiego, O., Lagares, D., Lamas, S. Role of endothelin in the cardiovascular system. Pharmacol Res. 63, 463-72 (2011).

Roger, V. L., Go, A. S., Lloyd-Jones, D. M. et al. Heart disease and stroke statistics – 2011 update: a report from the American Heart Association. Circulation 123(4) e18- e209 (2011). [Erratum, Circulation 123(6) e240 (2011).

Roggendorf, W., Cervós-Navarro, J. Ultrastructure of arterioles in the cat brain. Cell Tissue Res. 178, 495–515 (1977).

Roher, A.E., Esh, C., Rahman, A., et al. Atherosclerosis of cerebral arteries in Alzheimer disease. Stroke 35 (Suppl 1), 2623–2627 (2004).

Roher, A.E., Lowenson, J.D., Clarke, S., Woods, A.S., Cotter, R.J., Gowing, E., Ball, M.J. β-Amyloid - (1-42) is a major component of cerebrovascular deposits: Implicatons for the pathology of Alzheimer disease. Proc. Natl. Acad. Sci. USA 90, 10836-10840 (1993).

Ropper, A.H. and Brown, R.H. Adam and Victor's Principles of Neurology, 8th edn, McGraw-Hill, 2005.

Rosenegger, D.G., Tran, C.H., Wamsteeker, C. et al. Tonic local brain blood flow control by astrocytes independent of phasic neurovascular coupling. J Neurosci. 35, 13463-13474 (2015).

Rossi, D. J., Oshima, T., Attwell, D. Glutamate release in severe brain ischaemia is mainly by reversed uptake. Nature 403, 316-312 (2000).

Rouach, N., Koulakoff, A., Abudara, V., Willecke, K., Giaume, C. Astroglial metabolic networks sustain hippocampal synaptic transmission. Science 322, 1551-1555 (2008).

Rouget, C. Memoire sur le developpment, la structures et les proprieties des capillaires sanguis and lymphatiques. Archs Physiol Norm Pathol 5, 603-33 (1873)

Royal College of Physicians National Sentinal Stroke Clinical Audit 2010 Round 7 Public report for England, Wales and Northern Ireland. Prepared on behalf of the Intercollegiate Stroke Working Party p43 (2011)

Ruitenberg, A., den Heijer, T., Bakker, S.L. et al. Cerebral hypoperfusion and clinical onset of dementia: the Rotterdam Study. Ann Neurol. 57, 789–794 (2005).

Rustenhoven, J., Jansson, D., Smyth, L.C., Dragunow, M. Brain pericytes as mediators of neuroinflammation. Trends Pharmacol Sci 38, 291–304 (2017).

Sacco, R.L., Kasner, S.E., Broderick, J.P., et al. An updated definition of stroke for the 21st century: a statement for healthcare professionals from the American Heart Association/American Stroke Association. Stroke 44, 2064–89 (2013).

Sagare, A., Bell, R.D. Zhao, Z. et al. Pericyte loss influences Alzheimer-like neurodegeneration in mice. Nature communications 4, 1-14 (2013).

Saito, T.S., Matsuba, Y.M., Mihira, N. et al. Single A*pp* knock-in mouse

models of Alzheimer's disease. Nat Neurosci. 17, 661-663 (2014).

Sakagami, K., Kawamura, H., Wu, D.M., Puro, D. Nitric Oxide/cGMP-induced inhibition of calcium chloride currents in retinal pericytes. Microvasc. Res. 62, 196-203 (2001).

Salloway, S., Sperling, R., Fox, N.C., Blennow, K., Klunk, W., Raskind, M. et al. Two phase 3 trials of bapineuzumab in mild-to-moderate Alzheimer's disease N Engl J Med, 370, 322-333 (2014).

Sato, A., Sato, Y., Uchida, S. Regulation of regional cerebral blood flow by cholinergic fibres originating in the basal forebrain. Int J Dev Neurosci 19, 327-337 (2001).

Saver J.L., Goyal M., Bonafe A. et al. Stent-retriever thrombectomy after intravenous t-PA vs. t-PA alone in stroke. N Engl J Med 372, 2285-95 (2015).

Schaller, B. The role of endothelin in stroke: Experimental data underlying pathophysiology. Arch Med Sci 2, 146-58 (2011).

Scheltens, P., Blennow, K., Breteler, M.B.B. et al. Alzheimer's disease. Lancet 388, 505-517 (2016).

Segal, S.S. Integration and Modulation of Intercellular Signaling Underlying Blood Flow Control. J. Vasc. Res. *52*, 136–157 (2015).

Selkoe, D.J. The molecular pathology of Alzheimer's disease. Neuron 6, 487-498 (1991).

Selkoe, D.J. Alzheimer's disease is a synaptic failure. Science 298, 789-791 (2002).

Sengillo, J.D. et al. Deficiency in mural vascular cells coincides with blood-brain barrier disruption in Alzheimer's disease. Brain Pathol. 23, 303–310 (2013).

Serrano-Pozo, A. et al. Beneficial effect of human anti-amyloid-beta active immunization on neurite morphology and tau pathology. Brain 133, 1312–1327 (2010).

Shankar, G.M., Li, S., Mehta, T.H. et al. Amyloid-β protein dimers isolated directly from Alzheimer's brains impair synaptic plasticity and memory. Nat. Med. 14, 837–842 (2008).

Sharp, C.D., Hines, I., Houghton, J. et al. Glutamate causes a loss in human cerebral endothelial barrier integrity through activation of NMDA receptor. Am J Physiol Hear Circ Physiol 285, H2592– H2598 (2003).

Sheline, Y. I., Morris, J.C., Snyder, A.Z., et al. APOE4 allele disrupts resting state fMRI connectivity in the absence of amyloid plaques or decreased CSF Aβ42. J. Neurosci. 30, 17035–17040 (2010).

Shi, Y., Yamada, K., Liddelow, S.A. et al. ApoE4 markedly exacerbates tau-mediated neurodegeneration in a mouse model of tauopathy. Nature. 549, 523-527 (2017).

Shibata, M., Yamada, S., Ram Kumar, S. et al. Clearance of amyloid-β_{1-40} peptide from the brain by low density lipoprotein receptor-related protein-1 at the blood brain barrier. J. Clin. Invest. 106, 1489-99 (2000).

Shih, A.J., Blinder, P., Tsai, P.S. et al. The smallest stroke: occlusion of one penetrating vessel leads to infarction and a cognitive deficit. Nat Neurosci. 16, 55-63 (2013).

Shipp, S. Structure and function of the cerebral cortex. Curr. Biol 12, R443-R449 (2007).

Shohami, E., Jacobs, T.P., Hallenbeck, J.M., Feuerstein, G. Increase thromboxane A2 and 5-HETE production following spinal cord ischemia in the rabbit. Prostaglandins Leukot Med 28, 169-181 (1987).

Simard, J. M., Kent, T.A., Chen, M., Tarasov, K.V., Gerzanich, V. Brain oedema in focal ischaemia: molecular pathophysiology and theoretical implications. Lancet Neurol 6, 258-268 (2007).

Simpson, I.A., Carruthers, A., Vannucci, S.J. Supply and demand in cerebral energy metabolism: the role of nutrient transporters. J Cereb Blood Flow Metab 27, 1766-1791 (2007).

Sims, D. The pericyte-a review. Tissue & Cell 18 (2), 153-74 (1986).

Smith, E, E. & Greenberg, S.M. Beta-amyloid, blood vessels and brain function. Stroke 40, 2601-2606 (2009).

Song, S., Ewald, A.J., Stallcup, W., Werb, Z., Bergers, G. PDGFRbeta+ perivascular progenitor cells in tumours regulate pericyte differentiation and vascular survival. Nat. Cell Biol. 7, 870-79 (2005).

Soriano, P. Abnormal kidney development and hematological disorders in PDGF beta-receptor mutant mice. Genes Dev. 8, 1888-96 (1994).

Sotelo-Hitschfeld, T., Niemeyer, M.I., Mächler, P. et al. Channel-mediated lactate release by K^+-stimulated astrocytes. J Neurosci. 35, 4168-4178 (2015).

Spatz, M., Yasuma, Y., Strasser, A., McCarron, R.M. Cerebral postischaemic hypoperfusion is mediated by ET_A receptors. Brain Res. 726, 242-246 (1996).

Stephen, T.L., Higgs, N.F., Sheehan, D.F., Al Awabdh, S., López-Doménech, G., Arancibia-Carcamo, I.L., Kittler, J.T. Miro1 regulates activity-driven positioning of mitochondria within astrocytic processes apposed to synapses to regulate intracellular calcium signaling. J Neurosci. 35, 15996-16011 (2015).

Strittmatter, W. J., Saunders, A.M., Goedert, M. et al. Isoform-specific interactions of apolipoprotein E with microtubule-associated protein tau: implications for Alzheimer disease. Proc. Natl Acad. Sci. USA 91, 11183–11186 (1994).

Summers, W. K., Jamison, R.L. The no reflow phenomenon in renal ischemia. Lab. Invest. 25, 635-643 (1971).

Sun, X., He, G., Qing, H. et al. Hypoxia facilitates Alzheimer's disease pathogenesis by up-regulating BACE1 gene expression. *Proc. Natl. Acad. Sci. U.S.A.* 103,18727–18732 (2006).

Sun, W., McConnell, E., Pare, J.F., Xu, Q., Chen, M., Peng, W., Lovatt, D., Han, X., Smith, Y., Nedergaard, M. Glutamate-dependent neuroglial calcium signalling differs between young and adult brain. Science 339, 197-200 (2013).

Suo, Z., Humphrey, J., Kundtz, A., Sethi, F., Placzek, A., Crawford, F., Mullan, M. Soluble Alzheimers β-amyloid constricts the cerebral vasculature in vivo. Neurosci. Lett. 257, 77-80 (1998).

Suter, O. C., Sunthorn, T., Kraftsik, R., et al. Cerebral hypoperfusion generates cortical watershed microinfarcts in Alzheimer disease. Stroke 33, 1986–1992 (2002).

Suzuki, A., Stern, S.A., Bozdagi, O., Huntley, G.W., Walker, R.H., Magistretti, P.J., Alberini, C.M. Astrocyte-neuron lactate transport is required for long-term memory formation. Cell 144, 810-823 (2011).

Svensson, A., Özen, I., Genové, G., Paul, G., Bengzon, J. Endogenous brain pericytes are widely activated and contribute 1338 to mouse glioma microvasculature. PLoS One 10:e0123553 (2015).

Sweeney, M. D., Abhay, P., Zlokovic, B. V. Blood-brain barrier breakdown in Alzheimer Disease and other neurodegenerative disorders. Nat. Rev. Neurol. 14, 133-150 (2018).

Tachibana, M., Yamazaki, Y., Liu, C.C., Bu, G., Kanekiyo, T. Pericyte implantation in the brain enhances cerebral blood flow and reduces amyloid-pathology in amyloid model mice. Exp Neurol. 300, 13-21 (2017).

Takano, T., Tian, G.F., Peng, W., Lou, N., Libionka, W., Han, X., Nedergaard, M. Astrocyte mediated control of cerebral blood flow. Nat Neurosci 9, 260-267 (2006).

Taheri, S., Gasparovic, C., Huisa, B.N. et al. Blood–brain barrier permeability abnormalities in vascular cognitive impairment. Stroke 42, 2158–2163 (2011).

Tatu, L., Vuillier, F., Moulin, T. Arteries and veins of the brain: anatomical organization. In: Oxford Textbook of stroke and cerebrovascular disorders. 1st ed. Oxford University Press, 19-35 (2014)

Toledo, J.B., Arnold, S.E., Raible, K., et al. Contribution of cerebrovascular disease in autopsy confirmed neurodegenerative disease cases in the National Alzheimer's Coordinating Centre. Brain 136, 2697–2706 (2013).

Thal, D. R., Ghebremedhin, E., Rüb, U. et al. Two Types of Sporadic Cerebral Amyloid Angiopathy. J Neuropathol Exp Neurol. 61, 282-293 (2002).

Thambisetty, M., Beason-Held, L., An, Y., Kraut, M. A., Resnick, S. M. APOE e4 genotype and longitudinal changes in cerebral blood flow in normal aging. Arch. Neurol. 67, 93–98 (2010).

The National Institute of Neurological Disorders and Stroke rt-PA Stroke Study Group. Tissue plasminogen activator for acute ischaemic stroke. N Engl J Med 333, 1581-8 (1995).

Thomas, T., Miners, S., Love, S. Post-mortem assessment of hypoperfusion of cerebral cortex in Alzheimer's disease and vascular dementia. Brain 138, 1059-1069 (2016).

Thomas, T., Thomas, G., McLendon, C., Sutton, T., Mullan, M. β-Amyloid-mediated vasoactivity and vascular endothelial damage. Nature 380, 168–171 (1996).

Thorlakur, J.J.K. et al. A mutation in APP protects against Alzheimer's disease and age related cognitive decline. Nature 488, 96-9 (2012).

Toussay, X., Basu, K., Lacoste, B., Hamel, E. Locus coeruleus stimulation recruits a broad cortical neuronal network and increases cortical perfusion. J. Neurosci. 33, 3390–3401 (2013).

Townsend, M., Shankar, G. M., Mehta, T., Walsh, D. M., Selkoe, D. J. Effects of secreted oligomers of amyloid-β protein on hippocampal synaptic plasticity: a potent role for trimers. J. Physiol. 572, 477–492 (2006).

Townsend, N., Wickramasinghe, K., Bhatnagar, P., Smolina, K., Nichols, M.,

Luengo- Fernandez, R. and Rayner, M. Coronary heart disease statistics 2012 edition. British Heart Foundation: London p57 (2012).

Tokiyoshi, K., Ohnishi, T., Nii, Y. Efficacy and toxicity of thromboxane synthetase inhibitor for cerebral vasospasm after subarachnoid hemorrhage. Surg Neurol. 36, 112-118 (1991).

Turovsky, E., Theparambil, S.M., Kasymov, V. et al. Mechanisms of CO_2/H^+ sensitivity of astrocytes. J Neurosci. 36, 10750-10758 (2016).

Uhlirova, H., Kılıc, K., Tian, P., Thunemann, M., Desjardins, M., Saisan, P.A., Sakadzic_, S., Ness, T.V., Mateo, C., Cheng, Q., et al. Cell type specificity of neurovascular coupling in cerebral cortex. eLife *5*, 155 (2016b).

Van de Haar, H. J., Burgmans, S., Jansen, J.F.A. et al. Blood–brain barrier leakage in patients with early Alzheimer disease. Radiology 281, 527–535 (2016).

Venegas, C., Kumar, S., Bernardo, S., et al. Microglia-driven ASC specks cross-seed amyloid-β in Alzheimer's disease. Nature 552, 355-361 (2017).

Verbeek, M., de Waal, R., Schipper, J. and Van Nostrand, W. Rapid Degeneration of Cultured Human Brain Pericytes by Amyloid-β Protein. J Neurochem. 68(3), 1135-41 (1997).

Verghese, P.B., Castellano, J.M., Holtzman, D.M. Apolipoprotein E in Alzheimer's disease and other neurological disorders. *Lancet Neurol* 10, 241–252 (2011).

Vergouwen, M.D.I., Algra, A., Rinkel, G.J.E. Endothelin receptor antagonists for aneurysmal subarachnoid haemorrhage: A systematic review and meta-analysis update. Stroke 43, 2671-2676 (2012).

Vergouwen, M. D. I., Vermeulen, M., van Ginjn. J. et al. Definition of delayed cerebral ischaemia after aneurysmal subarachnoid haemorrhage as an outcome event in clinical trials and observational studies: proposal of a multidisciplinary research group. Stroke 41, 2391-5 (2010).

Villemagne, V.L. et al. Longitudinal assessment of Aβ and cognition in aging and Alzheimer disease. Ann. Neurol. 69, 181–192 (2011).

von Bartheld, C,S,, Bahney, J., Herculano-Houzel, S. The search for true numbers of neurons and glial cells in the human brain: A review of 150 years of cell counting. J Comp Neurol 524, 3865-3895 (2016).

von Kummer, R. After European Co-operative Acute Stroke Study 3: mission accomplished? Stroke. 40, 2268-70 (2009).

Walsh, D. M., Klyubin, I., Fadeeva, J.V., et al. Naturally secreted oligomers of amyloid-β protein potently inhibit hippocampal long-term potentiation *in vivo*. Nature 416, 535–539 (2002).

Waitt, A.E., Reed, L., Ransom, B.R., Brown, A.M. Emerging roles for glycogen in the CNS. Front Mol Neurosci. 10, 73 doi: 10.3389/fnmol.2017.00073 (2017).

Wang, Y., Mandelkow, E. Tau in physiology and pathology. Nat. Rev.

Neurosci. 17, 5-21 (2016).

Webster, S.J., Bachstetter, A.D., Nelson, P.T., Schmitt, F.A. & Van Eldik, L.J. Using mice to model Alzheimer's dementia: an overview of the clinical disease and the preclinical behavioral changes in 10 mouse models. Front. Genet. 5, 88 (2014).

Wechsler, L. R. Intravenous thrombolytic therapy for ischaemic stroke. N Engl J Med. 364, 2138-46 (2011).

Wei, S.W., Kang, H., Rashid, I.D. et al. Erythrocytes are oxygen-sensing regulators of the cerebral microcirculation. Neuron 91, 851-862 (2016).

Wilhelmus, M. M. M., Otte-Höller, I., van Triel, J.J.J. et al. Lipoprotein receptorrelated protein-1 mediates amyloid-ß-mediated cell death of cerebrovascular cells. Am. J. Pathol. 171, 1989–1999 (2007).

Williams, D. R., Holton, J.L., Strand, C. et al. Pathological tau burden and distribution distinguishes progressive supranuclear palsy-Parkinsonism from Richardson's syndrome. Brain 130, 1566–1576 (2007).

Willms-Kretschmer, K., G. Majno. Ischemia of the skin. Electron microscopic study of vascular injury. Am. J. Pathol. 54, 327-343 (1969).

Wimo, A., Prince, M. World Alzheimer Report 2010: The Global Economic Impact of Dementia (Alzheimer's Disease International (ADI), 2010).

Winblad, B., Amouyel, P., Andrieu, S. et al. Defeating Alzheimer's disease and other dementias: a priority for European science and society. Lancet Neurol 15, 455-532 (2016).

Winkler, E.A., Bell, R.D. & Zlokovic, B.V. Central nervous system pericytes in health and disease. Nat Neurosci. 14, 1398-1405 (2011).

Winkler, E.A., Bell, R.D., Zlokovic, B.V. Pericyte-specfic expression of PDGFR beta receptor in mouse models with normal and deficient PDGFR beta receptor signaling. Mol Neurodegener. 5 (32) 1-11 (2010).

Winkler, E.A., Sagare, A.P., Zlokovic, B.V. The pericyte – a forgotten cell type with implications for Alzheimer's disease? Brain Pathol. 24, 371-86 (2014).

Winkler, E.A., Sengillo, J.D., Sullivan, J.S., et al. Blood-spinal cord barrier breakdown and pericyte reductions in amyotrophic lateral sclerosis. Acta Neuropathol 125, 111–120 (2013).

Winship, I.R., Plaa, N., Murphy, T.H. Rapid astrocyte calcium signals correlate with neuronal activity and onset of the hemodynamic response in vivo. J Neurosci. 27, 6268-6272 (2007).

Wirth, M., Binette, A.P., Brunecker, P. Divergent regional patterns of cerebral hypoperfusion and gray matter atrophy in mild cognitive impairment patients. J. Cereb. Blood Flow Metab. 37, 814–824 (2016).

Woodruff, T., Thundyil, J., Tang, S. et al. Pathophysiology, treatment, and animal and cellular models of human ischemic stroke. Molecular Neurodegeneration 6, 11 (2011).

Woolsey, T.A., Rovainen, C.M. Whisker barrels: a model for direct observation of changes in the cerebral microcirculation with neuronal activity. In Brain Work and Mental Activity: Quantitative Studies with Radioactive Tracers: Proceedings of the Alfred Benzon Symposium 31 Held at the Premises of the Royal Danish Academy of Sciences and Letters, Copenhagen, August 12–16, 1990, N.A. Lassen, ed. (John Wiley & Sons), pp. 189–200 (1991).

Wu, D. M., Kawamura H., Sakagami, k., Kobayashi, M., Puro D. G. Cholinergic regulation of pericyte-containing retinal microvessels. Am. J. Physiol. Heart circ. Physiol. 284, H2083-H2090 (2003).

www.amidebio.com/wp-content/uploads/2016/07/Abeta_Quantitation_Protocol.pdf

Xie, L., Kang, H., Xu, Q. et al. Sleep drives metabolite clearance from the adult brain. Science 342, 373-77 (2013).

Yanagisawa, M., Kurihara, H., Kimura, S. et al. A novel potent vasoconstrictor peptide produced by vascular endothelial cells. Nature 332, 411-415 (1988).

Yarchoan, M., Xie, S.X., Kling, M.A., et al. Cerebrovascular atherosclerosis correlates with Alzheimer pathology in neurodegenerative dementias. Brain 135, 3749–3756 (2012).

Yemisci, M., Gursoy-Ozdemir, Y., Vural, A. et al. Pericyte contraction induced by oxidative-nitrative stress impairs capillary reflow despite successful opening of an occluded cerebral artery. Nat. Med. 15, 1031–1037 (2009).

Zhang, B., Gaiteri, C., Bodea, C. et al. Integrated systems approach identifies genetic nodes and networks in late-onset Alzheimer's disease. Cell 153, 707-720 (2013).

Zhang, E.T., Inman, C.B., and Weller, R.O. Interrelationships of the pia mater and the perivascular (Virchow-Robin) spaces in the human cerebrum. J. Anat. 170, 111–123 (1990).

Zhang, F., Eckman, C., Younkin, S., Hsiao, K. K., Iadecola, C. Increased susceptibility to ischemic brain damage in transgenic mice overexpressing the amyloid precursor protein. J. Neurosci. 17, 7655–7661 (1997).

Zhang, J., Yang, J., Zhang, C., Jiang, X., Zhou, H., Liu, M. Calcium antagonists for acute ischemic stroke. Cochrane Database of Systematic Reviews 2012, Issue 5. Art. No.: CD001928. DOI: 10.1002/14651858.CD001928.pub2.

Zhang, Y., Sloan, S.A., Clarke, L.E. et al. Purification and characterization of progenitor and mature human astrocytes reveals transcriptional and functional differences with mouse. Neuron 89, 37-53 (2016).

Zhang, X., Zhoue, K., Ruishan, W. et al. Hypoxia-inducible factor 1a (HIF-1a)-mediated hypoxia increases BACE1 expression and b-amyloid generation. J. Biol. Chem. 282, 10873–10880 (2007).

Zhang, Y., Chen, K., Sloan, S.A. et al. An RNA-sequencing transcriptome and splicing database of glia, neurons, and vascular cells of the cerebral cortex. J Neurosci. 34, 11929-11947 (2014).

Zhao, S., Ting, J.T., Atallah, H.E. et al. Cell type-specific channel rhodopsin-2 transgenic mice for optogenetic dissection of nerural circuitry function. Nat. Methods 8, 745-52 (2011).

Zimmerman, K. W. Der feinere bau der blutcapillaires. Z. Anat. Entwicklungsgesch 68, 3-109 (1923).

Ziv, I., Fleminger, G., Djaldetti, R., Achiron, A., Melamed, E., Sokolovsky, M. Increased plasma endothelin-1 in acute ischemic stroke. Stroke 23, 1014-1016 (1992).

Zlokovic, B. Neurovascular pathways to neurodegeneration in Alzheimer's disease and other disorders. Nat Rev Neurosci. 12, 723-738 (2011).

Zlokovic, B. The blood-brain barrier in health and chronic neurodegenerative disorder. Neuron 57, 178-201 (2008).

Zonta, M., Angulo, M.C., Gobbo, S., Rosengarten, B., Hossmann, K.A., Pozzan, T., Carmignoto, G. Neuron-to-astrocyte signalling is central to the dynamic control of brain microcirculation. Nat Neurosci 6, 43-50 (2003).